

AD-A046 365

FORD AEROSPACE AND COMMUNICATIONS CORP NEWPORT BEACH --ETC F/G 20/4
INVESTIGATION OF THE STRUCTURE OF A COOLED WALL TURBULENT SUPER--ETC(U)
OCT 77 A J LADERMAN, A DEMETRIADES

UNCLASSIFIED

U-6370

ARO-12505.1-E

NL

1 OF 2

AD
A046 365



ARO 12505.1-E

Aeronutronic Publication No. U-6370

(Handwritten signature and initials)

FINAL TECHNICAL REPORT
INVESTIGATION OF THE STRUCTURE OF A
COOLED WALL TURBULENT SUPERSONIC BOUNDARY LAYER

Prepared by

A. J. Laderman
A. Demetriades

FORD AEROSPACE & COMMUNICATIONS CORPORATION
AERONUTRONIC DIVISION
FORD ROAD
NEWPORT BEACH, CALIFORNIA

Supported by

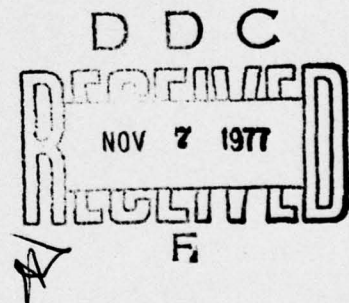
U. S. Army Research Office
Durham, N.C.

and

NASA Ames Research Center
Moffett Field, California

Under Contract
DAAG 29-75-C-0014

October 1977



Approved for public release; distribution unlimited.

AD No. —
DDC FILE COPY

AD A 0 46365

REPORT DOCUMENTATION PAGE		READ INSTRUCTIONS BEFORE COMPLETING FORM
1. REPORT NUMBER	2. GOVT ACCESSION NO.	3. RECIPIENT'S CATALOG NUMBER
6. TITLE (and Subtitle) Investigation of the Structure of a Cooled Wall Turbulent Supersonic Boundary Layer.		9. TYPE OF REPORT & PERIOD COVERED Final Report - 24 March 1975-23 July 1977
7. AUTHOR(s) 10. A. J. Laderman A. Demetriades		15. CONTRACT OR GRANT NUMBER(s) DAAG29-75-C-0014
9. PERFORMING ORGANIZATION NAME AND ADDRESS Ford Aerospace & Communications Corp Aeronutronic Division Ford Road, Newport Beach, CA 92663		10. PROGRAM ELEMENT, PROJECT, TASK AREA & WORK UNIT NUMBERS
11. CONTROLLING OFFICE NAME AND ADDRESS U. S. Army Research Office Post Office Box 12211 Research Triangle Park, NC 27709		12. REPORT DATE October 1977
14. MONITORING AGENCY NAME & ADDRESS (if different from Controlling Office) 12. 135p. 14. U-6370		13. NUMBER OF PAGES 123
16. DISTRIBUTION STATEMENT (of this Report) Approved for public release; distribution unlimited.		15. SECURITY CLASS. (of this report) Unclassified
17. DISTRIBUTION STATEMENT (of the abstract entered in Block 20, if different from Report) NA 18. ARO 19. 12505.1-E		15a. DECLASSIFICATION/DOWNGRADING SCHEDULE NA
18. SUPPLEMENTARY NOTES The findings in this report are not to be construed as an official Department of the Army position, unless so designated by other authorized documents.		
19. KEY WORDS (Continue on reverse side if necessary and identify by block number) Turbulent supersonic boundary layer Cooled wall Turbulent transport properties Mean flow profiles Turbulent shear stress		
20. ABSTRACT (Continue on reverse side if necessary and identify by block number) This report presents mean flow profiles across a two-dimensional, flat plate, compressible turbulent boundary layer. The mean flow properties were determined from pitot pressure and total temperature surveys carried out at three stream- wise locations for wall to freestream total temperature ratios of 0.94 (adiaba- tic case), 0.714 and 0.54. All tests were conducted for a freestream Mach number of 3.0 with Reynolds number, based on momentum thickness, varying from 3200 to 4200. Although the outer two thirds of the viscous sublayer was probed, no evidence was found of a linear velocity gradient near the wall. However,		

DD FORM 1 JAN 73 1473

EDITION OF 1 NOV 65 IS OBSOLETE

Unclassified

SECURITY CLASSIFICATION OF THIS PAGE (When Data Entered)

391 853 ii

7/3

Unclassified

SECURITY CLASSIFICATION OF THIS PAGE (When Data Entered)

the skin friction calculated using two conventional correlations were in good agreement with the trend of the data. Furthermore, comparison of the velocity profile with Coles Law-of-the-Wake correlation indicated that the boundary is characteristic of a fully developed zero pressure gradient, flat plate flow. The experimental profiles of total temperature versus velocity were also observed to be in good agreement with the theoretical predictions of Whitfield and High for nonunity Prandtl number. These results demonstrated that the linear Crocco relation, which assumes $Pr = 1.0$, cannot be used to judge the quality of the boundary layer flow for near adiabatic wall cases. Finally, the distribution of turbulent shear stress, mixing length and eddy viscosity across the boundary layer, were determined indirectly from the "time averaged" boundary layer equations using the experimental mean flow profiles. Results were in accord with those of other investigators for supersonic flows. In particular, the calculated eddy viscosity was in excellent agreement with the correlation derived by Maise and McDonald.

SECURITY CLASSIFICATION OF THIS PAGE (When Data Entered)

111

ABSTRACT

This report presents mean flow profiles across a two-dimensional, flat plate, compressible turbulent boundary layer. The mean flow properties were determined from pitot pressure and total temperature surveys carried out at three streamwise locations for wall to freestream total temperature ratios of 0.94 (adiabatic case), 0.714 and 0.54. All tests were conducted for a freestream Mach number of 3.0 with Reynolds number, based on momentum thickness, varying from 3200 to 4200. Although the outer two thirds of the viscous sublayer was probed, no evidence was found of a linear velocity gradient near the wall. However, the skin friction calculated using two conventional correlations were in good agreement with the trend of the data. Furthermore, comparison of the velocity profile with Coles Law-of-the-Wake correlation indicated that the boundary is characteristic of a fully developed zero pressure gradient, flat plate flow. The experimental profiles of total temperature versus velocity were also observed to be in good agreement with the theoretical predictions of Whitfield and High for nonunity Prandtl number. These results demonstrated that the linear Crocco relation, which assumes $Pr = 1.0$, cannot be used to judge the quality of the boundary layer flow for near adiabatic wall cases. Finally, the distribution of turbulent shear stress, mixing length and eddy viscosity across the boundary layer, were determined indirectly from the "time averaged" boundary layer equations using the experimental mean flow profiles. Results were in accord with those of other investigators for supersonic flows. In particular, the calculated eddy viscosity was in excellent agreement with the correlation derived by Maise and McDonald.

The findings in this report are not to be construed as an official Department of the Army position, unless so designated by other authorized documents.

ACCESSION for	
NTIS	Write Section <input checked="" type="checkbox"/>
DDC	Buff Section <input type="checkbox"/>
UNANNOUNCED	<input type="checkbox"/>
JUSTIFICATION	<input type="checkbox"/>
BY	
DISTRIBUTION/AVAILABILITY CODES	
01	SPECIAL
A	

CONTENTS

Section	Page
1 Introduction	1
2 The Experiment	2
2.1 Flat Plate Design	2
2.2 Instrumentation	2
2.2.1 Surface Diagnostics	2
2.2.2 Mean Flow Probes	3
2.3 Preliminary Flow Field Surveys	5
2.4 Test Matrix	5
3 Mean Flow Measurements	6
3.1 Mean Flow Properties	6
3.2 T versus u/u_e Profiles	7
3.3 Skin Friction	10
3.4 Gradients of Velocity and Temperature	13
3.5 Integral Properties	14
3.6 Calculation of Turbulent Shear Stress	15
4 Summary and Conclusions	20
References	73
Figures	75

FIGURES

Figure		Page
1	Photograph of flat plate installed in wind tunnel	75
2	Schematic of flat plate underside showing coolings and location of thermocouples (T_1, T_2, \dots) and static pressure taps (p_1, p_2, \dots)	76
3	Typical surface pressure distribution	77
4	Typical surface temperature distributions	78
5	Variation of hot film temperature T_{HF} held just above plate surface, as a function of wall temperature. Calibration of T_{HF} is approximate and is only meant to indicate smoothness of response through the frost formation stage	79
6	Typical X-Y plotter record of pitot pressure profile . . .	80
7	Typical pitot pressure measurements showing effect of probe size	81
8	Recovery factor calibration of total temperature probe. . .	82
9	Recovery temperature and computed total temperature profiles for adiabatic wall condition	83
10	Typical recovery temperature profiles for $T_w = 172^\circ K$. . .	84
11	Block diagram of mean flow instrumentation	85
12	a) Spark Schlieren photographs of flow over flat plate taken at different contrast to illustrate boundary layer development at $P_0 = 730$ mmHg.	86
	b) Features distinguished in Schlieren records.	87
13	Pitot probe traverses normal to the surface and at various lateral positions	88
14	Pitot probe traces parallel to and at various distances from the surface	89
15	Non-dimensional velocity profiles for $T_w/T_{oe} = .94$	90
16	Non-dimensional velocity profiles for $T_w/T_{oe} = .71$	91
17	Non-dimensional velocity profiles for $T_w/T_{oe} = .54$	92
18	Comparison of velocity profiles at $x = 38.79$ cm for $T_w/T_{oe} = .94, .71$ and $.54$	93
19	Non-dimensional total temperature profiles for $T_w/T_{oe} = .94$	94

FIGURES
(Continued)

Figure		Page
20	Non-dimensional total temperature profiles for $T_w/T_{oe} = .71$	95
21	Non-dimensional total temperature profiles for $T_w/T_{oe} = .54$	96
22	Effect of wall temperature on total temperature profiles . .	97
23	Plot of $\tilde{T} = T_o - T_w/T_{oe} - T_w$ versus u/u_e for $T_w = .94$	98
24	Plot of $\tilde{T} = T_o - T_w/T_{oe} - T_w$ versus u/u_e for $T_w = .71$	99
25	Plot of $\tilde{T} = T_o - T_w/T_{oe} - T_w$ versus u/u_e for $T_w = .54$	100
26	Typical correlation of experimental velocity profile in terms of the Law-of-the-Wall	101
27	Comparison of calculated wake function with assumed sine-squared variation	102
28	Variation of skin friction c_f , based on Hopkins and Inouye ¹¹ correlation, with Re_θ	103
29	Comparison of linear velocity profile near the wall, deduced from skin friction coefficient, with experimental measurements at $x = 38.79$ cm	104
30	Comparison of linear temperature profile, deduced from skin friction coefficient and Reynolds analogy, with experimental measurements at $T_w/T_{oe} = .54$	105
31	Non-dimensional normal velocity gradient versus y/δ for $x = 35.05$ cm and $T_w/T_{oe} = .94$	106
32	Non-dimensional normal total temperature gradient versus y/δ for $x = 35.05$ cm and $T_w/T_{oe} = .94$	107
33	Non-dimensional normal total temperature gradient in vicinity of wall for $x = 35.05$ cm and $T_w/T_{oe} = .94$	108
34	Non-dimensional normal total temperature gradient in vicinity of wall for $x = 42.52$ cm and $T_w/T_{oe} = .94$	109
35	Non-dimensional normal velocity gradient versus y/δ for $x = 35.05$ cm and $T_w/T_{oe} = .54$	110
36	Non-dimensional normal total temperature gradient versus y/δ for $x = 35.05$ cm and $T_w/T_{oe} = .54$	111
37	Non-dimensional normal velocity gradient in vicinity of wall for $x = 35.05$ cm and $T_e/T_{oe} = .54$	112

FIGURES
(Continued)

Figure		Page
38	Non-dimensional normal total temperature in vicinity of wall for $x = 35.05$ cm and $T_w/T_{oe} = .54$	113
39	Characteristic boundary layer thicknesses δ , δ^* and θ plotted as a function of T_w/T_{oe}	114
40	Variation of Re_θ with T_w/T_{oe}	115
41	Variation of incompressible form factor with Re_θ	116
42	Shear stress distribution, based on mean flow profiles for $T_w/T_{oe} = .94$, $x = 38.79$ cm	117
43	Shear stress distribution, based on mean flow profiles for $T_w/T_{oe} = .71$, $x = 38.79$ cm	118
44	Shear stress distribution, based on mean flow profiles for $T_w/T_{oe} = .54$, $x = 38.79$ cm	119
45	Turbulent shear stress, normalized by wall shear, versus y/δ	120
46	Density ratio, ρ/ρ_e , versus y/δ for $x = 38.79$ cm showing effect of T_w/T_{oe}	121
47	Variation of normalized mixing length ℓ/δ across the boundary layer.	122
48	Normalized eddy viscosity versus y/δ	123

TABLES

Table		Page
1	Location of Pressure Taps (P) and Thermocouples (TC) on Plate Surface	22
2	Matrix of Test Conditions	23
3	Summary of Mean Flow Profiles	24
4	Summary of Integral Properties and Edge Conditions	70
5	Summary of Velocity Correlation Calculations	71
6	Derivatives for Shear Stress Calculations	72

SYMBOLS

C_f	local skin friction coefficient
C_h	local heat transfer coefficient
C_p	specific heat at constant pressure
H_u	incompressible form factor defined in Equation 3.7
k	molecular thermal conductivity
ℓ	mixing length
M	Mach number
P	pressure
Pr	molecular Prandtl number
Pr_m	mixed Prandtl number
P_t	pitot pressure
q	heat transfer rate
Re	Reynolds number
Re_θ	Reynolds number based on momentum thickness
Re^+	boundary layer Reynolds number $\delta u_\tau / \nu_w$
T	temperature
T_{meas}	measured total temperature or recovery temperature
\bar{T}	Crocco parameter $\equiv T_o - T_w / T_{oe} - T_w$
u	longitudinal velocity
u^+	transformed velocity $\equiv u^* / u_\tau$ (see Equation 3.5)
u^*	Van Driest generalized velocity (see Equation 3.5)
u_τ	friction velocity $\equiv (\tau_w / \rho_w)^{1/2}$
v	velocity normal to surface
x	streamwise distance

SYMBOLS
(Continued)

y	distance normal to surface
y^+	transformed distance normal to surface (see Equation 3.5)
z	spanwise distance
θ	pressure gradient parameter $\equiv \frac{\theta}{\tau_w} \frac{dP}{dx}$
δ	boundary layer thickness
δ^*	displacement thickness
δ_i^*	kinematic boundary layer thickness $\equiv \int_0^\delta (1 - \frac{u}{u_e}) dy$
γ	ratio of specific heats
ϵ	eddy viscosity
η	recovery factor
μ	molecular viscosity
ν_u	kinematic viscosity = μ/ρ
θ	momentum thickness
π	parameter representing strength of wake component of boundary layer (normally = 0.6 for $dp/dx = 0$)
ρ	density
τ	shear stress
τ_L	laminar shear stress
τ_T	turbulent shear stress

SYMBOLS
(Continued)

Subscripts

aw	adiabatic wall
e	edge condition
0	stagnation condition
t	turbulent
w	wall condition
∞	freestream condition
m	evaluated at $y/\delta = 0.5$

Superscripts

()'	fluctuating value
($\bar{}$)	mean or time averaged value of fluctuation

SECTION 1

INTRODUCTION

Predictions of turbulent skin friction and heat transfer phenomena require accurate solutions to the "time averaged" equations of boundary layer flow. These equations, however, contain higher order turbulence terms, i.e., the turbulent transport properties, which cannot be derived from first principles. While recent advances in computational techniques make possible rapid calculation of compressible turbulent flows, the various calculation schemes lack appropriate models for the transport terms. There is, in fact, an acute need for direct measurement of the turbulent fluctuations and of their higher moments to serve as a basis for such turbulence "modeling."

At supersonic speeds, compressible turbulence is distributed among various "modes" including pressure, temperature and velocity fluctuations. While the available data base is restricted in scope, it does indicate that (1) the temperature (density) fluctuations become significant at high speeds and are sensitive to the wall temperature, (2) these same fluctuations are important, and perhaps even dominant, in the turbulent transfer process and thus are central to proper turbulence modeling, and (3) as a consequence, the cross-correlations, i.e., the Reynolds stress terms, may also be sensitive to the wall heat transfer. Based on present knowledge, estimating the influence of wall cooling on the turbulent fluctuations at any flow speed is possible over only a limited range of conditions. Consequently, the present task was undertaken to more clearly delineate the effect of wall temperature on the turbulence structure of the compressible supersonic boundary layers. Experiments were carried out in the flow over a zero pressure gradient flat plate at a fixed Mach number of 3.0 for wall temperatures $T_w/T_{Oe} = .94$ (adiabatic case), .714 and .54.

This report documents the results of the first phase of the program which was directed toward detailing the mean flow profiles of the boundary layer at several selected streamwise stations for each wall condition indicated above. Such measurements are required to demonstrate the two-dimensional, fully equilibrated nature of the flow and are needed to calculate the sensitivity coefficients of the hot wires used in subsequent measurements of the flow fluctuations. A report describing the results of the fluctuation measurements is forthcoming.

A description of the test hardware and instrumentation is presented in Section 2 of this report while Section 3 discusses the results of the mean flow measurements. In particular, Section 3 describes the mean flow profiles, includes an assessment of the measured total temperature-velocity profiles, presents the results of skin friction calculations and a comparison with the Law-of-the-Wake velocity correlation. Finally, it provides the distribution of turbulent shear stress, eddy-viscosity, and mixing length as deduced from the "time averaged" boundary layer equations using the known experimental mean flow profiles. A summary of the experimental findings is presented in Section 4.

SECTION 2

THE EXPERIMENT

2.1 FLAT PLATE DESIGN

The model consisted of a 7.62 cm wide, 66.04 cm long 2024 grade aluminum plate with a 0.475 cm thickness and a 5° leading edge. When installed, the plate spanned the test section completely, with its top surface coincident with the (2-dimensional) nozzle centerplane, and its leading edge located 10 cm upstream of and its trailing edge 55.9 cm downstream of the nozzle throat. The plate was supported by a windshield attached to the lower nozzle block and by a faired strut anchored in the stagnation chamber ahead of the throat. On the sides, the plate pressed against the glass sidewalls with long O-ring seals, thus avoiding metal-glass contacts and minimizing lateral heat transfer. A photograph of the flat plate installed in the wind tunnel is shown in Figure 1. The region above the plate was unobstructed except for diagnostic probes suspended through the upper nozzle wall, and in the working section where the experiment was performed. The region under the plate was available for protrusions needed for cooling, surface sensors, etc.

Cooling was accomplished using liquid nitrogen supplied to four loops of 0.5 cm diameter aluminum tubing epoxied on the plate underside in pairs, as shown in Figure 2. The eight ends of these tubes (4 inlets and 4 outlets) extend beyond the plate trailing edge; the inlets continue into the diffuser section where they exit through the tunnel wall and connect to the LN_2 supply. The outlets discharge the spent coolant into the diffuser section; because the tunnel is an open circuit facility, the test air stream was not contaminated by nitrogen.

2.2 INSTRUMENTATION

2.2.1 SURFACE DIAGNOSTICS

As shown in Figure 2 and listed in Table 1, the plate was instrumented with 9 static pressure taps (P1-P9) and 14 iron constantan thermocouples (T1-T14) to monitor the streamwise and spanwise uniformity of surface properties. The pressure tubes are 0.081 cm in diameter with a 0.05 cm diameter opening; the thermocouples, comprised of a twisted pair of 0.025 cm diameter wires, were epoxied in place in holes drilled through the plate. Both types of sensors were located flush with the upper surface of the model. The pressure taps were connected through a sampling valve to a 15 psi Dynesco pressure transducer with a sensitivity of approximately 0.05 mv/mmHg. Typical measurements of surface pressure are shown in Figure 3, which includes also the static pressure calculated from the tunnel stagnation pressure, P_0 , and the measured freestream pitot pressure $P_{t\infty}$. Since the level of surface pressure corresponds to only 3% of the maximum range of the transducer, the agreement between measurement and calculation is considered good. The pressure taps were used primarily to monitor the flow and insure the absence of non-uniformities, and the static

pressure used in the data reduction was calculated as indicated above. The surface thermocouples were connected to a Newport digital pyrometer. During the experiments, the output from surface thermocouple numbers 7,8, or 9 was plotted on a Mosely X-Y recorder to provide a continuous record of the temperature of the plate.

Typical surface temperature distributions for each of the three temperature levels used in this study are shown in Figure 4. This plot indicates the uniformity of the wall temperature, in both the streamwise and spanwise directions, within the survey region. The single low temperature recorded at the 16-inch station, for a nominal wall temperature of 172°K , is the output from thermocouple number 12 located 2.03 cm from the plate centerline where the surveys were conducted. It is sufficiently displaced from the region of interest to have had negligible effect on the measurements. In all cases the region of uniform temperature started at $x = 20$ cm or about 20 boundary layer thicknesses upstream of the first survey station.

It was originally feared that condensation of water vapor at low temperature would form a layer of frost or ice on the plate which could interfere with the measurements. The silica-gel drier of the tunnel provides a 236°K dew-point at the inlet, which for a Mach 3 expansion corresponds to a condensation temperature of 203°K in the test section. Thus the mixture in the test section is actually supersaturated, although condensation only occurs in the presence of a cold surface. During the experiments, a very fine frost layer appeared on the plate at $T_w \approx 210^{\circ}\text{K}$ and completely covered it at $T_w = 170^{\circ}\text{K}$. A microscopic view of this layer, made with the tunnel running, showed it to consist of mil-size particles which are, of course, very much smaller than the boundary layer thickness and the sublayer thickness. Tests also showed that the pressure taps operated properly with the frost present. A test was also carried out to demonstrate that the ice formation did not cause any abrupt changes in the flow characteristics. A thin film probe acting as a thermometer (operated at low current) was located at about $y = 0.075$ cm and its equilibrium temperature was monitored as T_w was decreased from 300°K through frost formation to about 170°K . The result is shown in Figure 5 where it is seen that the sensor temperature decreases smoothly through the frost point, evidence that the flow itself is not discontinuously affected by the formation of ice.

2.2.2 MEAN FLOW PROBES

The mean flow probes, either a pitot pressure tube or a total temperature thermocouple, were mounted in a two-degree of freedom actuator, extending through the tunnel ceiling, which permitted motion in the horizontal (streamwise) and vertical directions. The pitot probe consisted of a 0.010 cm od tube which gradually tapered at its tip to a 0.005 cm diameter opening. A miniaturized Kulite pressure transducer, Model VQH-250-10, was mounted within the actuator thereby drastically reducing the response time of the probe. The transducer sensitivity of approximately 11.0 mmHg/mv was checked by calibration prior to each run. An X-Y plotter record of a typical pitot pressure survey is shown in Figure 6. The profile is similar to those obtained for all test

conditions and is characteristic of a fully turbulent boundary layer. (Note that the indicated height above the surface, y , requires a small zero correction to account for the true location of the wall.)

In order to document the sublayer, it was necessary to probe in detail within .05 cm of the wall. Although probe corrections were found to be negligible through the boundary layer, interference effects caused by the proximity of the wall were apparent for $y < 0.015$ cm. This was verified by measurements made with a larger pitot probe, comprised of a 0.051 cm od x 0.0406 cm id tube, flattened at its tip to a height of 0.018 cm. Typical pitot pressure measurements with both probes are shown in Figure 7 where it is seen the interference effects become evident when $y \leq 1.5$ times the probe height.

Total temperature measurements were made with a Ch-Al bare wire thermocouple, with its 0.0038 cm diameter wires welded to form a 0.0127 cm diameter sphere. Measurements were initially made with a shielded thermocouple but, because of interference effects near the wall, this probe was discarded in favor of the bare wire thermocouple. The probe was calibrated in the wind tunnel free-stream and the recovery factor plotted against Reynolds number, based on total temperature and sphere diameter, is shown in Figure 8. The recovery factor in Figure 8 is defined as $(T_{\text{meas}} - T)/(T_0 - T)$ and therefore accounts for the effects of local Mach number.

A typical record of the measured, or recovery, temperature for the adiabatic wall condition, together with the computed total temperature profile, is shown in Figure 9. Included as an insert in Figure 9 is the sublayer region plotted with an expanded scale. The zero slope of the T_0 profile near the wall and the overshoot near the outer edge of the boundary layer are characteristic of the adiabatic wall condition for non-unity Prandtl number. Typical recovery temperature profiles for $T_w = 170^\circ\text{K}$ are shown in Figure 10. The viscous sublayer is readily apparent and approximately 0.04 - 0.05 cm thick and experiences about one-half the change in total temperature across the boundary layer.

The mean flow profiles were obtained by feeding the probe output and a voltage signal from the probe actuator, which was proportional to the y position, to a pair of digital voltmeters. The DVM readings, in turn, were output to a paper printer that could be actuated manually or triggered by the actuator signal. A block diagram of the instrumentation is shown in Figure 11. The probe signal was allowed to equilibrate before data was recorded. The resolution of the DVMs was 0.01 mv, corresponding to a 0.1 mmHg or 0.5°C resolution for the pitot pressure and total temperature probes, respectively, and to 0.0001 cm for the probe position. The probe tip was viewed with a 10 power microscope and the wall location was determined from the actuator reading when the probe contacted the surface; in this manner the wall or $y = 0$ position could be determined with an accuracy of less than 0.0025 cm. The tunnel stagnation pressure was measured with a 0-800 mmHg Heise pressure gauge with a least count of 1 mmHg and stagnation temperature was sensed by a Precision digital temperature indicator which read directly in degrees

Fahrenheit with a resolution of 1°F (0.6°K). Mean flow properties were calculated by means of standard gas dynamic equations using an iterative procedure to account for the calibrated recovery factor characteristics of the T_o probe. The data reduction procedure was programmed for the Honeywell 6000 digital computer.

2.3 PRELIMINARY FLOW FIELD SURVEYS

Prior to the final measurements, several tests were carried out to judge the quality of the flow above the plate and to demonstrate the repeatability and two-dimensionality of the boundary layer. Extensive Spark-Schlieren studies were carried out for tunnel pressures ranging from $1/3$ to 1.0 atm. Figure 12 shows typical Schlieren records of the flow over the plate at $.973 \times 10^5 \text{ N/M}^2$ (730 mmHg). Each photograph is a mosaic composed of frames obtained from the nozzle throat region to beyond the plate trailing edge. They were obtained with a knife edge parallel to the flow so that when the density increases going up, the flow region appears light and vice versa. Figure 12b interprets the major features of the Schlieren photograph. These records show a very smooth, uniform flow, as can be judged by observing "calibration" shocks introduced deliberately at two points.

Pitot surveys of the boundary layer were made to determine the two-dimensionality and repeatability of the flow and to gain an idea of the overall flow quality. The region surveyed extended from $x = 25$ to $x = 48$ cm from the nozzle throat, from $0 < y < 1.65$ cm above the plate, and from $1.65 \text{ cm} < z < +1.65 \text{ cm}$. The survey thus covered approximately half the plate length, half the span, and half the height from the plate surface to the tunnel ceiling.

Figure 13 shows several vertical traverses of pitot pressure at fixed $x (=48.8 \text{ cm})$ for $z = 0, \pm 0.76 \text{ cm}$, and $z = \pm 1.65 \text{ cm}$. It is seen that the profiles are (1) nearly identical, attesting to the two-dimensionality of the flow, (2) typically turbulent, and (3) show that the freestream is quite uniform, verifying the Schlieren records. Figure 14 shows continuous traverses taken again at fixed x and along the z axis for various values of y . Again, the two-dimensionality of the flow is apparent and it is noted that there are no shocks or other wavelets evident in the surveyed volume. This implies that there are no discontinuities, leaks, throat waves or other localized disturbance sources in the flow.

2.4 TEST MATRIX

The matrix of final test conditions is shown in Table II which lists the three streamwise stations and three wall temperatures for which data surveys were conducted and indicates the type of survey. In all cases the tunnel was operated at $P_o = .973 \times 10^5 \text{ N/M}^2$ (730 mmHg) and $T_o = 318^{\circ}\text{K}$ corresponding to nominal $M_{\infty} = 3$ and unit Reynolds number $= 6.57 \times 10^6/\text{meter}$. Mean flow measurements were made at all three x locations in order to document the streamwise progress of the turbulent flow.

SECTION 3

MEAN FLOW MEASUREMENTS

3.1 MEAN FLOW PROPERTIES

The mean flow profiles for the three axial stations and three wall temperatures indicated in Table 2 are presented in Table 3. The integral properties δ^* and θ , together with the static pressure (assumed constant across the boundary layer) and the edge values of mass and momentum flux (used later in shear stress calculations) are listed in Table 4. The pitot pressure variation in the freestream was found to be uniform (constant with y) or showed a small linear increase with increasing y . The boundary layer thickness δ , was defined as that point where the pitot pressure profile within the layer merged with the straight line representing the distribution of pitot pressure in the freestream. On this basis δ was found to range from 0.75 to 1.0 cm (depending on x and T_w). The corresponding Re_θ ranged from 3200 to 4400.

The velocity profiles for the three survey stations are plotted in Figures 15 to 17 for wall temperatures T_w/T_{oe} of .94, .71 and .54, respectively. In each case, the figure includes for comparison, the one-seventh power law profile commonly used to characterize turbulent boundary layers. The agreement between the data and the power law expression is close and indicates the utility of the latter as a simple approximation to the turbulent velocity profile. The data also indicate that the sublayer thickness is approximately $.05\delta$, corresponding to 0.04 to 0.05 cm, regardless of the test parameters. In addition, for each wall temperature condition the velocity profiles are apparently independent of x position, although in view of the relatively short interval between survey stations ($\Delta x/\delta \sim 5$) the agreement is not a conclusive test of self-similarity. However, results described later in this section confirm the maturity of the boundary layer flow and establish that self-similarity is indeed a reasonable assumption. Figure 18, which is a plot of u/u_e versus y/δ at the mid-survey station, $x = 38.79$ cm for each surface condition shows that the velocity profiles are independent of wall temperature as well as x station.

The total temperature profiles, T_o/T_{oe} versus y/δ , are plotted in Figures 19 to 21 for wall temperature ratios of .94, .71 and .54, respectively. Each figure includes data from the three survey stations and, similar to the velocity measurements, shows that the T_o profiles are independent of stream-wise station. The data shows clearly the T_o overshoot expected for non-unity Prandtl number flows and that the overshoot vanishes as the wall temperature is reduced. In addition, the T_o profiles show that the thickness of the thermal boundary layer coincides with the values of δ defined above on the basis of the pitot pressure. The T_o profiles, particularly for the adiabatic measurements, also confirm that the sublayer thickness is about $0.05 y/\delta$. The effect of wall temperature on the total temperature profile is demonstrated in Figure 22 where T_o/T_{oe} versus y/δ at the mid-survey station has been plotted for each wall condition. It is of interest to note, especially for the non-adiabatic cases, that approximately one-half the change

in T_0 occurs across the viscous sublayer.

3.2 \bar{T} VERSUS u/u_e PROFILES

While the velocity and total temperature profiles presented in Figures 15 to 22 indicate that the boundary layer is well behaved and characteristic of fully turbulent flow, a better insight to the turbulent structure is provided by plotting \bar{T} versus u/u_e . It has become common practice to compare experimental profiles to the linear Crocco relation $\bar{T} = u/u_e$. The Crocco relation, however, is restricted to unity Prandtl number, an assumption made to eliminate the turbulent shear stress terms from the energy equation. As a result, the simple Crocco expression cannot predict the total temperature overshoot in adiabatic, non-unity Prandtl number flows that has been observed in numerous experimental investigations and confirmed by the numerical analysis of Van Daele.¹

It has been further observed experimentally that the $\bar{T} - u/u_e$ profiles for boundary layers growing over aerodynamic models (flat plates, cones) differs from those on nozzle walls (see, for example, the data review in Reference 2 as well as the results of References 3 and 4.) The latter conform more closely to the Walz⁵ quadratic law $\bar{T} = (u/u_e)^2$ which is valid for $P_r < 1.0$ but is limited to zero heat transfer. However, the Walz relation also ignores the turbulent shear stress terms in the energy equation and, similar to the Crocco expression, is unable to account for the T_0 overshoot in the adiabatic case. The quadratic behavior has been attributed by several investigators^{6,7} to various effects associated with the upstream history of the nozzle expansion which tend to delay the attainment of an equilibrium boundary layer structure.

More recently, Meier, et al,⁸ and Whitfield and High⁹ have examined the $\bar{T} - u/u_e$ relationship for non-unity Prandtl number flows by including approximate models for the turbulent shear stress distribution across the boundary layer. The former present a numerical analysis, while the latter derive an analytic solution which is used here for comparison to the experimental data. For convenience, the solutions of Whitfield and High are repeated:

$$\bar{T} = \frac{T/T_\infty + \frac{\gamma-1}{2} M_\infty^2 (u/u_e)^2 - T_w/T_\infty}{1 + \frac{\gamma-1}{2} M_\infty^2 - T_w/T_\infty} \quad (3-1)$$

where, for the constant wall temperature (cold wall) case:

$$T/T_\infty = T_w/T_\infty + (1 + \frac{\gamma-1}{2} M_\infty^2 - T_w/T_\infty) u/u_e - \frac{\gamma-1}{2} M_\infty^2 (u/u_e)^2 \quad (3-2)$$

$$+ e \left\{ \frac{4\alpha (\gamma-1) M_\infty^2 (u/u_e)}{(\alpha+1) (\alpha+2)} (1 - (u/u_e)^{-\alpha+1}) \right. \\ - \frac{4(1 + \frac{\gamma-1}{2} M_\infty^2 - T_w/T_\infty) u/u_e}{\alpha + 1} (1 - (u/u_e))^{-2} \\ + \frac{\gamma-1}{2} M_\infty^2 (u/u_e) \left[1 - (u/u_e) \right] + \left[1 - (u/u_e) \right] f(o) \\ \left. + (u/u_e) f(1) - f(u) \right\}$$

and

$$\alpha = 17.5$$

$$e = 1 - \text{Pr}_m$$

$$\text{Pr}_m, \text{ the mixed Prandtl number} = c_p(\mu + \mu_t)/(k + k_t)$$

$$f(u/u_e) = \frac{\Delta}{(\gamma-1)M_\infty^2} \left[(\xi - \Delta) \ln|\xi - \Delta| - (\xi + \Delta) \ln|\xi + \Delta| \right]$$

$$\xi = 1 + \frac{\gamma-1}{2} M_\infty^2 - T_w/T_\infty - (\gamma-1)M_\infty^2(u/u_e)$$

$$\Delta = \left[2(\gamma-1)M_\infty^2 (T_w/T_\infty) + (1 + \frac{\gamma-1}{2} M_\infty^2 - T_w/T_\infty)^2 \right]^{\frac{1}{2}}$$

while for the adiabatic case:

$$T/T_{\infty} = 1 + \frac{\gamma-1}{2} M_{\infty}^2 \left[1 - (u/u_e)^2 \right] \quad (3-3)$$

$$+ \epsilon \left[\frac{4\alpha(\gamma-1)M_{\infty}^2}{(\alpha+1)(\alpha+2)} (1 - (u/u_e)^{-\alpha+2}) \right. \\ \left. + \frac{\gamma-1}{2} M_{\infty}^2 (1 - (u/u_e)^2) + f(1) - f(u/u_e) \right]$$

where $f(u/u_e)$ is the same as for the cold wall case but now:

$$\xi = - (\gamma-1) M_{\infty}^2 (u/u_e)$$

$$\Delta = 2(\gamma-1) M_{\infty}^2 \left(1 + \frac{\gamma-1}{2} M_{\infty}^2 \right)^{\frac{1}{2}}$$

To evaluate the above equations, it is necessary to know the mixed Prandtl number Pr_m . Whitfield and High examined the variation of Pr_m , based on measured recovery factors, as a function of Mach number and indicate that Pr_m is about 0.9 at $M_{\infty} = 3$. It was found that the results are insensitive to small variations in Pr_m and therefore a value of 0.88 was selected for the present calculations.

Equation 3-1 evaluated for the adiabatic case (i.e., with Equation 3-3) is shown in Figure 23 which includes the Crocco relation, the quadratic expression and the experimental results for the three survey stations. It is clear that the linear Crocco relation is a completely inadequate representation of the data which instead is in good accord with both the results of Whitfield and High and the trend of the quadratic law. More important the T_0 overshoot calculated from the theory confirms the experimental observations. The "kink" in the profile at $u/u_e = 0.6$ corresponds to the edge of the sublayer and is similar to the behavior observed by other investigators.^{3,4,10}

The results for the cold wall cases are shown in Figures 24 and 25 for $T_w/T_{oe} = 0.71$ and 0.54, respectively, where again both figures include the Crocco relation and the data for the three survey stations. It is immediately evident that with heat transfer, even at moderate rates, the $\bar{T} - u/u_e$ profile becomes nearly linear and that the Crocco relation is now an accurate approximation of the data. In fact, the theory of Whitfield and High indicates that the shift to a linear-like behavior occurs quickly as the wall temperature is

decreased below its adiabatic value.

The present results show that the \bar{T} versus u/u_e profiles in non-unity Prandtl number boundary layer flows can be accurately calculated provided the turbulent shear stresses are taken into account. While the Crocco relation appears to be valid for finite heat transfer rates, it is not an appropriate basis of comparison for the case of an adiabatic wall when $P_r < 1.0$. In view of the agreement between the data and the Whitfield and High theory, it is suggested that relaxation effects in nozzle wall boundary layers may be less important than previously considered.

3.3 SKIN FRICTION

It was originally intended to measure skin friction using a Preston tube and, provided that the sublayer could be probed in sufficient detail, from the slope of the experimentally determined velocity profile. However, the velocity profile approached, but did not attain, a linear variation near the wall, so that this method could provide only a lower bound to the skin friction coefficient. In addition, the Preston tube measurements indicated c_f values considerably higher than implied by the trend of the velocity data. (This is apparently a consequence of the large scatter inherent in existing Preston tube correlations.)

Consequently, the skin friction coefficient was calculated using two approaches. The first involved the correlation of Hopkins and Inouye¹¹ and the second is based on Coles Law-of-the-Wake correlation.¹² The results of the two procedures are in good agreement with each other and with the trend indicated by the velocity profiles and are therefore considered an accurate representation of the skin friction.

The correlation of Hopkins and Inouye, which is based on the Karman-Schönherr incompressible formula for c_f and utilizes the Van Driest velocity transformation, is expressed as:

$$\frac{1}{\bar{c}_f} = 17.08 (\text{Log}_{10} \bar{Re}_\theta)^2 + 25.11 \text{Log}_{10} \bar{Re}_\theta + 6.012 \quad (3-4)$$

where

$$\bar{c}_f = F_c c_f, \quad \bar{Re}_\theta = F_\theta Re_\theta \quad \text{and}$$

$$F_c = rm / (\sin^{-1} \alpha + \sin^{-1} \beta)^2$$

$$F_\theta = u_e / \mu_w$$

$$\alpha = (2A^2 - B) / (4A^2 + B^2)^{1/2}$$

$$\beta = B/(4A^2 + B^2)^{\frac{1}{2}}$$

$$A = (rm/F)^{\frac{1}{2}}$$

$$B = (1 + rm - F)/F$$

$$F = T_w/T_e$$

$$m = 0.2 M_e^2$$

$$r = 0.9$$

In the above expression, c_f and Re_θ are the compressible values of skin friction coefficient and Reynolds number based on momentum thickness and \bar{c}_f and \bar{Re}_θ are the equivalent or transformed incompressible values.

Coles Law-of-the-Wake can be expressed as

$$u^+ = u^*/u_\tau = 2.43 \ln(y^+) + 5 + 2.43 \tilde{\pi} w(y/\delta) \quad (3-5)$$

where $y^+ \equiv yu_\tau/\nu_w$, u_τ is the friction velocity $(\tau_w/\rho_w)^{\frac{1}{2}}$, $\tilde{\pi}$ is a parameter representing the strength of the wake component of the boundary layer, W is the Coles tabulated wake function which is approximated by $2 \sin^2(\pi y/2\delta)$ and u^* , the generalized velocity proposed by Van Driest¹³ to account for the effects of compressibility and heat transfer, is given by:

$$u^* = \frac{u_e}{K_1} \left\{ \sin^{-1} \left[\frac{2K_1^2(u/u_e) - K_2}{(K_2^2 + 4K_1^2)^{\frac{1}{2}}} \right] + \sin^{-1} \left[\frac{K_2}{(K_2^2 + 4K_1^2)^{\frac{1}{2}}} \right] \right\}$$

$$K_1^2 = m/F$$

$$K_2 = (1 + m)/F - 1$$

where m and F have been defined in Equation 3-4.

The quantities u_τ , δ and $\tilde{\pi}$ are treated as unknown constants and are determined by adjusting their values until the velocity data fits Equation 3-5 with a minimum rms error. Data for $y^+ < 50$ and $y > 0.9\delta$ are excluded from the curve fitting process since the former are in or near the viscous sublayer and the latter are influenced by small errors in the velocity measurements.

The transformed velocity profile for a typical case is shown in Figure 26. The data for $y^+ < 50$ which was omitted from the analysis is included in the plot for comparison with the theoretical sublayer and wall region profiles. The agreement between the universal correlation and the data is considered good. Once the parameters u_τ , δ and $\tilde{\pi}$ are determined the measured velocities can be used to calculate the variation of W through the boundary layer. A comparison of the calculated values of W and the approximation $2 \sin^2(\pi y/2\delta)$ is shown in Figure 27 where the agreement between the two completely justifies the use of the trigonometric function in the correlation procedure.

The skin friction coefficients calculated from the method of Hopkins and Inouye were consistently 10% greater than those deduced from the Law-of-the-Wake correlation. However, the latter also resulted in values of δ about 10% smaller than those defined from the pitot pressure profiles. This is due to the fact that the velocity approaches its freestream value slightly faster than the other properties (density, total temperature, etc.). Since the correlation described in Equation 3-5 relies only on the transformed velocity, the equivalent boundary layer thickness can be expected to be less than δ based on the experimental observations. In fact, the value of δ found in this manner can be considered as the velocity boundary layer thickness. Consequently, the Law-of-the-Wake correlation procedure was modified by specifying δ in Equation 3-5 as the known δ based on the pitot pressure profile, and the curve fit process carried out to determine only c_f and $\tilde{\pi}$. The skin friction coefficients found by the modified procedure were slightly larger than the results of the original method but still ranged from 2 to 10% less than the results of Hopkins and Inouye. A summary of the skin friction calculations is given in Table 5. It is noted that the values of $\tilde{\pi}$ range from .57 to .84 for the Law-of-the-Wake correlation, while those for the modified correlation vary from .42 to .72. In both cases $\tilde{\pi}$ is close to the value 0.6 which is typical of flat plate, zero pressure gradient boundary layers.

A plot of c_f versus Re_θ , using the results of the Hopkins and Inouye correlation and showing the influence of wall temperature, is shown in Figure 28. The computed skin friction coefficients were compared with the data by converting c_f to $(du/dy)_{wall}$ and plotting the corresponding linear u versus y relation. Typical results at the mid-survey station ($x = 38.79$ cm) for each wall temperature condition are shown in Figure 29 which includes also the experimental velocity profile. While the data is not sufficient to accurately determine $(du/dy)_{wall}$, the agreement between the trend indicated by the experimental velocity distribution and the results of Hopkins and Inouye is encouraging.

The simple Reynolds Analogy states that:

$$C_h \equiv q_w / \rho_e u_e c_p (T_w - T_{aw}) = c_f / 2 \quad (3-6)$$

since

$$q_w = -k_w dT/dy)_w$$

then

$$\frac{dT}{dy} \bigg|_w = - \frac{\rho_e u_e c_p (T_w - T_{aw})}{k_w} \frac{c_f}{2}$$

so that it was possible to convert the calculated skin friction coefficients c_f to $dT/dy|_w$ and then to compute the corresponding linear temperature-distance profile adjacent to the surface. The results for the three survey stations at a wall temperature of $.54 T_{oe}$ are shown in Figure 30, which includes the experimental profiles of T_o/T_{oe} and T/T_{oe} . Both sets of data have been plotted since the slopes $d(T_o/T_{oe})/d(y/\delta)$ and $d(T/T_{oe})/d(y/\delta)$ become identical at the surface where $u = 0$. The agreement between the linear profile and the data is again considered good and thus provides further confidence in the computed skin friction coefficients.

3.4 GRADIENTS OF VELOCITY AND TEMPERATURE

In a recent paper, Horstmann and Owen¹⁴ presented detailed data on the distribution of velocity and total temperature gradients across a turbulent boundary layer. While their measurements were obtained for $M_\infty = 7.2$ and $T_w/T_{oe} = 0.46$, it is instructive to compare the results of Horstmann and Owen with those of the present investigation. Similar to Reference 14 a simple two-point differencing scheme was used to convert the velocity and temperature profile data to gradients in these quantities. The non-dimensional gradients $d(u/u_e)/d(y/\delta)$ and $d(T_o/T_{oe})/d(y/\delta)$ for the adiabatic case and $x = 35.05$ cm are plotted versus (y/δ) in Figures 31 and 32, respectively, which include also the results of Horstmann and Owen. Also shown in Figure 31 is the velocity gradient at the wall computed from c_f . The velocity gradients are seen to be quite similar in spite of the difference in the heat transfer rates in the two experiments. However, this difference obviously accounts for the smaller total temperature gradients observed in the present test. The T_o gradient in the vicinity of the wall is replotted to an expanded y scale in Figure 33 where it is seen that the scatter in the data is quite small and that the y variation in the gradient can be accurately represented by the dashed line drawn through the data points. This curve is redrawn in Figure 34 where the total temperature gradient at the $x = 42.52$ cm station for the adiabatic case has been plotted. The trend of the data at the downstream station is in excellent agreement with the results of the upstream survey, thereby confirming the similarity in the total temperature profiles.

The gradients $d(u/u_e)/d(y/\delta)$ and $d(T_o/T_{oe})/d(y/\delta)$ for the cold wall case $T_w/T_{oe} = 0.54$ are plotted against y/δ in Figures 35 and 36, respectively. These figures include the gradients at the wall, $y = 0$, evaluated from c_f , and the results of Horstmann and Owen. Outside the sublayer, the distributions of $d(u/u_e)/d(y/\delta)$ across the boundary layer are in good agreement for the two experiments, demonstrating again the relative insensitivity of the velocity profile to the freestream conditions. (The gradients near the wall will differ,

of course, due to differences in the skin friction.) Since the wall temperature ratio T_w/T_{oe} of the present test is similar to that of Reference 14, the distributions of the gradients $d(T_o/T_{oe})/d(y/\delta)$ are also in good agreement.

The gradients of velocity and total temperature are plotted to an expanded y/δ scale in Figures 37 and 38. These figures illustrate clearly that the trend of the experimental data, indicated by the dashed lines faired through the data points, is in good agreement with the wall gradients determined from the calculated skin friction coefficients. Similar findings were observed for all the test conditions of the present experiment, reinforcing the early conclusion, based on Figure 29, that the results of the Hopkins and Inouye¹¹ and the Coles Law-of-the-Wake¹² correlations provide an accurate representation of the skin friction.

3.5 INTEGRAL PROPERTIES

The values of the boundary layer thickness δ , the displacement thickness δ^* and the momentum thickness θ listed in Table 4 are plotted against wall temperature ratio T_w/T_{oe} in Figure 39. As expected, the momentum thickness θ increases with decreasing temperature (about 5 to 10% for a 50% reduction in T_w) while δ^* diminishes (about 20%). The corresponding values of Reynolds number based on momentum thickness Re_θ are plotted as a function of x station for each wall temperature condition in Figure 40. Since the freestream unit Reynolds number was essentially constant for all test conditions, the variations in Re_θ reflects the change in θ .

The incompressible shape factor is defined as:

$$H_u = \frac{\int_0^\delta (1 - \frac{u}{u_e}) dy}{\int_0^\delta \frac{u}{u_e} (1 - \frac{u}{u_e}) dy} \quad (3-7)$$

which, for the incompressible case, reduces to δ^*/θ . A plot of this parameter versus Re_θ is shown in Figure 41 where it is compared to the results of previous investigations of supersonic boundary layers with zero and favorable pressure gradient.⁴ The present data show relatively little effect due to wall temperature, reflecting the fact that the velocity profiles are essentially independent of T_w . Interestingly enough, while the present data correspond to a slightly adverse pressure gradient $\beta = +0.04$, they are in better agreement with the trend of the favorable pressure gradient results of Reference 4 ($\beta = -0.1$ to -0.2) than the zero pressure gradient results of Reference 3.

3.6 CALCULATION OF TURBULENT SHEAR STRESS

Under suitable assumptions, the turbulent shear stress can be extracted from experimental mean flow data. For a two-dimensional compressible flow, contributions from the flow fluctuations yield the following expression for the turbulent shear stress:

$$\frac{\partial}{\partial y} (\rho \overline{u'v'} + u \overline{\rho'v'} + v \overline{\rho'u'} + \rho \overline{u'v'})$$

The second term can be masked by reformulating the governing boundary layer equations in "mass-averaged" coordinates, so that the above shear expression reduces to:

$$\frac{\partial}{\partial y} (\rho \overline{u'v'} + v \overline{\rho'u'} + \rho \overline{u'v'}) = \frac{\partial}{\partial y} (\overline{\rho v}) \overline{u'}$$

If, in addition, the last two terms on the left hand side are assumed to be negligible, the expression for the turbulent shear stress reduces to its incompressible form $\partial(\rho u'v')/\partial y$. However, for complete generality, the compressible formulation will be retained.

The time-averaged conservation equations for the two-dimensional flat plate boundary layer are:

Continuity:

$$\partial(\rho u)/\partial x + \partial(\rho \tilde{v})/\partial y = 0 \quad (3-8)$$

Momentum:

$$\partial(\rho u^2)/\partial x + \partial(\rho u \tilde{v})/\partial y = -dp/dx + \partial\tau/\partial y \quad (3-9)$$

where $\tilde{v} = v + \overline{\rho'v'}/\rho$ and the total shear stress τ is the sum of a laminar and a turbulent term:

$$\begin{aligned} \tau &= \tau_L + \tau_T \\ &= \mu \partial u / \partial y - (\overline{\rho v})'u' \end{aligned}$$

In preceding paragraphs, the present data were shown to be representative of a fully developed turbulent boundary layer and evidence was presented which indicates that the mean flow profiles are self-similar, i.e. that u/u_e , ρ/ρ_e , etc., are functions of only y/δ . This allows then $\partial f/\partial x$ to be replaced with $(f/f_e)df_e/dx$ for constant y/δ , where $f = \rho u$ or ρu^2 . Integrating Equation (3-8) with respect to y yields an expression for $\rho \tilde{v}$ which can be substituted

into Equation (3-9). The latter can then be integrated with respect to y/δ yielding the following expression for the total shear:¹⁴

$$\begin{aligned} \frac{\tau}{\rho_e u_e^2} = \frac{c_f}{2} + \left[\frac{\delta}{\rho_e u_e^2} \frac{d}{dx} (\rho_e u_e^2) + \frac{d\delta}{dx} \right] & \left[\int_0^{y/\delta} \frac{\rho}{\rho_e} \left(\frac{u}{u_e} \right)^2 d \left(\frac{y}{\delta} \right) \right] \\ & - \left[\frac{\delta}{\rho_e u_e} \frac{d}{dx} (\rho_e u_e) + \frac{d\delta}{dx} \right] \frac{u}{u_e} \left[\int_0^{y/\delta} \frac{\rho}{\rho_e} \frac{u}{u_e} d \left(\frac{y}{\delta} \right) \right] \\ & + \frac{\delta}{\rho_e u_e^2} \frac{y}{\delta} \frac{dp}{dx} \end{aligned} \quad (3-10)$$

where it has been assumed that the static pressure is constant across the boundary layer.

Evaluation of $\tau/\rho_e u_e^2$ using Equation 3-10 was restricted to the midsurvey station ($x = 38.79$ cm) for each wall temperature condition. The x derivatives of $\rho_e u_e$ and $\rho_e u_e^2$ were found by applying a simple two-point differencing scheme to the edge properties listed in Table 4, yielding average values between the first and second stations and the second and third stations. These values were then further averaged to determine the derivatives at the midsurvey station.

Since the boundary layer thickness δ was determined from inspection of the measured pitot pressure profile, its value was influenced by the density of data points near the edge of the layer and by small errors in the pressure measurements. Therefore, δ lacks the precision of the integral properties, which depend on the variation of velocity and density within the boundary layer and are insensitive to the location of the edge of the layer. The uncertainties in δ are further accentuated in determining $d\delta/dx$ since the increase in the boundary layer thickness is relatively small over the limited interstation intervals of the present tests. Consequently, it was assumed that δ could be related to the momentum thickness θ through a simple form factor k so that $\delta = k\theta$ and $d\delta/dx = kd\theta/dx$. The value of k was the average value for the three survey stations.

The streamwise derivatives used in Equation 3-10 are listed in Table 6 where it is seen that the $d\delta/dx$ term is 4-5 times greater than the $\rho_e u_e$ and $\rho_e u_e^2$

derivatives and as much as 30 times greater than the dp/dx term. Nevertheless, as shown later, the dp/dx term cannot be ignored since it balances the contributions from the $\rho_e u_e$ and $\rho_e u_e^2$ derivatives which are of opposite sign. It is further shown that the $d\delta/dx$ contribution is dominant since the shear stress evaluated ignoring all derivations except $d\delta/dx$ is similar to the result obtained with all terms included.

The calculated shear stress distributions for $T_w/T_{oe} = .94, .71$ and $.54$ are shown in Figures 42-44, respectively. In each case, it is seen that the shear stress does not completely vanish at $y/\delta = 1.0$, probably reflecting errors in evaluating the streamwise derivatives. However, the discrepancy is not large, with the maximum residue occurring for the adiabatic case where it is negative in sign and only about 15% of the wall shear. The results, overall, are considered quite satisfactory.

Figure 43 shows the effect of neglecting all derivatives except $d\delta/dx$. The resulting shear stress distribution is everywhere within 10% of the results of the complete solution showing the significance of the $d\delta/dx$ contribution. Also indicated is the magnitude of the dp/dx contribution, illustrating the necessity of including the small but finite static pressure gradient observed in the mean flow measurements in order to achieve a complete momentum balance.

A final plot of the turbulent shear stress, normalized now by the wall shear, is shown as a function of y/δ in Figure 45. The results for each wall temperature are presented and included also is the "best estimate" suggested by Sanborn¹⁵ based on his review of both hot wire measurements and mean flow calculations for Mach numbers ranging from 0 to 6.8. The present results are seen to be in good agreement with Sanborn's distribution and furthermore indicate that the shear stresses are insensitive to wall temperature. The latter finding is not surprising since it has already been shown that to first approximation the $d\rho_e u_e/dx$, $d\rho_e u_e^2/dx$, and $d\rho_e/dx$ terms can be omitted and the shear stress given by

$$\frac{\tau}{\rho_e u_e^2} = \frac{c_f}{2} + \left\{ \int_0^{y/\delta} \frac{\rho}{\rho_e} \left(\frac{u}{u_e} \right)^2 d \left(\frac{y}{\delta} \right) + \frac{u}{u_e} \int_0^{y/\delta} \frac{\rho}{\rho_e} \frac{u}{u_e} d \left(\frac{y}{\delta} \right) \right\} \frac{d\delta}{dx} \quad (3-11)$$

It has already been demonstrated that u/u_e is essentially independent of T_w/T_{oe} and c_f varies by about 10% over the range $T_w/T_{oe} = 0.94$ to 0.54 . The density ratio ρ/ρ_e , plotted versus y/δ in Figure 46, is also seen to be largely insensitive to T_w/T_{oe} except for the region near the wall, $y/\delta < 0.2$ where the integral terms are small compared to $c_f/2$. Thus, according to

Equation 3-11, the shear stress distribution can be expected to be weakly dependent on wall temperature.

With the turbulent shear stress distribution determined from the mean flow profiles, it is possible to calculate the mixing length ℓ , and the eddy viscosity ϵ . These quantities are defined as:

$$\tau_t = \rho \ell^2 \left| \frac{\partial u}{\partial y} \right| \frac{\partial u}{\partial y} = \rho \epsilon \frac{\partial u}{\partial y} \quad (3-12)$$

from which the normalized mixing length can be expressed as:

$$\frac{\ell}{\delta} = \left\{ \frac{(\tau_t / \rho_e u_e^2)}{(\rho / \rho_e) [\partial(u/u_e) / \partial(y/\delta)]^2} \right\}^{1/2} \quad (3-13)$$

The mixing length distribution is plotted in Figure 47 where it is compared to the results of Horstman and Owen¹⁴, obtained at $M_\infty = 7.2$ and Re_θ from ranging 4900 to 9700, and to those of Yanta and Lee¹⁶ acquired at $M_\infty = 2.9$ and Re_θ from 10,000 to 14,000. Included in the figure is the mixing length calculated by Maise and McDonald¹⁷ on the basis of a correlation of earlier two-dimensional, adiabatic supersonic flow measurements. They found that for M_∞ up to 5 and Re_θ from 10^3 to 10^5 , the Mach number and Reynolds number effects are quite small and generally within the experimental uncertainty of ℓ/δ , so that for this range of conditions the mixing distribution could be represented by the incompressible variation of ℓ/δ versus y/δ . As seen, the present results compare favorably with the Maise and McDonald¹⁷ model throughout the entire boundary layer, although they indicate slightly lower values for $y/\delta > 0.5$. The present data also show a slight separation due to T_w/T_{oe} and surprisingly, while the separation is small, it suggests that ℓ/δ increases as T_w/T_{oe} decreases. It is of interest to note that the results of Horstman and Owen¹⁴ and Yanta and Lee¹⁶ are in agreement with the present findings and the correlation of Maise and McDonald only near the wall ($y/\delta < 0.2$). For larger y/δ , the results of references 14 and 16 are 20 to 30% less than the value indicated by the correlation.

Solving Equation 3-12 for ϵ yields:

$$\frac{\epsilon}{u_e \delta_i^*} = \frac{\tau_t / \rho_e u_e^2}{(\rho / \rho_e) (\partial(u/u_e) / \partial(y/\delta)) (\delta_i^* / \delta)} \quad (3-14)$$

where it has been shown by Maise and McDonald¹⁷ that when ϵ is normalized by the kinematic boundary layer thickness δ_i^* , its distribution across the boundary layer is sensitive to Mach number and to Re_θ . The present calculations

of eddy viscosity are plotted in Figure 48 where they are compared to those of Horstman and Owen¹⁴ and Yanta and Lee¹⁶ and to the Maise and McDonald¹⁷ model. It is seen that for $y/\delta > 0.2$ the present results are significantly larger than both those of References 14 and 18. However, they are in reasonable agreement with the predictions of Maise and McDonald although yielding slightly larger values for $y/\delta < 0.3$ and slightly smaller values of normalized eddy viscosity for $y/\delta > 0.3$. In particular, the peak value of $\epsilon/u_e \delta^+_{*1} = 0.02$ at $y/\delta \sim 0.3$ calculated in the present case is in agreement with the maximum value deduced from the Maise and McDonald model. Again, the trend of the present data suggests a slight wall temperature effect with $\epsilon/u_e \delta^+_{*1}$ increasing as T_w/T_{oe} is reduced.

In closing, it should be mentioned that in a recent paper, Lee and Smith¹⁸ presented the results of a study at Mach 5 of the effect of wall temperature on shear stress, mixing length and eddy viscosity, with the transport properties calculated using the "inverse" procedure described above. Their measurements, also obtained on the nozzle wall, led to shear stress values, however, which were considerably less than those expected from Sanborn's "best estimate",¹⁵ with the discrepancy attributed by the authors to the influence of upstream heat transfer. A similar decrease was observed in their results for mixing length and eddy viscosity. Although the present study was carried out in a wind tunnel channel similar to that used in Reference 18, no such effect of upstream cooling was detected.

A study of wall cooling effects on hypersonic boundary layers (Mach 11) has been reported by Watson.¹⁹ While his findings were in general agreement with those presented here, the influence of cooling was somewhat obscured by the larger effects associated with the low Re^+ conditions of his experiments. In an earlier paper, Bushnell, et al²⁰ examined the effect of Re^+ on the outer region (i.e., $y/\delta = 0.5$) mixing length. They demonstrated that in the low Reynolds number regime, the $(\ell/\delta)_m$ for flat plates increases significantly with decreasing Re^+ , while for nozzle walls $(\ell/\delta)_m$ decreases slightly as Re^+ decreases. They attributed the difference in behavior to the fact that flat plate measurements are generally made near the end of the transition zone and are therefore, influenced by the transitional flow structure, while for nozzle walls, the measurement station is usually far downstream from transition where the transitional structure has vanished. While Bushnell, et al²⁰ conservatively selected $Re^+ = 2000$ as the lower bound for fully developed flow, both their data and Watson's²¹ recent assessment of Pletcher's²² low Re^+ mixing length model indicates that fully developed flow persists for Re^+ as low as 500. Although the minimum Re^+ in the present experiments was 350, the agreement shown with the high Reynolds number data of other investigators indicates that low Re^+ effects are absent. The results, therefore, are considered representative of a fully developed flow and provide systematic evidence of the influence of wall temperature on the detailed structure of turbulent compressible boundary layers.

SECTION 4

SUMMARY AND CONCLUSIONS

On the basis of the preceding discussion, the results of the mean flow measurements can be summarized as follows:

1. For each wall temperature condition, the boundary layer appears to be well behaved, two-dimensional, and fully equilibrated. The normalized velocity and total temperature profiles are independent of stream wise location implying a self-similar boundary layer flow. The nominal boundary thickness was one centimeter, while the thickness of the sublayer was 0.04 to 0.05 cm. Since valid flow measurements extended to within 0.01 cm of the surface, this marks one of the few instances where the sublayer flow has been documented.

2. Within the extent of the measurements, no evidence of a linear velocity profile near the wall was observed even for the adiabatic case. Therefore, the surface shear stress was calculated using the empirical correlation of Hopkins and Inouye and by curve fit of the velocity profile to the Coles incompressible "Law-of-the-Wake." For all test conditions, the results of the two procedures agreed within 5-10% and were in good agreement with the trend of the experimental data. The "Law-of-the-Wake" curve fit also indicated a wake parameter of approximately 0.6 which is characteristic of zero pressure gradient, flat plate boundary layers. Using the computed skin friction coefficients and the simple Reynolds Analogy, the temperature gradient at the surface was calculated and, for the low wall temperature case in particular, conformed closely to the measured temperature profile. These calculations further substantiate that the boundary layer flow was fully equilibrated and self-similar.

3. The experimental profiles of total temperature versus velocity were also found to be in good agreement with predictions based on the theory of Whitfield and High for the case of non-unity Prandtl number. For the adiabatic wall condition, the results exhibited the expected temperature overshoot near the outer edge of the boundary layer and a quadratic-like behavior within, the boundary layer. This differs considerably from the linear Crocco relation, which arises from assuming a unity Prandtl number and therefore cannot account for a total temperature "overshoot". The results further indicate that with increasing heat transfer, the total-temperature-velocity profile quickly approaches a linear-like relationship independent of the Prandtl number. Consequently, the present results demonstrate clearly that, for near adiabatic walls, the Crocco relation does not provide a valid test of the boundary layer flow for practical cases where the Prandtl number departs from unity.

There are a number of boundary layer transformations and correlations which utilize the linear Crocco relation in their derivation. In view of the above finding, the validity of these correlations may be questioned. It should be pointed out, however, that in the adiabatic case, the Crocco parameter \bar{T} is extremely sensitive to uncertainties in the total temperature. In the present instance, for example, where $T_{0e} - T_w$ is only 5 to 10% of T_{0e} , using the extremes of a constant T_0 on the one hand and a linear T_0 variation on the other, produces

a difference of only a few percent in the corresponding profiles of velocity and density. Hence the mathematical simplification afforded by the Crocco relation justifies its use in approximating the T_0 - u variation. The point to be emphasized is that the Crocco relation, cast in its usual form T versus u/u_e , cannot be used to judge the quality of the boundary layer flow.

4. Finally, the distribution of turbulent shear stresses at each wall temperature condition was determined by means of the "indirect" method of integrating the "time averaged" conservation equations across the boundary layer using the experimental mean flow profile data. The results, normalized, by the wall stress, were found to be only slightly dependent on wall temperature over the range investigated, and were in accord with similar calculations by other investigators. Further clarification of this point awaits the actual fluctuation measurements. In addition, values of mixing length and eddy viscosity deduced from the computed turbulent stresses are in excellent agreement with the correlation derived by Maise and McDonald for freestream Mach numbers ranging from 0 to 5.

TABLE 1
LOCATION OF PRESSURE TAPS (P) AND
THERMOCOUPLES (TC) ON PLATE SURFACE

<u>SENSOR</u>	<u>X (CM)</u>	<u>Z (CM)</u>
P1	8.9	- 2.03
P2	8.9	0
P3	8.9	2.03
P4	20.3	- 2.03
P5	20.3	2.03
P6	34.3	- 2.03
P7	34.3	2.03
P8	45.7	- 2.03
P9	45.7	2.03
TC1	11.4	-2.03
TC2	11.4	0
TC3	11.4	2.03
TC4	17.8	0
TC5	20.3	-0.25
TC6	27.9	-2.03
TC7	27.9	0.38
TC8	27.9	2.03
TC9	40.6	-2.03
TC10	40.6	-0.38
TC11	40.6	0.38
TC12	40.6	2.03
TC13	54.6	-2.03
TC14	54.6	2.03

TABLE 2
MATRIX OF TEST CONDITIONS

$$P_o = .973 \times 10^5 \text{ N/M}^2$$

$$T_o = 318^\circ\text{K}$$

$$M_\infty = 3 \text{ (nominal)}$$

$$Re_\infty = 6.57 \times 10^6/\text{meter (nominal)}$$

X (cm)	T_w/T_{oe}		
	.94	.714	.54
35.05	$P_t, T_t(111)$	$P_t, T_t(112)$	$P_t, T_t(113)$
38.79	$P_t, T_t(121)$	$P_t, T_t(122)$	$P_t, T_t(123)$
42.52	$P_t, T_t(131)$	$P_t, T_t(132)$	$P_t, T_t(133)$

P_t - pitot pressure survey

T_t - total temperature survey

Number in parenthesis denotes run number

Table 3
Summary of Mean Flow Profiles

MEAN FLOW PROFILES, RUN NO 111

P0,N/M2= 97309
T0, DEG K= 318.8889
TW, DEG K= 298.3333
X, CM= 35.052
RHOE, KG/M3= .0778892
UE, M/SEC= 644.666
RHOUE2, N/M2= 32287.14
RHOUE, KG/M2SEC= 50.18182
RE, M-1= 6454139

Y (CM)	Y/D T/TE	M T0/TDE	U/UE RE/REE	RHO/RHOE H
.00508	.0060096 2.579528	.4144576 .9367443	.218966 .0367728	.3876679 .0186813
.007112	.0084135 2.561507	.4592525 .9372396	.241783 .0411138	.3903951 .0263655
.01016	.0120192 2.541056	.5068813 .9379668	.2657907 .0458454	.3935372 .0376467
.013208	.015625 2.512237	.5693154 .9391817	.2968313 .0522502	.3980516 .0564953
.016256	.0192308 2.454325	.6828507 .9420319	.3518992 .064576	.4074439 .1007119
.018288	.0216346 2.414799	.7530869 .9439615	.3849568 .0727238	.4141132 .1306453
.022352	.0264423 2.343853	.8695768 .9473373	.4379248 .0872748	.426648 .1830168
.024384	.0288462 2.287984	.9560002 .9501033	.4756756 .099003	.437066 .2259266
.026416	.03125 2.241226	1.025493 .9523567	.5050121 .1090971	.4461843 .2608855
.029464	.0348558 2.199977	1.085376 .9543557	.5295609 .1183073	.4545501 .2918967
.032512	.0384615 2.161207	1.140573 .9561821	.5515664 .1272575	.4627045 .3202304

Table 3 (continued) Run 111

.03556	.0420673 2.133292	1.179592 .9573926	.5667393 .1338802	.468759 .3390093
.037592	.0444712 2.109367	1.21286 .9584441	.5794464 .1397171	.4740759 .3553215
.04064	.0480769 2.080284	1.252842 .9596298	.5944074 .1469929	.4807036 .3737166
.042672	.0504808 2.059123	1.281805 .9604821	.6050475 .1524392	.4856437 .3869381
.046736	.0552885 2.031311	1.319222 .9613904	.6184895 .1597428	.4922929 .4010298
.048768	.0576923 2.017471	1.337463 .9617051	.6249019 .1634286	.4956701 .4059122
.053848	.0637019 1.983738	1.381844 .962436	.6402178 .1726825	.5040987 .4172497
.059944	.0709135 1.957029	1.41621 .9626908	.6517072 .1802061	.5109787 .4212028
.064008	.0757212 1.943698	1.433046 .9626804	.6572051 .1840212	.5144831 .4210424
.069088	.0817308 1.922009	1.461174 .9629248	.6663556 .190472	.5202889 .4248336
.075184	.0889423 1.897769	1.492648 .9631693	.6764031 .1979145	.5269346 .428626
.080264	.0949519 1.879474	1.516603 .9633973	.6839377 .2037246	.5320638 .4321642
.087376	.1033654 1.863612	1.537025 .9634268	.6902161 .2088357	.5365925 .4326215
.090424	.1069712 1.853242	1.550986 .9636765	.6945452 .2123223	.5395948 .4364944
.095504	.1129808 1.83961	1.569384 .9640035	.7001944 .2169905	.5435934 .4415677
.100584	.1189904 1.828505	1.584533 .9643184	.7048161 .2208832	.5468948 .4464524
.114808	.1358173 1.79709	1.629033 .9657958	.7183586 .2324726	.5564551 .4693723
.127	.1502404 1.772703	1.665448 .9676223	.7294161 .2421142	.5641103 .4977075

Table 3 (continued) Run 111

.141224	.1670673 1.752571	1.700322 .9710779	.7404494 .251051	.5705903 .5513174
.153416	.1814904 1.727301	1.734749 .9714194	.7499756 .2612515	.5789379 .5566151
.166624	.1971154 1.700546	1.768438 .9704647	.7585958 .2720634	.5880465 .5418033
.178816	.2115385 1.680122	1.796202 .970485	.7658646 .2809428	.5951947 .542119
.206248	.2439904 1.635016	1.864278 .9730386	.7841479 .3026949	.6116149 .5817341
.232664	.2752404 1.592562	1.930994 .9760884	.8015961 .325116	.6279189 .6290471
.260096	.3076923 1.552443	1.995359 .9790472	.8178154 .3480439	.6441462 .674949
.287528	.3401442 1.511435	2.062177 .9819589	.8339637 .3733549	.6616228 .7201198
.313944	.3713942 1.476946	2.121628 .9853469	.8481604 .3967156	.6770728 .7726785
.34036	.4026442 1.433486	2.193358 .9875064	.8638388 .4276958	.6976003 .8061808
.366776	.4338942 1.399626	2.254481 .9908988	.8773623 .4546928	.7144768 .8588088
.379984	.4495192 1.38597	2.27929 .9921771	.8826792 .4661175	.7215163 .878639
.393192	.4651442 1.360685	2.324081 .9937766	.8917777 .4878521	.7349238 .9034535
.4064	.4807692 1.348186	2.347155 .9948511	.8964853 .4992023	.7417375 .9201229
.417576	.4939904 1.331341	2.377903 .9960026	.9025375 .5148804	.7511223 .937987
.432816	.5120192 1.313519	2.41118 .9973679	.9090217 .5322273	.7613139 .9591675
.446024	.5276442 1.295145	2.445929 .9987656	.91565 .5508906	.7721144 .9808496
.459232	.5432692 1.277024	2.479256 .9995094	.9216103 .5697971	.7830709 .9923892

Table 3 (continued) Run 111

.471424	.5576923 1.257962	2.514953 1.000338	.9278765 .5906364	.7949364 1.00524
.485648	.5745192 1.248701	2.53539 1.002022	.9319666 .6018089	.8008325 1.031376
.498856	.5901442 1.225574	2.580699 1.003412	.9397956 .6293235	.8159444 1.052935
.512064	.6057692 1.21425	2.602642 1.003838	.9433976 .6432592	.8235539 1.059545
.526288	.6225962 1.20014	2.630312 1.004376	.9478722 .6612089	.8332358 1.067893
.540512	.6394231 1.186052	2.658274 1.004901	.9523093 .6798008	.8431331 1.076039
.552704	.6538461 1.169955	2.690658 1.005493	.9573472 .7019098	.8547336 1.085214
.566928	.6706731 1.160092	2.710966 1.005952	.9604984 .715996	.8620007 1.092334
.580136	.6862981 1.143373	2.744737 1.006246	.9654306 .740461	.8746055 1.096899
.592328	.7007212 1.128516	2.77465 1.006254	.9695907 .7630116	.8861195 1.097019
.606552	.7175481 1.120023	2.790765 1.005734	.9715455 .7759988	.8928387 1.088961
.61976	.7331731 1.105986	2.821067 1.006336	.9759209 .7991049	.9041707 1.098287
.631952	.7475962 1.095012	2.846095 1.007256	.9796824 .8181228	.9132318 1.11257
.646176	.7644231 1.081304	2.875559 1.007446	.9836091 .8421037	.9248095 1.115517
.659384	.7800481 1.072303	2.893487 1.006848	.9856136 .8578901	.9325723 1.10623
.671576	.7944712 1.061791	2.914539 1.006094	.9879066 .8768286	.9418047 1.094533
.684784	.8100962 1.05463	2.930635 1.006275	.9900071 .8905621	.9481997 1.097354
.699008	.8269231 1.046521	2.948245 1.006146	.9921195 .9062377	.9555466 1.09534

Table 3, (continued) Run 111

.7112	.8413462 1.038911	2.963373 1.005353	.9935778 .9208237	.9625464 1.083042
.724408	.8569711 1.033267	2.973682 1.004331	.9943222 .9315479	.9678044 1.067196
.737616	.8725961 1.026489	2.987112 1.003514	.9955316 .9449731	.9741948 1.054507
.75184	.8894231 1.018632	3.004409 1.003245	.9974567 .9613979	.9817088 1.050339
.765048	.9050481 1.014402	3.01224 1.002435	.9979781 .96991	.9858024 1.037774
.77724	.9194712 1.010754	3.018491 1.001506	.9982494 .9771672	.9893603 1.023357
.79248	.9375 1.008075	3.021612 1.000186	.9979566 .9820646	.9919892 1.002884
.805688	.953125 1.005309	3.026288 .9994371	.9981284 .9876345	.9947192 .9912678
.818896	.96875 1.001295	3.034843 .999092	.9989497 .9963724	.9987071 .9859145
.83312	.9855769 .9962531	3.047247 .9993389	1.000504 1.008034	1.003761 .9897438
.845312	1 .9984722	3.041051 .9989202	.9995812 1.002638	1.00153 .9832483
.85852	1.015625 .9966437	3.04415 .9984108	.9996834 1.006418	1.003368 .9753463
.872744	1.032452 .9973647	3.041051 .9978122	.9990267 1.004306	1.002642 .9660593
.885952	1.048077 .9951177	3.044925 .9972115	.9991718 1.008988	1.004906 .9567407
.900176	1.064904 .9930177	3.048794 .9967511	.9993853 1.013473	1.007031 .9495982
.912368	1.079327 .9929105	3.048794 .9966435	.9993314 1.013637	1.00714 .947929
.925576	1.094952 .9928081	3.05034 .9971982	.9997867 1.014308	1.007244 .9565349

Table 3 (Continued) Run 111

.940816	1.112981 .9938626	3.048794 .9975992	.9998104 1.012182	1.006175 .9627554
.954024	1.128606 .9890929	3.05729 .9964146	1.000188 1.022348	1.011027 .9443784
.966216	1.143029 .9899626	3.054203 .9959792	.9996172 1.019971	1.010139 .9376241
.979424	1.158654 .9896472	3.054975 .9959897	.9997106 1.020717	1.010461 .9377862
.992632	1.174279 .9914049	3.05034 .9957889	.99908 1.01646	1.00867 .9346713
1.003808	1.1875 .9890841	3.056519 .9960782	.9999311 1.022104	1.011036 .9391587
1.020064	1.206731 .9892318	3.057827 .9967827	1.000434 1.022313	1.010885 .9500887
1.032256	1.221154 .9894242	3.05729 .9967484	1.000355 1.021835	1.010689 .9495557
1.03632	1.225962 .9895332	3.05706 .9967602	1.000335 1.021589	1.010578 .94974

DELSTAR,CM=	.2742376
THETA,CM=	.0507142
RE THETA=	3273.162

Table 3 (continued) Run 112

MEAN FLOW PROFILES, RUN NO 112

P0,N/M2= 97309
 T0, DEG K= 318.8889
 TW, DEG K= 227.7778
 X, CM= 35.052
 RHDE, KG/M3= .0794545
 UE, M/SEC= 643.2428
 RHDEUE2, N/M2= 32790.7
 RHDEUE, KG/M2SEC= 51.07723
 RE, M-1= 6516402

Y (CM)	Y/D T/TE	M T0/TOE	U/UE RE/REE	RHO/RHDE H
.00508	.0061881 2.104702	.4873122 .7803326	.2340194 .0567365	.4751265 .2311641
.009144	.0111386 2.152001	.5884648 .8144461	.2857532 .0665399	.4646837 .3505614
.01016	.0123762 2.141966	.6501583 .8222346	.3149739 .0739685	.4668609 .3778213
.012192	.0148515 2.131677	.7093012 .8304179	.3427999 .0812094	.4691142 .4064626
.0131064	.0159653 2.118542	.7493579 .8340636	.3610415 .086496	.4720227 .4192228
.0145288	.017698 2.110371	.7824422 .8384177	.3762539 .0907755	.4738503 .434462
.0159512	.0194307 2.100599	.8097158 .8409923	.3884664 .0945159	.4760548 .4434732
.0170688	.0207921 2.089819	.8356109 .8429795	.3998597 .0982025	.4785104 .4504283
.018288	.0222772 2.065356	.8871044 .8460815	.4220088 .1058877	.484178 .4612854
.0194056	.0236386 2.042418	.934017 .8490369	.4418515 .1131468	.4896158 .471629
.0210312	.0256188 2.00624	1.00589 .853799	.4716187 .1247758	.4984449 .4882965
.0231648	.0282178 1.980775	1.059629 .8585261	.4936519 .1336932	.5048528 .5048415
.0239776	.0292079 1.958577	1.09943 .8608192	.509316 .1408132	.5105747 .5128671
.0247904	.030198 1.948054	1.119647 .8623806	.517286 .1444367	.5133327 .5183321

Table 3 (continued) Run 112

.0262128	.0319307 1.91964	1.169062 .8651705	.5361627 .1538017	.5209311 .5280967
.0281432	.0342822 1.907184	1.193732 .8674266	.5456982 .1584218	.5243333 .535993
.0298704	.0363861 1.890183	1.225608 .8700132	.557767 .1646158	.5290492 .5450462
.0312928	.0381188 1.875058	1.252646 .8719454	.5677864 .1700715	.5333167 .5518091
.034544	.0420792 1.852641	1.293717 .8752364	.5828867 .1785112	.53977 .5633275
.0362712	.0441832 1.829278	1.331497 .8770425	.5961141 .1868926	.5466638 .5696488
.0398272	.0485149 1.812224	1.361179 .8791193	.6065556 .1934897	.5518081 .5769177
.0419608	.0511139 1.79292	1.393493 .8810522	.6176387 .2009722	.5577495 .5836826
.0433832	.0528465 1.788695	1.401856 .8819361	.620613 .202825	.5590668 .5867765
.0470408	.057302 1.776626	1.424979 .884206	.6287178 .20807	.5628647 .5947211
.049276	.0600248 1.76679	1.442857 .8857237	.6348413 .2122725	.5659981 .6000328
.052832	.0643564 1.753615	1.466849 .8877844	.6429864 .2180061	.5702506 .6072453
.054864	.0668317 1.745134	1.481642 .8888879	.6478983 .2216601	.5730218 .6110765
.059944	.0730198 1.73556	1.498908 .8903251	.6526483 .2259276	.576183 .616138
.0654304	.079703 1.713054	1.532787 .8912352	.6640742 .2351787	.5837527 .6193231
.0705104	.0858911 1.700326	1.553915 .8924627	.6707219 .2408592	.5881226 .6236194
.0752856	.0917079 1.690783	1.573248 .8946899	.6771585 .2457382	.5914421 .6314147
.0808736	.0985149 1.682046	1.593774 .8978072	.6842187 .2507142	.5945142 .6423251
.0862584	.1050743 1.672782	1.614008 .9005482	.6909945 .2558236	.5978067 .6519186
.0918464	.1118812 1.665481	1.631128 .9031679	.6967984 .2600908	.6004271 .6610876
.0968248	.1179455 1.658908	1.645242 .9050339	.7014396 .2637674	.6028062 .6676188

Table 3 (continued) Run 112

.1096264	.1335396 1.634273	1.686272 .9074076	.7135742 .2759561	.6118929 .6759266
.1220216	.1486386 1.613858	1.724578 .9109993	.7252118 .2871498	.6196332 .6884976
.1345184	.1638614 1.598917	1.761466 .9171203	.737287 .2970774	.6254234 .7099209
.1481328	.1804455 1.579278	1.794975 .9191785	.7466843 .3079412	.6332009 .7171246
.1616456	.1969059 1.567542	1.817779 .9214897	.7533554 .3150886	.6379415 .7252139
.1749552	.2131188 1.55844	1.858799 .932777	.7681159 .3248085	.6416673 .7647196
.1882648	.2293317 1.534339	1.894059 .932724	.7766107 .3382067	.6517465 .7645341
.2017776	.2457921 1.518318	1.926268 .9362105	.7856831 .3490166	.6586236 .7767369
.2019808	.2460396 1.519903	1.923902 .936208	.7851276 .3480817	.6579366 .7767279
.2154936	.2625 1.498448	1.97066 .9423083	.7985126 .3636757	.6673571 .7980791
.2286	.2784653 1.48195	1.998165 .9433856	.8051883 .3744975	.6747864 .8018495
.2424176	.295297 1.468991	2.027526 .9474273	.8134396 .3846985	.6807393 .8159954
.26924	.3279703 1.42725	2.102553 .9518133	.8314694 .4154052	.7006483 .8313466
.2949448	.3592822 1.393387	2.16981 .9575734	.8478262 .4434547	.7176758 .8515069
.3219704	.392203 1.363529	2.237045 .9656539	.8646817 .4714302	.733391 .8797886
.3475736	.4233911 1.333811	2.299327 .9712844	.879017 .4999654	.7497313 .8994953
.3744976	.4561881 1.303145	2.362859 .976277	.8928602 .5311097	.767374 .9169695
.4005072	.4878713 1.277005	2.420976 .9818262	.9055992 .5601899	.7830822 .9363918
.427736	.5210396 1.248981	2.481432 .986484	.9179722 .5927801	.8006529 .952694
.453136	.5519802 1.222401	2.537775 .9899622	.9287725 .6253413	.8180618 .9648679
.4809744	.5858911 1.190935	2.598705 .990864	.9387509 .6649997	.8396763 .9680239

Table 3 (continued) Run 112

.508	.6188119 1.168069	2.65631 .9968695	.9503034 .69917	.8561139 .9890434
.5357368	.652599 1.142109	2.711926 .9988527	.9593584 .7376015	.8755731 .9959844
.5622544	.684901 1.124422	2.764703 1.006391	.9704261 .7693304	.8893454 1.022369
.587756	.7159653 1.096297	2.814078 1.002595	.9753253 .8127521	.9121613 1.009083
.6142736	.7482673 1.072007	2.858442 .999478	.9796646 .8532989	.9328301 .9981732
.626872	.7636139 1.064306	2.88074 1.00194	.9837543 .8691691	.9395791 1.006791
.64008	.779703 1.056668	2.898933 1.002615	.9864082 .8840333	.9463713 1.009151
.653288	.7957921 1.050453	2.917018 1.004539	.9896387 .8973582	.9519704 1.015887
.667512	.8131188 1.040541	2.935777 1.003148	.9912927 .9159221	.9610385 1.011016
.678688	.8267327 1.039134	2.949771 1.00785	.9953444 .9221394	.9623398 1.027474
.692912	.8440594 1.030924	2.962158 1.005231	.9955676 .9369936	.970004 1.018308
.70612	.8601485 1.019728	2.973727 .9992709	.9940138 .9560676	.9806539 .9974483
.72136	.8787129 1.022839	2.985253 1.007293	.9993877 .955428	.9776711 1.025525
.733552	.8935644 1.015961	2.990617 1.002825	.9978119 .9668158	.9842897 1.009888
.747776	.9108911 1.016601	3.000556 1.007742	1.001443 .9691188	.9836701 1.027097
.765048	.9319307 1.006327	3.007419 1.000495	.9986487 .9861681	.9937129 1.001731
.775208	.9443069 1.004	3.011986 1.000135	.9990081 .9910867	.9960162 1.000471
.788416	.960396 1.005317	3.015027 1.002751	1.000673 .9901461	.9947109 1.00963
.800608	.9752475 1.002815	3.017306 1.001231	1.000182 .9945907	.9971933 1.004309
.820928	.9991134 1	3.021859 .9994804	.9998407 1.001612	1.000887 .9981815

Table 3 (continued) Run 112

.82804	1.008663 .9989913	3.021859 .9993582	.9997796 1.001795	1.00101 .9977538
.841248	1.024752 1.003295	3.021859 1.003664	1.001931 .9953788	.9967157 1.012823
.854456	1.040842 .997787	3.024133 .9991246	.9999288 1.004358	1.002218 .9969363
.867664	1.056931 .9975151	3.02489 .999176	1.000043 1.005019	1.002491 .997116
.880872	1.07302 1.000024	3.023375 1.00104	1.000798 1.00075	.9999761 1.00364
.89408	1.089109 .9985835	3.024133 .9999222	1.000328 1.003161	1.001418 .9997278
.908304	1.106436 .9923568	3.027919 .995297	.9984527 1.013859	1.007702 .9835396
.91948	1.12005 .9964929	3.027919 .9994454	1.000531 1.007569	1.003519 .9980589
.93472	1.138614 .9968631	3.027919 .9998167	1.000717 1.00701	1.003147 .9993584
.947928	1.154703 .9941448	3.029433 .9977354	.9998513 1.011637	1.00589 .9920739
.961136	1.170792 .9902176	3.028676 .9934727	.9976252 1.017394	1.009879 .9771546
.973328	1.185644 .9955967	3.029433 .9991925	1.000581 1.009431	1.004423 .9971739
.987552	1.20297 .9951886	3.030189 .9991059	1.000626 1.010302	1.004835 .9968705
.993648	1.210396 .9940524	3.030945 .9982878	1.000304 1.012283	1.005983 .9940073

DELSTAR,CM=
THETA,CM=
RE THETA=

.244234
.0519245
3383.608

Table 3 (continued) Run 113

MEAN FLOW PROFILES, RUN NO 113

P0, N/M2= 97309
 T0, DEG K= 318.3333
 TW, DEG K= 172.2222
 X, CM= 35.052
 RHOE, KG/M3= .0790366
 UE, M/SEC= 643.3206
 RHOUE2, N/M2= 32626.15
 RHOUE, KG/M2SEC= 50.81478
 RE, M-1= 6517718

Y (CM)	Y/D T/TE	M T0/TDE	U/UE RE/REE	RHO/RHOE H
.00508	.0060916 1.631829	.7772044 .6450083	.327719 .1270111	.6128094 .2265771
.0058928	.0070663 1.645265	.8088949 .6561522	.342483 .1307074	.6078048 .2508562
.0079248	.0095029 1.683525	.8459379 .6786896	.3623075 .1324499	.5939918 .2999587
.009144	.0109649 1.731745	.8565537 .7003364	.3720708 .1290379	.5774522 .3471208
.0104648	.0125487 1.776239	.8838528 .7242827	.38883 .1286362	.5629872 .3992928
.0113792	.0136452 1.774541	.912965 .7301374	.4014451 .1330458	.5635261 .4120483
.013208	.0158382 1.762081	.9945691 .7443572	.4357897 .1463311	.5675107 .4430292
.0149352	.0179094 1.730404	1.085152 .7539681	.4711869 .1636483	.5778998 .4639685
.0158496	.0190058 1.712147	1.12623 .7569835	.4864372 .1723181	.584062 .4705381
.0185928	.0222953 1.679141	1.222618 .7692042	.5229538 .1921118	.5955424 .4971635
.021336	.0255848 1.657124	1.295331 .7805179	.5504114 .2072547	.603455 .5218128
.023876	.0286306 1.635761	1.359916 .790241	.574118 .2215033	.6113363 .5429966

Table 3 (continued) Run 113

.026924	.0322856 1.623529	1.411138 .8005855	.5935108 .2322336	.6159421 .5655342
.0328168	.0393519 1.600576	1.481737 .8123233	.6187828 .2486883	.624775 .5911074
.0381	.0456871 1.590488	1.524166 .8215107	.6344925 .258054	.6287379 .6111242
.0424688	.0509259 1.581733	1.550212 .8259223	.6435567 .2644752	.632218 .6207357
.0478536	.057383 1.56932	1.586168 .8319229	.6558943 .2735777	.6372187 .6338092
.0526288	.0631092 1.557803	1.613996 .8356025	.6649481 .2812349	.6419298 .6418261
.0581152	.0696881 1.547604	1.64272 .840343	.6745629 .2888617	.6461601 .6521542
.0627888	.0752924 1.541573	1.660253 .8433652	.6804331 .2935328	.6486879 .6587386
.0693928	.0832115 1.537382	1.677684 .8473814	.6866417 .2977394	.6504564 .6674888
.0748792	.0897904 1.534693	1.693606 .8517095	.6925517 .3012976	.6515961 .6769184
.0887984	.1064815 1.515457	1.739114 .857732	.70669 .3148753	.6598668 .6900396
.1014984	.1217105 1.487768	1.800653 .8649187	.724981 .3345192	.6721479 .7056973
.113792	.1364522 1.481369	1.827419 .8713451	.7341736 .3415446	.6750512 .7196987
.1278128	.1532651 1.479843	1.84127 .8757513	.7393573 .3446305	.6757476 .7292985
.1394968	.1672758 1.46251	1.877261 .8792998	.7493819 .3572144	.6837558 .7370296
.154432	.1851852 1.454036	1.913731 .8883839	.7617237 .3671354	.6877409 .7568212
.1678432	.2012671 1.443512	1.948297 .8955461	.7726708 .3775998	.6927547 .7724255
.1811528	.2172271 1.432671	1.976423 .8999747	.7808763 .387134	.697997 .7820741
.2065528	.2476852 1.411138	2.035871 .9101883	.7982961 .4073803	.708648 .8043266
.2333752	.2798489 1.388896	2.097268 .9207017	.8158643 .4291928	.7199961 .8272322

Table 3 (continued) Run 113

.2599944	.311769 1.365031	2.157941 .9297384	.8322234 .452589	.7325839 .8469206
.2873248	.3445419 1.350175	2.218999 .9450696	.851101 .4726854	.7406448 .8803227
.3147568	.3774366 1.318871	2.278401 .9480095	.8636947 .5018326	.7582244 .8867279
.3401568	.4078947 1.296264	2.338256 .9570242	.878755 .5279048	.7714479 .9063683
.3675888	.4407895 1.27179	2.396623 .9637457	.8921473 .5560764	.7862933 .9210126
.3929888	.4712476 1.24682	2.455498 .969946	.9050459 .586226	.8020403 .934521
.4204208	.5041423 1.221153	2.51486 .9753911	.9173348 .6187041	.8188985 .9463845
.4478528	.537037 1.200092	2.571339 .9828842	.9298129 .6487435	.8332696 .9627096
.4732528	.5674951 1.176297	2.629093 .9883153	.9412253 .6829027	.8501253 .9745425
.4986528	.5979532 1.157694	2.676262 .9931193	.9505055 .7114974	.8637861 .9850089
.5271008	.6320663 1.136075	2.731536 .9985251	.9610357 .7464844	.8802237 .9967866
.5535168	.6637427 1.109308	2.786148 .9985754	.9686329 .788518	.9014631 .9968963
.5667248	.6795809 1.09945	2.809372 .9997793	.9723578 .8056021	.9095455 .9995192
.5789168	.6942008 1.089946	2.831603 1.000778	.9758071 .8224312	.9174763 1.001694
.5931408	.7112573 1.081788	2.856119 1.003927	.9805654 .8387995	.9243951 1.008555
.6063488	.7270955 1.06986	2.876881 1.001839	.9822331 .8588558	.9347014 1.004007
.6195568	.7429337 1.063103	2.897685 1.00452	.9862069 .873217	.9406423 1.009847
.6327648	.7587719 1.052332	2.916764 1.002576	.9876582 .8923335	.9502703 1.005611
.6449568	.7733918 1.045709	2.93336 1.003427	.9901473 .9058601	.9562892 1.007465
.6581648	.78923 1.038095	2.949084 1.002893	.9918243 .9206586	.9633029 1.006303

Table 3 (continued) Run 113

.6744208	.8087232 1.031181	2.967069 1.003953	.9945444 .9355271	.9697615 1.008611
.6855968	.8221247 1.025837	2.977966 1.003436	.9956068 .9462574	.9748141 1.007487
.6977888	.8367446 1.020381	2.988051 1.00243	.9963186 .9570378	.9800259 1.005295
.7120128	.8538012 1.018873	2.997332 1.004941	.9986745 .9621299	.9814763 1.010765
.7252208	.8696394 1.015946	3.004275 1.005039	.9995486 .9685076	.9843048 1.010979
.7384288	.8854776 1.010979	3.011203 1.003098	.999402 .9778682	.9891399 1.00675
.7526528	.9025341 1.009836	3.013509 1.002953	.9996017 .9802722	.9902597 1.006434
.7658608	.9183723 1.007121	3.017349 1.001902	.999529 .9854771	.9929292 1.004143
.7790688	.9342105 1.012604	3.022716 1.009672	1.004029 .9792561	.9875528 1.021072
.7922768	.9500487 1.008574	3.026545 1.007301	1.003298 .9863542	.9914991 1.015906
.8054848	.9658869 .9988994	3.026545 .9976387	.9984748 1.000672	1.001102 .9948554
.8186928	.9817251 1.001714	3.02578 1.000122	.9996274 .9962171	.9982893 1.000266
.8339328	1 1.012709	3.028075 1.012092	1.005861 .9808409	.9874507 1.026346
.8471408	1.015838 1.000573	3.029605 1.000618	1.000321 .9991774	.999427 1.001347
.8593328	1.030458 1.000589	3.029605 1.000634	1.000329 .999154	.9994113 1.001381
.8715248	1.045078 1.000088	3.02884 .9998057	.9998261 .9996511	.9999123 .9995768
.8857488	1.062134 .9996454	3.029605 .9996903	.9998573 1.000565	1.000355 .9993252
.8979408	1.076754 .9997193	3.029605 .9997641	.9998943 1.000455	1.000281 .999486
.9111488	1.092593 .9993141	3.030369 .9996854	.9999438 1.001315	1.000686 .9993145
.9233408	1.107212 .9993161	3.030369 .9996874	.9999449 1.001311	1.000684 .999319

Table 3 (continued) Run 113

.9375648	1.124269 .999992	3.02884 .99971	.9997782 .9997943	1.000008 .9993682
.9497568	1.138889 .9997527	3.029605 .9997975	.999911 1.000405	1.000247 .9995589
.9639808	1.155945 1.00007	3.02884 .9997879	.9998171 .9996778	.9999302 .9995379
.9771888	1.171784 .9992808	3.030369 .9996521	.9999272 1.001364	1.00072 .9992421
.9883648	1.185185 .9996274	3.029605 .9996722	.9998483 1.000592	1.000373 .9992858

DEL STAR, CM=	.2225505
THETA, CM=	.0538501
RE THETA=	3509.796

Table 3 (continued) Run 121

MEAN FLOW PROFILES, RUN NO 121

P0,N/M2= 97309
 T0,DEG K= 318.3333
 TW,DEG K= 297.7778
 X,CM= 38.7858
 RHOE,KG/M3= .0792901
 UE,M/SEC= 642.9455
 RHOUE2,N/M2= 32692.64
 RHOUE,KG/M2SEC= 50.94803
 RE,M-1= 6520915

Y(CM)	Y/D T/TE	M T0/TDE	U/UE RE/REE	RHO/RHOE H
.00508	.0056433 2.563219	.4388289 .940774	.2322921 .0394952	.3901345 .0827979
.008128	.0090293 2.54734	.4721628 .9404139	.2491619 .042834	.3925663 .0772202
.011176	.0124153 2.505821	.5645352 .9420473	.2954693 .0523027	.3990708 .1025164
.014224	.0158014 2.46723	.6405746 .9435201	.3326756 .0605413	.4053128 .1253244
.017272	.0191874 2.398967	.7634002 .9466555	.3909406 .0748042	.4168461 .1738807
.02032	.0225734 2.328118	.8788534 .9498988	.443369 .0895227	.4295315 .2241083
.022352	.0248307 2.312841	.9017248 .9503232	.4534123 .0926404	.4323687 .2306815
.024384	.027088 2.254745	.9899689 .9530564	.4914922 .1051285	.4435092 .2730082
.027432	.030474 2.203823	1.064068 .9552412	.5222809 .1164191	.453757 .3068441
.03048	.03386 2.169463	1.112878 .9566419	.5419633 .1242919	.4609436 .3285349
.033528	.037246 2.136745	1.158721 .9579429	.5600176 .1320207	.4680015 .3486829

Table 3 (continued) Run 121

.03556	.0395034 2.102824	1.206203 .9594258	.5783202 .1403572	.475551 .3716482
.038608	.0428894 2.076894	1.241708 .9603539	.5916611 .1468743	.4814883 .3860212
.041656	.0462754 2.063839	1.258984 .9606197	.5980045 .1501642	.4845339 .3901377
.043688	.0485327 2.045914	1.283428 .9612636	.6069623 .1548574	.4887792 .4001094
.046736	.0519187 2.032002	1.301851 .9615679	.6135779 .158507	.4921255 .4048217
.047752	.0530474 2.01621	1.323552 .9622146	.6213773 .1628261	.4959801 .4148366
.0508	.0564334 2.002648	1.34132 .9624447	.6275973 .166498	.4993388 .4184005
.052832	.0586907 1.992072	1.355338 .9626848	.6324796 .1694268	.5019898 .4221185
.05588	.0620767 1.983844	1.365742 .9626783	.6360172 .1716704	.5040719 .4220181
.06096	.0677201 1.958269	1.399785 .9632993	.6476552 .1790185	.510655 .4316353
.06604	.0733634 1.942877	1.419768 .9634654	.6543143 .183497	.5147005 .4342068
.072136	.0801354 1.924309	1.444313 .9638192	.6624377 .1890814	.519667 .439687
.077216	.0857788 1.906309	1.468405 .964259	.6703302 .1946699	.5245739 .4464981
.083312	.0925508 1.892494	1.486445 .9644021	.6761026 .198993	.5284032 .4487131
.087376	.0970655 1.880664	1.502178 .9646236	.6811196 .2027993	.5317272 .4521441
.1016	.1128668 1.845418	1.548301 .9648978	.695423 .2144145	.5418827 .4563898
.113792	.1264108 1.817436	1.587059 .9658778	.7074063 .2243597	.5502258 .4715677
.125984	.1399549 1.789948	1.626214 .9671878	.7193567 .2346834	.5586754 .4918543

Table 3 (continued) Run 121

.140208	.1557562 1.764759	1.66204 .9682719	.7300129 .2445077	.5666496 .5086431
.166624	.1851016 1.72125	1.727149 .971247	.7492006 .2628639	.580973 .5547172
.194056	.2155756 1.674423	1.796521 .9737548	.7686192 .2839253	.5972206 .5935535
.219456	.2437923 1.635372	1.855679 .9760196	.7846168 .3029299	.6114818 .6286277
.246888	.2742664 1.599537	1.911675 .978484	.7993883 .3217451	.6251807 .6667936
.27432	.3047404 1.555339	1.982199 .981636	.8173464 .3468056	.6429468 .7156069
.300736	.3340858 1.516426	2.045687 .9844866	.8329065 .3707451	.6594454 .7597516
.326136	.3623025 1.481234	2.104291 .9871025	.8467671 .3940741	.6751129 .8002627
.352552	.3916479 1.445834	2.164445 .9897541	.8605026 .4193186	.6916423 .8413263
.377952	.4198646 1.411474	2.223972 .9922949	.873599 .4456864	.7084792 .8806754
.405384	.4503386 1.377119	2.284937 .9948999	.8865565 .4741332	.7261538 .9210174
.4318	.479684 1.34438	2.344312 .9973669	.898717 .503353	.7438371 .9592227
.460248	.5112867 1.309735	2.408895 1.000083	.9114986 .5368313	.763513 1.001286
.484632	.5383747 1.28075	2.462524 1.001601	.921423 .5666473	.7807927 1.024791
.51308	.5699774 1.24791	2.525959 1.003831	.9329626 .6033557	.80134 1.059324
.526288	.5846501 1.23792	2.544998 1.004243	.9362246 .6149877	.8078067 1.065702
.540512	.6004515 1.224259	2.57121 1.004765	.9406339 .6313573	.8168207 1.073799

Table 3 (continued) Run 121

.55372	.6151242 1.208589	2.601651 1.005357	.9456595 .6508506	.8274111 1.082959
.565912	.6286682 1.192141	2.634068 1.005977	.9509052 .672185	.8388267 1.092558
.580136	.6444695 1.174838	2.668689 1.006621	.9563863 .6956489	.8511811 1.102535
.592328	.6580135 1.163301	2.692075 1.007045	.9600188 .7119058	.8596225 1.109096
.606552	.6738149 1.153198	2.712781 1.007421	.9631925 .7265693	.8671536 1.114918
.618744	.6873589 1.136496	2.747415 1.008021	.9683996 .7517086	.8798978 1.124216
.630936	.7009029 1.126155	2.769147 1.008392	.9716089 .7678676	.8879775 1.129963
.64516	.7167043 1.114162	2.794856 1.008918	.9753938 .7872673	.8975355 1.138114
.659384	.7325056 1.105856	2.812149 1.008976	.977764 .8008974	.9042768 1.139009
.67056	.744921 1.09329	2.838316 1.008937	.981239 .8220629	.9146706 1.138398
.683768	.7595937 1.082476	2.86081 1.008766	.9841121 .8408119	.9238077 1.135755
.699008	.7765237 1.068467	2.890372 1.008551	.9878265 .866009	.9359207 1.132421
.725424	.8058691 1.055407	2.917286 1.007884	.9909127 .8901339	.9475015 1.122093
.737616	.8194131 1.049702	2.929084 1.007553	.9922275 .9009469	.9526516 1.116974
.752856	.8363431 1.038586	2.953327 1.007352	.9951283 .9228773	.9628478 1.113861
.765048	.8498871 1.033338	2.963437 1.006632	.9960091 .9330373	.9677374 1.102701
.778256	.8645598 1.027235	2.975062 1.005699	.996959 .9449919	.9734873 1.088252

Table 3 (continued) Run 121

.793496	.8814898 1.020278	2.988186 1.004531	.9979602 .9588184	.9801253 1.070175
.805688	.8950339 1.017998	2.992036 1.003943	.9981289 .9632606	.9823201 1.061071
.819912	.9108352 1.014154	2.999721 1.003453	.9988013 .9712005	.9860438 1.053475
.832104	.9243792 1.010102	3.008153 1.003061	.9996064 .9797674	.9899989 1.04741
.847344	.9413092 1.010102	3.006622 1.002404	.9990975 .9792684	.9899988 1.037225
.859536	.9548533 1.004803	3.01809 1.002053	1.000275 .9907573	.9952195 1.03179
.872744	.969526 1.003019	3.021142 1.00158	1.000396 .9943973	.99699 1.024464
.885952	.9841986 1.002769	3.020379 1.001003	1.000019 .9945168	.9972386 1.01554
.900176	1 .9999633	3.025713 1.000482	1.000383 1.000456	1.000037 1.007468
.913384	1.014673 .9998468	3.02419 .9997144	.9998211 1.000127	1.000153 .9955778
.92456	1.027088 1.001286	3.021142 .9998495	.999532 .9969711	.9987153 .9976693
.938784	1.042889 1.002787	3.018854 1.000368	.9995228 .9939886	.9972212 1.005696
.951992	1.057562 1.002537	3.01809 .9997923	.9991457 .9941074	.9974696 .9967829
.9652	1.072235 .9984853	3.027236 .9996539	1.000146 1.003177	1.001517 .9946398
.978408	1.086907 1.001324	3.020379 .9995612	.9992985 .9966631	.9986775 .9932039
.992632	1.102709 .9995014	3.024952 .9996946	.9999001 1.000896	1.000499 .99527
.994664	1.104966 1.000125	3.023429 .9996664	.999708 .9994595	.9998755 .9948345

DELSTAR,CM=
THETA,CM=
RE THETA=

.291671
.0534867
3487.824

Table 3 (continued) Run 122

MEAN FLOW PROFILES, RUN NO 122

P0,N/M2=	97309
T0,DEG K=	318.3333
TW,DEG K=	227.7778
X,CM=	38.7858
RHOE,KG/M3=	.0792205
UE,M/SEC=	643.0206
RHOUE2,N/M2=	32671.56
RHOUE,KG/M2SEC=	50.90924
RE,M-1=	6518724

Y(CM)	Y/D T/TE	M T0/T0E	U/UE RE/REE	RHO/RHOE H
.00508	.0059319 2.143941	.4410314 .7868443	.2134415 .0500076	.4664308 .2506857
.0075184	.0087792 2.162431	.4820922 .7994214	.2343171 .0540503	.4624426 .2948984
.0085344	.0099656 2.153203	.5332469 .8039114	.2586269 .0601222	.4644245 .3106825
.01016	.0118638 2.170942	.5467725 .8127753	.266277 .0609868	.4606294 .3418421
.0110744	.0129315 2.142697	.6474933 .8204105	.3132697 .0734739	.4667016 .3686823
.0125984	.0147111 2.120047	.7257169 .8278282	.3492552 .0835097	.4716876 .3947581
.0140208	.016372 2.099375	.785208 .833089	.3760388 .0915298	.4763321 .4132516
.0155448	.0181516 2.066483	.8596727 .8379196	.4084622 .1023219	.483914 .4302328
.0168656	.0196939 2.040621	.9155545 .8417358	.432283 .1108051	.4900469 .4436481
.0176784	.020643 2.015143	.9661257 .8447747	.4533039 .1188905	.4962427 .4543309
.018796	.021948 1.996576	1.006279 .8481633	.4699636 .1253644	.5008576 .4662427
.020828	.0243208 1.983844	1.04314 .853343	.4856228 .1310676	.504072 .4844512
.021844	.0255072 1.958374	1.091133 .8565604	.5046944 .1394793	.5106276 .4957615

Table 3 (continued) Run 122)

.0232664	.0271681 1.941006	1.127328 .8599757	.5191187 .1458304	.5151967 .5077673
.0242824	.0283545 1.925547	1.157674 .8625599	.5309654 .1513657	.5193329 .5168517
.0260096	.0303713 1.913677	1.186953 .8665244	.5427136 .1564839	.5225542 .5307883
.0271272	.0316764 1.897087	1.217284 .8687866	.554164 .1623664	.5271239 .5387405
.0285496	.0333373 1.894619	1.223232 .8695995	.5565095 .163445	.5278106 .5415982
.0295656	.0345237 1.873403	1.25817 .8713366	.5691905 .170675	.533788 .5477048
.0321056	.0374896 1.859307	1.288237 .8748382	.580596 .1765379	.5378348 .5600142
.0347472	.0405742 1.841082	1.321073 .8774081	.5924696 .1834558	.5431588 .569048
.0374904	.0437774 1.828224	1.344196 .8792409	.6007313 .1884401	.5469791 .5754912
.0405384	.0473366 1.819845	1.363406 .8818991	.6079183 .1923221	.5494973 .5848356
.0427736	.0499466 1.802241	1.394185 .8841759	.6186282 .1992651	.5548646 .5928392
.0458216	.0535058 1.794681	1.409289 .885836	.6240171 .2025731	.557202 .598675
.0476504	.0556412 1.785261	1.424213 .8865202	.628968 .2061828	.5601421 .6010803
.0504952	.0589631 1.774439	1.442219 .8876171	.6349868 .210518	.5635584 .6049363
.05334	.062285 1.76998	1.451937 .8889035	.6384616 .2126613	.5649782 .6094584
.0557784	.0651323 1.761833	1.46638 .8900589	.6433271 .2161262	.5675907 .61352
.0583184	.0680982 1.755018	1.477507 .8906778	.6469537 .2189157	.5697947 .6156956
.06096	.0711828 1.748348	1.48921 .8915814	.6508377 .2217949	.5719686 .6188721
.0658368	.0768774 1.737949	1.511168 .8943681	.658467 .2268993	.5753908 .6286683
.0718312	.0838771 1.725895	1.53583 .8973286	.6668886 .2327988	.5794094 .6390753

Table 3 (continued) Run 122

.0769112	.089809 1.720252	1.546481 .8983843	.6704145 .2354624	.5813103 .6427865
.0826008	.0964527 1.707891	1.570522 .9009712	.6783859 .2414873	.5855176 .6518803
.0869696	.1015542 1.697791	1.586812 .9018133	.6833931 .245977	.5890006 .6548407
.0915416	.1068929 1.690146	1.600003 .9027719	.6875206 .249557	.5916649 .6582105
.0974344	.1137739 1.678834	1.620283 .9044759	.6939009 .2550533	.5956517 .6642006
.1100328	.128485 1.657086	1.661906 .9087545	.7071018 .2663233	.6034688 .6792413
.1232408	.1439079 1.637398	1.696405 .9113604	.7174795 .2763525	.6107252 .6884018
.1375664	.1606359 1.615422	1.740439 .9164018	.731147 .2888495	.6190333 .706124
.150368	.1755843 1.602838	1.770701 .9212959	.7409569 .2970588	.6238934 .7233287
.1638808	.1913632 1.586288	1.801686 .9241886	.75002 .3066219	.6304027 .7334972
.177292	.2070234 1.574604	1.83461 .9307007	.7609082 .3154348	.6350803 .7563896
.2044192	.2386997 1.531757	1.908257 .9352068	.7806108 .3409015	.6528452 .7722299
.23114	.2699015 1.506284	1.969721 .9450218	.7990264 .3601978	.6638852 .806733
.257556	.3007474 1.467237	2.039277 .9494309	.8164494 .3868654	.6815531 .8222325
.2832608	.3307628 1.437405	2.098141 .9548605	.8314326 .409676	.6956981 .8413195
.3095752	.3614901 1.404232	2.161735 .9597011	.8466906 .4362104	.7121332 .8583357
.33528	.3915055 1.378896	2.22038 .9674221	.8617788 .4597289	.725218 .8854775
.362712	.4235378 1.351007	2.277496 .9723778	.8749623 .4854242	.7401885 .9028987
.38862	.4537905 1.321577	2.338118 .9773226	.8884144 .5142209	.7566715 .9202812
.4156456	.4853482 1.29476	2.396257 .9826702	.9012199 .5426755	.772344 .9390798

Table 3 (continued) Run 122

.442468	.5166686 1.267967	2.453971 .9874127	.9133267 .5726648	.7886644 .9557513
.4701032	.5489382 1.240402	2.511303 .9908956	.9244498 .6048809	.80619 .9679949
.496824	.58014 1.218439	2.562182 .995572	.9347915 .6332671	.820722 .9844341
.5236464	.6114604 1.187312	2.628718 .9991119	.9467371 .6745506	.8422382 .996878
.549656	.6418318 1.164186	2.680071 1.002075	.9557853 .7077013	.8589695 1.007295
.57658	.6732709 1.138774	2.734165 1.003766	.9643757 .745637	.8781374 1.013239
.6013704	.7022185 1.117373	2.782705 1.006043	.9722303 .7802722	.8949561 1.021245
.6288024	.7342508 1.094936	2.832933 1.007662	.9797912 .8184088	.9132955 1.026936
.6552184	.7650967 1.07829	2.873199 1.009848	.9861351 .8490099	.927394 1.034618
.6816344	.7959426 1.056276	2.916918 1.008123	.9908682 .8886378	.946722 1.028554
.7090664	.8279748 1.042116	2.945982 1.007154	.9940105 .9156459	.959586 1.025149
.7212584	.8422114 1.03123	2.96469 1.004689	.9950841 .9359598	.969716 1.016485
.7354824	.8588207 1.027771	2.977099 1.006675	.9975725 .9445888	.972979 1.023463
.7497064	.8754301 1.026034	2.987918 1.009652	1.000351 .9504123	.9746261 1.033929
.7629144	.890853 1.020522	2.995624 1.007552	1.000233 .9605418	.9798902 1.026548
.7771384	.9074623 1.016391	3.00331 1.006784	1.000768 .9688496	.9838734 1.023849
.7903464	.9228853 1.011132	3.01251 1.005528	1.001233 .9793704	.9889909 1.019434
.8035544	.9383082 1.009019	3.014806 1.004414	1.000949 .9831831	.9910619 1.015515
.8167624	.9537312 1.008248	3.017864 1.004961	1.001581 .9853041	.9918194 1.017439
.8320024	.9715269 1.007655	3.019393 1.005027	1.001794 .9866699	.9924031 1.01767

Table 3 (continued) Run 122

.3431784	.9845771 1.006338	3.021683 1.004697	1.001898 .9893502	.9937022 1.016511
.3563864	1 1.004138	3.02626 1.004464	1.002319 .9940948	.9958794 1.015693
.3695944	1.015423 1.005688	3.02626 1.006015	1.003092 .991805	.9943439 1.021145
.3838184	1.032032 1.007078	3.02626 1.007405	1.003785 .9897612	.992972 1.026031
.3960104	1.046269 1.002366	3.027785 1.003346	1.001938 .9972243	.9976394 1.011761
.4102344	1.062878 1.000844	3.027785 1.001822	1.001177 .9994927	.9991564 1.006405
.4224264	1.077115 1.002263	3.027785 1.003243	1.001887 .9973773	.9977417 1.011399
.4366504	1.093724 1.002391	3.028546 1.003698	1.002203 .9974378	.9976143 1.012998
.4488424	1.107961 1.003616	3.023973 1.002961	1.001301 .9941149	.9963968 1.010409
.4620504	1.123384 1.001182	3.029308 1.002813	1.00185 .9994916	.9988196 1.009888

DELSTAR, CM=	.2607856
THETA, CM=	.0538006
RE THETA=	3507.112

Table 3 (continued) Run 123

MEAN FLOW PROFILES, RUN NO 123

P0,N/M2= 97309
 T0, DEG K= 318.3333
 TW, DEG K= 172.3333
 X, CM= 38.7858
 RHOE, KG/M3= .0782125
 UE, M/SEC= 643.9181
 RHOEUE2, N/M2= 32345.95
 RHOEUE, KG/M2SEC= 50.33162
 RE, M-1= 6477771

Y (CM)	Y/D T/TE	M T0/TOE	U/UE RE/REE	RHO/RHOE H
.00508	.0059074 1.737725	.6365394 .6602315	.2762483 .0951489	.575465 .259744
.0069088	.008034 1.856596	.6020392 .6998187	.2700643 .082275	.5386201 .3459929
.0084328	.0098062 1.900125	.6474876 .7238114	.2938369 .0857709	.5262811 .398266
.0104648	.0121692 1.924003	.6634437 .735736	.3029637 .0864254	.5197497 .4242462
.0113792	.0132325 1.916159	.6987115 .7392072	.3184178 .0915191	.5218773 .4318087
.0125984	.0146503 1.912758	.7270173 .743321	.3310232 .0954538	.5228053 .4407716
.0148336	.0172495 1.908636	.7750383 .7513961	.3525075 .1020535	.5239344 .4583649
.015748	.0183129 1.883874	.8413027 .755831	.3801561 .1127382	.530821 .4680271
.0176784	.0205577 1.870602	.8967724 .7631828	.403791 .1213194	.5345873 .4840447
.0188976	.0219754 1.866461	.9224646 .7676258	.4148995 .1251679	.5357732 .4937246
.0196088	.0228025 1.844905	.9732815 .7712531	.4352203 .1341467	.5420333 .5016276
.0216408	.0251654 1.839829	1.011982 .7790671	.4519028 .1400001	.5435288 .5186519
.0244856	.0284735 1.811545	1.087258 .7872128	.4817715 .1535959	.552015 .536399

Table 3 (continued) Run 123

.026924	.0313091 1.787384	1.146543 .7933519	.5046415 .1649436	.5594767 .5497744
.0293624	.0341446 1.781069	1.168214 .7968287	.5132706 .1688701	.5614607 .5573492
.0321056	.0373346 1.757517	1.220137 .8016124	.5325278 .179594	.5689845 .5677716
.0348488	.0405246 1.705392	1.318121 .8076516	.5666972 .202146	.5863755 .5809292
.0371856	.043242 1.679812	1.366603 .8109065	.583118 .2139612	.5953046 .5880207
.0405384	.0471408 1.668374	1.392698 .813829	.5922258 .2200991	.5993859 .5943878
.0429768	.0499764 1.651864	1.426653 .8168908	.6036555 .2285654	.6053768 .6010587
.04572	.0531664 1.642153	1.449894 .8198055	.6116835 .2341798	.6089567 .6074089
.0481584	.0560019 1.638689	1.45973 .8213725	.615183 .2364544	.610244 .610823
.0505968	.0588374 1.628534	1.479813 .8230406	.6217116 .2417681	.6140492 .6144572
.0535432	.0622637 1.611368	1.513435 .8257638	.632477 .2509006	.6205908 .6203904
.0581152	.0675803 1.613049	1.519744 .8287951	.6354449 .2515843	.6199441 .6269946
.0628904	.0731333 1.60567	1.538498 .8314774	.6418135 .2563059	.6227928 .6328386
.0686816	.0798677 1.599863	1.560058 .8359825	.6496294 .2612018	.6250536 .6426539
.0737616	.085775 1.581667	1.594767 .8386492	.660296 .2712713	.6322442 .6484639
.0794512	.0923913 1.580124	1.605164 .8415263	.6642765 .2734091	.6328616 .6547322
.0841248	.0978261 1.571356	1.625735 .8441973	.6709199 .279056	.6363932 .6605515
.0918464	.1068053 1.579145	1.646018 .8557483	.6809721 .2806085	.6332541 .6857177
.1019048	.1185019 1.56709	1.675837 .8601271	.6906573 .288742	.6381253 .6952579
.1151128	.1338611 1.543467	1.708023 .8589767	.6985958 .3005603	.6478922 .6927516

Table 3 (continued) Run 123

.1289304	.1499291 1.530831	1.748905 .867152	.7123829 .3112943	.65324 .7105632
.1408176	.1637524 1.517296	1.784819 .8730205	.7237907 .3216422	.6590672 .7233488
.1555496	.1808837 1.503814	1.822533 .8796441	.7357937 .332555	.664976 .7377798
.1678432	.1951796 1.49134	1.851852 .883641	.7445233 .3418612	.6705379 .7464878
.181356	.2108932 1.477861	1.884404 .8882889	.7541792 .3523193	.6766536 .7566142
.1941576	.2257798 1.471346	1.912707 .895488	.7638175 .3598315	.6796496 .772299
.2180336	.2535444 1.449127	1.966836 .9033559	.7794805 .3780024	.6900704 .7894407
.2475992	.2879253 1.423159	2.036557 .9150898	.7998471 .401492	.702662 .8150056
.2754376	.3202977 1.395889	2.094318 .9209669	.8146138 .4243152	.7163892 .8278101
.3016504	.3507798 1.378353	2.148313 .9315923	.8303507 .4431167	.7255034 .8509597
.3279648	.38138 1.36833	2.189251 .9418967	.8430913 .4562599	.7308181 .8734099
.354076	.4117439 1.337631	2.246123 .9444826	.8552348 .4834641	.7475903 .8790439
.3812032	.4432892 1.323874	2.297516 .956499	.8702931 .5018709	.7553589 .9052241
.4077208	.4741257 1.297922	2.348776 .9594778	.8809468 .5277994	.7704623 .911714
.432816	.5033081 1.280387	2.397974 .9675328	.8933029 .5494682	.7810141 .9292634
.4626864	.5380435 1.260032	2.450967 .9749104	.9057575 .5746989	.7936308 .9453371
.4850384	.5640359 1.245799	2.487874 .9798601	.9141892 .5929806	.802698 .956121
.5134864	.5971172 1.222573	2.541833 .9849151	.9252692 .6225388	.8179473 .9671344
.5409184	.629017 1.19965	2.59509 .9895184	.935758 .6532588	.8335762 .9771636
.5653024	.6573724 1.178488	2.640884 .991925	.9438338 .6822128	.848545 .9824069

Table 3 (continued) Run 123

.5937504	.6904537 1.1516	2.70418 .9966808	.9553671 .7224865	.8683568 .9927683
.6211824	.7223535 1.127017	2.768722 1.003387	.9676721 .76348	.8872982 1.007379
.6323584	.7353497 1.114058	2.800818 1.005848	.9732457 .7855606	.8976195 1.012742
.6465824	.7518904 1.094688	2.835076 1.003217	.9765484 .8159694	.9135019 1.007009
.6618224	.7696125 1.084712	2.86298 1.006197	.9816557 .8352075	.9219038 1.013501
.6729984	.7826087 1.074752	2.884983 1.006513	.9846482 .8531786	.9304473 1.014189
.6862064	.7979679 1.063027	2.903601 1.003585	.9855819 .872743	.9407103 1.00781
.6994144	.813327 1.056264	2.924512 1.006248	.9895169 .8873851	.9467334 1.013613
.7126224	.8286862 1.050206	2.940501 1.0074	.99207 .8998842	.9521938 1.016123
.7268464	.8452268 1.039472	2.957201 1.0043	.9925924 .9189179	.9620268 1.009369
.7400544	.860586 1.031703	2.974601 1.004279	.9946946 .934703	.9692712 1.009323
.7522464	.8747637 1.027558	2.985624 1.004989	.9963728 .9438105	.9731815 1.01087
.7664704	.8913043 1.022178	2.996609 1.004449	.9974175 .9547256	.9783034 1.009693
.7796784	.9066635 1.018987	3.006775 1.005685	.9992381 .9624433	.9813667 1.012387
.7939024	.9232042 1.011677	3.015352 1.002144	.9984878 .9756207	.9884574 1.004672
.8050784	.9362004 1.007294	3.022353 1.000794	.9986353 .9842537	.9927593 1.001731
.8213344	.955104 1.006938	3.027012 1.002436	.9999983 .9862907	.9931093 1.005308
.8345424	.9704631 1.000544	3.030889 .9977226	.998095 .9970111	.9994561 .9950382
.8477504	.9858223 1.00189	3.033987 1.000388	.999787 .9960244	.9981135 1.000845
.8599424	1 1.002444	3.037856 1.002596	1.001338 .9964706	.9975624 1.005656

Table 3 (continued) Run 123

.8741664	1.016541 1.001288	3.038629 1.001771	1.001016 .9984459	.9987135 1.003859
.8853424	1.029537 .9989971	3.040948 1.000469	1.000633 1.00264	1.001004 1.001021
.8995664	1.046077 1.004032	3.040948 1.005511	1.003151 .9951243	.9959841 1.012007
.9117584	1.060255 1.008714	3.042493 1.010866	1.005998 .9887271	.9913612 1.023675
.9259824	1.076796 .9990214	3.042493 1.001153	1.001153 1.003113	1.00098 1.002512
.9412224	1.094518 .9938268	3.042493 .9959473	.9985472 1.010977	1.006212 .9911704
.9554464	1.111059 .9957448	3.04558 .9991849	1.000524 1.009084	1.004273 .9982241
.9696704	1.127599 .9989974	3.04558 1.002449	1.002157 1.004167	1.001004 1.005335

DELSTAR,CM=
THETA,CM=
RE THETA=

.2629874
.0611951
3964.077

Table 3 (continued) Run 131

MEAN FLOW PROFILES, RUN NO 131

P0,N/M2= 97309
 T0, DEG K= 318.8889
 TW, DEG K= 298.8889
 X, CM= 42.5196
 RHOE, KG/M3= .0809837
 UE, M/SEC= 640.8831
 RHOEUE2, N/M2= 33177.05
 RHOEUE, KG/M2SEC= 51.86932
 RE, M-1= 6530758

Y (CM)	Y/D T/TE	M T0/T0E	U/UE RE/REE	RHO/RHOE H
.00508	.0052854 2.501346	.4902074 .9402954	.2592958 .0462082	.3997848 .0480427
.008128	.0084567 2.486652	.5185562 .9398727	.2734841 .0492503	.4021472 .0413041
.01016	.0105708 2.479707	.532029 .9397657	.2801975 .0507111	.4032734 .0395983
.013208	.0137421 2.423634	.6478058 .9422638	.3372928 .0635851	.4126036 .0794279
.01524	.0158562 2.409852	.6726737 .9425823	.3492436 .0665119	.4149633 .0845066
.018288	.0190275 2.358166	.7650363 .9448298	.3929145 .0777874	.4240583 .1203412
.021336	.0221987 2.290968	.8763317 .9479275	.4436156 .0924994	.4364967 .169733
.024384	.02537 2.270273	.9076935 .9484767	.4574115 .0969445	.4404757 .1784893
.026416	.0274841 2.213836	.9946475 .951168	.4949607 .109769	.4517047 .2214014
.029464	.0306554 2.166042	1.065654 .9533652	.52454 .1210063	.4616717 .2564339

Table 3 (continued) Run 131

.032512	.0338266 2.139482	1.103903 .954411	.5400251 .1273916	.4674028 .273109
.034544	.0359408 2.121362	1.12975 .9551138	.5503243 .1318376	.4713952 .2843145
.036576	.038055 2.096653	1.16498 .956148	.5641707 .1380583	.4769506 .3008039
.039624	.0412262 2.072462	1.198799 .9570007	.5771896 .1442538	.4825179 .3143995
.039624	.0412262 2.051095	1.229511 .9581072	.5889171 .149986	.4875445 .3320421
.044704	.0465116 2.039242	1.244502 .9579958	.5943727 .1529815	.4903783 .3302661
.047752	.0496829 2.020295	1.270202 .9584611	.603822 .1580802	.4949773 .3376853
.049784	.051797 2.003149	1.293503 .9589107	.6122839 .1628078	.4992141 .3448544
.054864	.0570825 1.981626	1.321502 .9590156	.6221675 .1687328	.5046362 .346526
.059944	.0623679 1.967936	1.338648 .9588295	.6280594 .1725037	.5081467 .3435591
.065024	.0676533 1.946427	1.367223 .9591459	.6379508 .1787812	.5137618 .3486042
.07112	.0739958 1.927797	1.391876 .9593721	.6463386 .1843531	.5187269 .3522104
.0762	.0792812 1.908815	1.417639 .9598366	.6550528 .1902624	.5238854 .3596166
.080264	.0835095 1.897066	1.433477 .960074	.6603297 .1939826	.5271299 .363402
.08636	.089852 1.885271	1.449124 .9602046	.6654588 .1977434	.5304277 .3654838
.09144	.0951374 1.870639	1.469189 .9606102	.6720499 .2025853	.5345767 .3719508
.09652	.1004228 1.860173	1.483472 .9608633	.6766825 .2061	.5375844 .3759874
.100584	.1046512 1.847142	1.501678 .9613334	.6825834 .2106079	.5413768 .3834828

Table 3 (continued) Run 131

.10668	.1109937 1.835309	1.518151 .9617239	.6878571 .2147657	.5448675 .3897093
.112776	.1173362 1.819822	1.540295 .9624504	.6949397 .2203977	.5495042 .4012924
.11684	.1215645 1.810696	1.553411 .9628943	.6990978 .2237854	.5522739 .4083703
.12192	.1268499 1.809688	1.554861 .9629433	.6995554 .2241624	.5525815 .4091509
.128016	.1331924 1.795703	1.574999 .9636211	.7058726 .2294546	.556885 .4199585
.141224	.1469345 1.767463	1.61582 .9649816	.7184508 .2405	.5657827 .4416514
.154432	.1606765 1.754018	1.635119 .9655349	.7242611 .2459026	.5701197 .4504736
.16764	.1744186 1.727277	1.674279 .9668726	.7359317 .2570963	.5789461 .4718022
.181864	.1892178 1.708415	1.703366 .9683547	.7446177 .2654982	.585338 .495433
.19812	.2061311 1.701589	1.715096 .969381	.7482466 .2687879	.5876858 .5117967
.20828	.2167019 1.685722	1.739574 .970567	.7553786 .2761286	.5932178 .5307066
.222504	.2315011 1.664554	1.772467 .9721735	.7648141 .2862482	.6007616 .5563225
.235712	.2452431 1.643892	1.804704 .9737051	.7738761 .2964801	.6083123 .5807421
.24892	.2589852 1.625377	1.833914 .9751304	.7819604 .3059961	.615242 .6034681
.262128	.2727273 1.606527	1.863815 .9765637	.7900881 .3160107	.6224608 .6263214
.276352	.2875264 1.587452	1.894374 .9780469	.7982608 .3265189	.6299404 .6499706
.288544	.3002114 1.567985	1.925562 .9794539	.8064127 .3375937	.6377611 .6724038

Table 3 (continued) Run 131

.301752	.3139535 1.551257	1.952843 .9807783	.8134632 .347492	.6446387 .6935202
.313944	.3266385 1.537672	1.975274 .9819089	.8191965 .3557913	.6503338 .711547
.327152	.3403805 1.513311	2.014996 .9835592	.8290241 .3710803	.6608028 .7378606
.34036	.3541226 1.49577	2.044247 .984899	.8361699 .3826226	.6685519 .7592233
.352552	.3668076 1.477816	2.074297 .9861976	.8433541 .394838	.6766741 .7799282
.366776	.3816068 1.457779	2.108101 .9876107	.8512674 .4089992	.6859752 .8024599
.381	.3964059 1.443084	2.135163 .989543	.8578388 .4201665	.6929602 .8332683
.393192	.4090909 1.425526	2.165959 .9910479	.8649012 .4336084	.7014956 .8572642
.4064	.422833 1.408489	2.194304 .9916917	.8709684 .4467691	.7099805 .8675287
.433832	.4513742 1.375968	2.251868 .9940571	.8834379 .4738403	.7267609 .9052433
.461264	.4799154 1.344231	2.309897 .9966547	.8956913 .5023731	.7439197 .9466612
.488696	.5084567 1.310628	2.370228 .9982874	.9075253 .5343812	.7629929 .9726944
.515112	.5359408 1.282064	2.426348 1.001287	.9188336 .5645099	.7799921 1.020527
.541528	.5634249 1.249367	2.486556 1.002261	.9295484 .6003366	.8004054 1.03605
.566928	.589852 1.232701	2.51745 1.002562	.9347998 .6196453	.8112265 1.040854
.593344	.6173361 1.197214	2.587916 1.004597	.9470326 .6644152	.8352722 1.073301
.607568	.6321353 1.182744	2.61703 1.005312	.9518816 .6838268	.8454912 1.084703
.61976	.6448203 1.166349	2.649457 1.005665	.9569736 .7064699	.8573765 1.090328

Table 3 (continued) Run 131

.632968	.6585624 1.152188	2.677099 1.005625	.9610698 .7266382	.8679138 1.089685
.647192	.6733615 1.140094	2.700461 1.005343	.964355 .7443399	.8771209 1.085198
.659384	.6860465 1.127245	2.726775 1.005562	.9682497 .7641353	.8871185 1.088685
.672592	.6997886 1.115031	2.752695 1.006027	.9721435 .7837924	.8968361 1.096092
.6858	.7135306 1.105187	2.772789 1.005948	.9749079 .7998405	.9048242 1.094834
.699008	.7272727 1.092794	2.798316 1.005816	.978351 .8206784	.915086 1.092725
.713232	.7420719 1.081009	2.822845 1.005661	.9815907 .8411792	.9250619 1.090257
.727456	.756871 1.068814	2.847181 1.004895	.9844528 .8627336	.9356167 1.078054
.739648	.769556 1.060783	2.863289 1.004344	.9862958 .8773258	.9427 1.069267
.753872	.7843552 1.050011	2.886379 1.004146	.9891886 .8978431	.9523707 1.066101
.76708	.7980972 1.043303	2.899385 1.003363	.990467 .9104847	.9584939 1.053617
.781304	.8128964 1.033506	2.91917 1.002475	.9925322 .929607	.9675805 1.039462
.794512	.8266385 1.025561	2.935057 1.001611	.9940908 .9454337	.9750764 1.025687
.80772	.8403805 1.019209	2.947107 1.00059	.9950764 .9581195	.9811529 1.009411
.820928	.8541226 1.013825	2.957613 .9998155	.9959822 .9691409	.986364 .9970584
.83312	.8668076 1.009848	2.965843 .9994251	.9967929 .9775401	.9902484 .9908339
.847344	.8816068 1.005527	2.974797 .998986	.9976611 .986773	.9945031 .9838327

Table 3 (continued) Run 131

.862584	.897463 1.001342	2.981495 .9976939	.9978245 .9951631	.9986597 .9632314
.87376	.9090909 .9994899	2.985953 .9977558	.9983917 .9994068	1.00051 .9642179
.885952	.9217759 .9973374	2.991146 .9978276	.9990505 1.00437	1.00267 .9653628
.89916	.935518 .9961113	2.994109 .9978684	.9994254 1.007212	1.003904 .9660136
.912368	.94926 .9967406	2.992628 .9978648	.9992465 1.005766	1.00327 .9659553
.926592	.9640592 .9945992	2.99781 .9979357	.9999009 1.010747	1.00543 .9670857
.9398	.9778013 .9942941	2.998549 .9979459	.9999942 1.011459	1.005739 .9672489
.953008	.9915433 .99367	3.000028 .9979518	1.000173 1.012907	1.00637 .967343
.961136	1 .9933654	3.000767 .9979619	1.000266 1.013621	1.006679 .9675043

DELSTAR,CM=	.3085885
THETA,CM=	.0584319
RE THETA=	3816.049

Table 3 (continued) Run 132

MEAN FLOW PROFILES, RUN NO 132

P0,N/M2= 97309
 T0, DEG K= 318.3333
 TW, DEG K= 227.7778
 X, CM= 42.5196
 RHOE, KG/M3= .0817021
 UE, M/SEC= 640.7846
 RHOUE2, N/M2= 33461.06
 RHOUE, KG/M2SEC= 52.32138
 RE, M-1= 6615950

Y (CM)	Y/D T/TE	M T0/TOE	U/UE RE/REE	RHO/RHOE H
.00508	.0056548 2.132226	.4523192 .7940295	.220455 .0522857	.4689934 .2759442
.0078232	.0087084 2.149966	.5515759 .815964	.2699475 .0630699	.4651237 .3530515
.0092456	.0102918 2.132305	.626696 .8227656	.3054498 .0724392	.468976 .3769611
.0102616	.0114228 2.10552	.7049318 .8281252	.3414168 .0828474	.4749421 .3958022
.011684	.0130061 2.081569	.7643312 .8317035	.368074 .0911918	.4804069 .4083811
.0130048	.0144764 2.0575	.8174306 .8344514	.3913623 .099035	.4860268 .4180408
.0143256	.0159466 2.040798	.8655532 .8395041	.4127167 .1060008	.4900043 .4358027
.0156464	.0174169 2.024257	.906595 .8432338	.4305309 .1122292	.4940085 .4489141
.0164592	.0183216 2.00355	.9475136 .8454841	.4476553 .1189038	.4991141 .4568246
.0180848	.0201312 1.984243	.9907587 .8492373	.4658258 .1259391	.5039705 .4700183
.0189992	.0211491 1.969654	1.021273 .8516456	.4784041 .1310976	.5077035 .4784843
.0207264	.0230717 1.953671	1.057237 .8551842	.4932375 .137194	.511857 .4909236
.0217424	.0242027 1.941321	1.082408 .8572593	.5033821 .1416525	.5151132 .4982182

Table 3 (continued) Run 132

.0234696	.0261253 1.927568	1.113201 .8605111	.5158659 .1470708	.5187884 .5096493
.024384	.0271432 1.919632	1.130246 .8622206	.5226853 .1501476	.5209331 .5156589
.0263144	.029292 1.898586	1.171335 .8656139	.5387091 .1579167	.5267079 .5275876
.0271272	.0301968 1.890189	1.187225 .8668547	.5448085 .1610115	.5290475 .5319493
.028956	.0322325 1.87784	1.21054 .8687025	.5536898 .1656219	.5325266 .5384451
.0307848	.0342683 1.865747	1.233281 .8705269	.562272 .1702021	.5359785 .5448585
.0341376	.0380005 1.851449	1.262794 .8736149	.5735174 .1760851	.5401175 .5557139
.0364744	.0406017 1.8337	1.295003 .8760488	.5853196 .1829313	.5453456 .5642698
.0392176	.0436553 1.825009	1.312484 .8778491	.5918132 .1865905	.5479424 .5705983
.0418592	.0465958 1.815634	1.32969 .8792453	.5980298 .1903536	.5507719 .5755065
.0450088	.0501018 1.801806	1.351675 .8801487	.6055979 .1955071	.5549987 .5786823
.0468376	.0521375 1.791388	1.366654 .8802789	.6105365 .1992281	.5582264 .5791401
.0499872	.0556435 1.781443	1.381447 .8805737	.6154296 .2029062	.5613427 .5801764
.0530352	.0590364 1.772657	1.396061 .8813793	.6204047 .2064293	.5641249 .5830082
.0561848	.0625424 1.765056	1.410505 .8827194	.6254779 .2097823	.5665542 .5877192
.0583184	.0649174 1.760511	1.421624 .8844135	.6295967 .2121761	.5680168 .5936746
.0607568	.0676318 1.75658	1.434215 .8869579	.6344631 .2147049	.5692879 .602619
.0666496	.0741914 1.749757	1.459035 .8925031	.6441881 .2195765	.5715078 .6221122
.0712216	.0792807 1.74941	1.469748 .8962536	.6488539 .2212484	.5716213 .6352963
.0765048	.0851617 1.743731	1.49305 .9019578	.6580704 .2257504	.5734831 .6553486

Table 3 (continued) Run 132

.0016864	.0909297 1.735056	1.512534 .9047406	.6649976 .2302507	.5763503 .6651312
.086868	.0966976 1.718898	1.528802 .9024001	.6690129 .2357071	.5817682 .6569035
.1001776	.1115132 1.682385	1.570785 .8988959	.6800451 .2493743	.5943944 .6445851
.1135888	.126442 1.663291	1.611545 .904131	.6937207 .2598689	.6012176 .662988
.1266952	.1410314 1.642432	1.647129 .9064195	.7045787 .2702393	.6088532 .6710331
.1405128	.1564126 1.620826	1.680276 .9072864	.7140143 .2807359	.6169695 .6740805
.1533144	.1706627 1.605409	1.711958 .9110021	.7240094 .2898148	.6228942 .6871422
.1670304	.1859308 1.595159	1.746543 .9188374	.736274 .2982901	.6268969 .7146862
.1938528	.2157883 1.56137	1.814761 .9265157	.7568861 .3192408	.6404633 .7416779
.2200656	.2449672 1.530381	1.876787 .9331994	.7749488 .3394523	.6534322 .7651734
.2464816	.2743723 1.496335	1.941218 .9387765	.792587 .3622655	.6682996 .7847786
.2729992	.3038905 1.469301	1.994701 .9439464	.8070333 .3818399	.6805956 .8029527
.2986024	.3323909 1.44471	2.053174 .9526149	.8237101 .4024303	.6921805 .8334253
.3250184	.361796 1.415462	2.108144 .9564961	.8371581 .4252448	.7064831 .8470691
.351536	.3913142 1.387983	2.166757 .9628112	.8520409 .4493112	.7204701 .8692687
.378968	.4218503 1.359473	2.224785 .9678225	.8658278 .4750846	.7355794 .8868851
.4049776	.450803 1.333933	2.281321 .9739557	.8794509 .5004442	.7496626 .9084456
.4320032	.4808867 1.304114	2.341177 .9780016	.892381 .5303773	.766804 .9226681
.4598416	.5118751 1.282598	2.3968 .9860515	.906015 .5560391	.7796674 .9509663
.486156	.5411672 1.250725	2.455657 .9871057	.9166566 .5906251	.7995364 .9546722

Table 3 (continued) Run 132

.511556	.5694413 1.228779	2.51054 .9937494	.9288856 .6194062	.8138159 .9780272
.5381752	.5990726 1.195758	2.570474 .9930988	.9381948 .6596495	.8362895 .9757401
.5640832	.6279122 1.173724	2.625439 .9987842	.9493869 .6921768	.8519887 .995726
.5904992	.6573173 1.149215	2.67981 1.001647	.9588769 .7285452	.870159 1.005788
.6169152	.6867225 1.126673	2.731612 1.004598	.9677792 .7644263	.8875686 1.016163
.6311392	.702556 1.116735	2.757374 1.007035	.972588 .7817096	.8954677 1.02473
.6443472	.7172585 1.104381	2.78053 1.006028	.9753158 .8012388	.9054848 1.021189
.6575552	.7319611 1.093655	2.806668 1.007685	.9796918 .8204489	.9143648 1.027015
.6717792	.7477946 1.081953	2.828672 1.006502	.982076 .8400753	.9242541 1.022858
.6849872	.7624972 1.07188	2.850522 1.006648	.9850441 .8583183	.9329403 1.023371
.6981952	.7771997 1.065306	2.869585 1.008786	.988586 .8719403	.9386976 1.030886
.7124192	.7930332 1.057979	2.886423 1.009184	.9909613 .8860472	.9451987 1.032287
.7256272	.8077358 1.04648	2.904686 1.006135	.9917972 .9061904	.9555845 1.021567
.7388352	.8224384 1.037199	2.923594 1.005391	.9938169 .9242133	.9641351 1.01895
.7520432	.8371409 1.036041	2.934133 1.008844	.9968422 .929083	.9652127 1.03109
.7662672	.8529744 1.03267	2.943886 1.009797	.9985272 .9366914	.9683636 1.034441
.7794752	.867677 1.025984	2.958831 1.009736	1.000343 .9505735	.9746738 1.034226
.7947152	.8846415 1.017917	2.968508 1.005974	.9996606 .9649438	.9823982 1.021001
.8048752	.8959511 1.015853	2.972221 1.005538	.999896 .9690743	.9843942 1.019468
.8180832	.9106537 1.012208	2.979636 1.005126	1.00059 .9767057	.9879391 1.01802

Table 3 (continued) Run 132

.8312912	.9253563 1.012746	2.984816 1.007899	1.002596 .9776293	.9874141 1.027768
.8444992	.9400588 1.013739	2.989249 1.010808	1.004577 .9776541	.9864474 1.037993
.8587232	.9558923 1.009098	2.992201 1.007455	1.003265 .9853323	.9909844 1.026207
.8709152	.9694639 1.008779	2.992201 1.007137	1.003106 .9857956	.991297 1.02509
.8841232	.9841665 1.003213	2.996624 1.003482	1.001814 .9954314	.996797 1.012239
.8983472	1 1.002741	2.99736 1.003326	1.001824 .9963757	.9972664 1.011692
.9115552	1.014703 1.002623	2.998833 1.003841	1.002257 .9970408	.9973842 1.013502
.9146032	1.018095 1.003278	2.99736 1.003863	1.002092 .99558	.9967325 1.013581

DELSTAR,CM=	.2764242
THETA,CM=	.0583841
RE THETA=	3862.663

Table 3 (continued) Run 133

MEAN FLOW PROFILES, RUN NO 133

P0,N/M2= 97309
 T0,DEG K= 318.8889
 TW,DEG K= 172.2222
 X,CM= 42.5196
 RHDE,KG/M3= .0825342
 UE,M/SEC= 640.5367
 RHDEUE2,N/M2= 33775.73
 RHDEUE,KG/M2SEC= 52.83385
 RE,M-1= 6639482

Y(CM)	Y/D T/TE	M T0/TDE	U/UE RE/REE	RHD/RHDE H
.00508	.0058106 1.454867	1.024466 .632583	.4138968 .1996525	.6873482 .2011464
.0065024	.0074375 1.477278	1.019615 .6412745	.4150975 .194509	.6769208 .2200439
.0078232	.0089483 1.490507	1.026877 .6486094	.4199217 .1934748	.6709127 .2359916
.0087376	.0099942 1.509815	1.041147 .660214	.4285059 .1926817	.6623327 .2612228
.0104648	.0119698 1.572748	1.07326 .6954087	.4508349 .1877025	.6358299 .3377446
.012192	.0139454 1.629242	1.12301 .7331833	.4801305 .1870934	.6137822 .4198758
.0170688	.0195235 1.619663	1.208395 .7520462	.515115 .2029547	.6174124 .4608883
.0200152	.0228937 1.615729	1.249117 .7618409	.5318268 .2104961	.6189158 .4821843
.022352	.0255665 1.615341	1.282982 .7716138	.5461798 .2162743	.6190644 .5034331
.0250952	.0287042 1.623437	1.302096 .7812469	.5557044 .2179944	.6159769 .5243777
.0307848	.0352121 1.63287	1.339349 .7973345	.5732612 .2224559	.6124187 .5593561
.0334264	.0382336 1.624351	1.364067 .8009763	.5823157 .228193	.6156303 .5672743
.0387096	.0442766 1.615319	1.39147 .8052892	.5923603 .2345666	.6190728 .5766515

Table 3 (continued) Run 133

.044704	.0511331 1.605793	1.430694 .8133161	.6072596 .2431476	.6227453 .5941039
.0511048	.0584544 1.59832	1.462738 .8201823	.6194145 .2501942	.6256571 .6090327
.057912	.0662406 1.592198	1.485713 .8247931	.6279377 .2554702	.6280625 .6190578
.0644144	.0736781 1.581997	1.515252 .8295881	.6383673 .2628674	.6321124 .6294832
.0719328	.0822777 1.572693	1.541294 .8337064	.6474262 .2695698	.635852 .6384373
.078232	.0894829 1.563625	1.565442 .8373309	.6556715 .2759883	.6395394 .6463179
.0860552	.0984311 1.55665	1.586407 .8409885	.6629687 .281418	.6424053 .6542705
.0911352	.1042417 1.54905	1.605698 .8437385	.6693903 .2867748	.6455569 .6602497
.1038352	.1187682 1.536066	1.64352 .850234	.6822801 .2969711	.6510137 .6743724
.117856	.1348053 1.521619	1.68137 .8560012	.6947033 .3078182	.6571946 .6869118
.1304544	.1492156 1.509087	1.718926 .8628016	.7072894 .3183297	.6626525 .7016975
.1436624	.1643231 1.508196	1.746586 .8726834	.7184588 .3237176	.6630438 .7231828
.156972	.1795468 1.483391	1.782327 .8717777	.7271067 .3380569	.6741311 .7212137
.1710944	.1957002 1.470331	1.8173 .8774063	.7381032 .3489693	.6801191 .7334515
.1827784	.2090645 1.458231	1.848045 .8819965	.7474954 .358994	.6857626 .7434319
.2101088	.2403254 1.433408	1.912463 .89194	.766939 .3805469	.6976381 .7650514
.2365248	.2705404 1.410494	1.975747 .902627	.7859589 .4021371	.7089715 .7882876
.2629408	.3007554 1.392184	2.034824 .9146181	.8041891 .4218498	.7182957 .814359
.2907792	.3325973 1.36772	2.095604 .9232249	.820901 .4454588	.7311435 .8330724
.3167888	.3623475 1.350755	2.153622 .9357075	.8383795 .4659494	.7403266 .8602126

Table 3 (continued) Run 133

.3438144	.3932597 1.318598	2.212041 .9376023	.8508095 .4952415	.758381 .8643323
.370332	.4235909 1.29344	2.267984 .9430131	.863965 .5218966	.7731319 .8760966
.395732	.4526438 1.27638	2.322573 .9535638	.8789056 .5446945	.7834657 .8990364
.410972	.4700755 1.260771	2.354902 .9556054	.8856739 .5620938	.7931656 .9034754
.450596	.515398 1.234885	2.431644 .9685879	.9050992 .5979626	.809792 .9317025
.477012	.545613 1.208799	2.485283 .9710416	.9152419 .6302507	.8272671 .9370374
.503428	.575828 1.193977	2.53518 .9806315	.9278752 .6544722	.8375374 .9578882
.531876	.6083672 1.165187	2.591346 .9810999	.9369277 .6930701	.8582314 .9589066
.552196	.6316095 1.150898	2.634517 .9877307	.9466782 .7173763	.8688868 .9733235
.58166	.6653109 1.122131	2.690887 .9872536	.9547732 .7602945	.8911612 .9722863
.609092	.696688 1.105689	2.743904 .9956855	.9664252 .7922124	.9044138 .9906192
.636524	.7280651 1.085541	2.792618 .9985851	.97458 .8283439	.9211999 .9969237
.661924	.7571179 1.069533	2.829034 .9995968	.9799822 .8577034	.9349876 .9991234
.676148	.7733876 1.057504	2.852822 .9986277	.9826495 .8794722	.9456228 .9970163
.687324	.7861708 1.05466	2.868511 1.002746	.986724 .8878344	.9481729 1.005971
.702564	.8036026 1.047968	2.888836 1.005197	.9905578 .9025803	.9542279 1.0113
.715772	.8187101 1.043271	2.897826 1.004593	.9914112 .9114272	.9585236 1.009986
.72898	.8338175 1.035186	2.913494 1.003582	.9929017 .9269779	.9660101 1.007789
.733044	.838466 1.031382	2.920927 1.003109	.9936042 .9344296	.9695727 1.006761

Table 3 (continued) Run 133

.753364	.8617083 1.022567	2.940169 1.002825	.9958667 .9526458	.9779307 1.006142
.782828	.8954096 1.014419	2.957826 1.002427	.9978474 .9698322	.9857862 1.005276
.796036	.9105171 1.009843	2.965153 1.001055	.9980608 .9787974	.9902531 1.002294
.808228	.9244625 1.006782	2.971003 1.000533	.998513 .9851713	.9932638 1.00116
.822452	.9407321 1.006211	2.973924 1.001221	.999211 .9869738	.9938277 1.002656
.83566	.9558396 1.004386	2.976842 1.00066	.9992843 .9906167	.9956328 1.001434
.848868	.9709471 1.002573	2.98267 1.001356	1.000336 .9952326	.9974338 1.002948
.862076	.9860546 1.001972	2.984125 1.001381	1.000525 .9966077	.9980315 1.003003
.874268	.9994554 1	2.98558 .9994897	.9997545 1.000839	1.000545 .9988905
.887476	1.015107 .9985458	2.98558 .9985801	.9992994 1.002199	1.001456 .9969128
.900684	1.030215 1.002235	2.984853 1.001957	1.0009 .9964613	.99777 1.004254
.913892	1.045322 1.007497	2.981214 1.005645	1.0023 .987513	.9925591 1.012273

DELSTAR,CM=	.2504473
THETA,CM=	.0632969
RE THETA=	4202.583

TABLE 4
SUMMARY OF INTEGRAL PROPERTIES
AND
EDGE CONDITIONS

x Sta. cm	δ cm	δ^* cm	θ cm	Re_θ	P_w N/M ²	$\rho_e u_e$ Kg/M ² sec	$\rho_e u_e^2$ N/M ²
$T_w/T_{oe} = .94$							
35.05	.846	.2743	.0508	3273	2497	50.18	32286
38.79	.899	.2916	.0533	3487	2554	50.96	32693
42.52	.960	.3086	.0584	3816	2651	51.89	33176
$T_w/T_{oe} = .714$							
35.05	.820	.2441	.0518	3384	2567	51.06	32789
38.79	.856	.2609	.0536	3507	2550	50.91	32674
42.52	.899	.2764	.0584	3862	2663	52.32	33459
$T_w/T_{oe} = .54$							
35.05	.836	.2225	.0538	3509	2539	50.81	32626
38.79	.861	.2629	.0612	3964	2505	50.33	32344
42.52	.876	.2504	.0632	4203	2707	52.82	33775

TABLE 5
SUMMARY OF VELOCITY CORRELATION CALCULATIONS

x sta inches	T_w/T_{oe}	δ (1) cm	c_f (2)	c_f (3)	π (3)	δ (4) cm	c_f (4)	π (4)
35.05	.94	.846	.00199	.00196	.54	.765	.00188	.70
38.79		.899	.00196	.00192	.56	.800	.00183	.74
42.52		.960	.00192	.00183	.67	.848	.00176	.84
35.05	.714	.820	.00216	.00208	.55	.721	.00201	.70
38.79		.856	.00215	.00204	.58	.757	.00197	.73
42.52		.899	.00210	.00196	.67	.797	.00191	.80
35.05	.54	.836	.00233	.00228	.42	.721	.00221	.57
38.79		.861	.00227	.00206	.68	.800	.00204	.75
42.52		.876	.00224	.00204	.72	.780	.00199	.84

- (1) Determined from pitot profile
(2) Calculated from skin friction correlation (Reference 11)
(3) Calculated from velocity correlation using δ from pitot profile
(4) Calculated from velocity correlation (Reference 12)

TABLE 6

DERIVATIVES FOR SHEAR STRESS CALCULATIONS

x = 38.79 inches

T_w/T_{oe}	$\frac{d\delta}{dx}$	$\frac{\delta}{\rho_e u_e}$	$\frac{d\rho_e u_e}{dx}$	$\frac{\delta}{\rho_e u_e^2}$	$\frac{d\rho_e u_e^2}{dx}$	$\frac{1}{\rho_e u_e^2}$	$\frac{dp}{dx}$ (inch ⁻¹)
.94	.0169		.00404		.00328		.00063
.714	.0136		.00280		.00235		.000393
.54	.0184		.00445		.00409		.000693

REFERENCES

1. Van Driest, E.R., "The Turbulent Boundary Layer with Variable Prandtl Number", 50 Jahre Grenzschichtforschung Vierneg and Sohn, Braunschweig, 1955, pp 257-271
2. Bertram, M.H., and Neal, L., "Recent Experiments in Hypersonic Turbulent Boundary Layers", NASA-TMX-56355, May 1965
3. Lee, R.E., Yanta, W.J. and Leonas, A.C., "Velocity Profile, Skin Friction Balance, and Heat Transfer Measurements of the Turbulent Boundary Layer at Mach 5 and Zero Pressure Gradient", Naval Ordnance Laboratory, White Oak, TR 69-106, June 1969
4. Brott, D.L., Yanta, W.J., Voisient, R.L., and Lee, R.E., "An Experimental Investigation of the Compressible Turbulent Boundary Layer with a Favorable Pressure Gradient", Naval Ordnance Laboratory, White Oak, TR 69-143, August 1969
5. Walz, A., "Compressible Turbulent Boundary Layers", pp 300-350, Mechanique de La Turbulence, Centre National de la Recherche Scientifique, Paris 1962
6. Bushnell, D.M., Johnson, C.B., Harvey, W.D. and Feller, W.V., "Comparison of Prediction Methods and Studies of Relaxation in Hypersonic Turbulent Nozzle Wall Boundary Layers", NASA TND-5433, 1969
7. Feller, W.V., "Effects of Upstream Wall Temperatures on Hypersonic Tunnel Wall Boundary Layer Profile Measurements", AIAA Journal, Vol. 11, No. 4, pp 556-557, April 1973
8. Meier, H.U., Voisinet, R.L., and Gates, D.F., "Temperature Distributions Using the Law-of-the-Wall for Compressible Flow with Variable Turbulent Prandtl Numbers", Paper No. 74-596, AIAA 7th Fluid & Plasma Dynamics Conference, June 1974
9. Whitfield, D.L., and High, M.D., "Velocity-Temperature Relations in Turbulent Boundary Layers with Non-Unity Prandtl Numbers", AIAA Journal, Vol. 15, No. 3, pp 431-434, March 1977
10. Gates, D.G., "Measurements of Upstream History Effects in Compressible Turbulent Boundary Layers", Naval Ordnance Laboratory, White Oak, TR 73-152, July 1973
11. Hopkins, E.J., and Inouye, M., "An Evaluation of Theories for Predicting Turbulent Skin Friction and Heat Transfer on Flat Plates at Supersonic and Hypersonic Mach Numbers", AIAA Journal, Vol. 9, No. 6, pp 993-1003, June 1971

REFERENCES

(Continued)

12. Coles, D.E., "The Young Person's Guide to the Data", Proceedings AFOSR-IFP - Stanford Conference on Computation of Turbulent Boundary Layers, Vol. 2, edited by D.E. Coles and E.A. Hirst, Stanford University, 1969
13. Van Driest, E.R., "Turbulent Boundary Layer in Compressible Fluids", Journal of Aeronautical Sciences, Vol. 18, No. 3, pp 145-160, March 1951
14. Horstman, C.C. and Owen, F.K. , "Turbulent Properties of a Compressible Boundary Layer", AIAA Journal, Vol. 10, No. 11, pp 1418-1424, Nov. 1972
15. Sandborn, V.A., "A Review of Turbulence Measurements in Compressible Flow", NASA TMX-62, 337 March 1974
16. Yanta, W.J. and Lee, R.E., "Determination of Turbulence Transport Properties with the Laser Doppler Velocimeter and Conventional Time Averaged Mean Flow Measurements at Mach 3", Paper No. 74-575, AIAA 7th Fluid & Plasma Dynamics Conference, June 1974
17. Maise, G. and McDonald, H. , "Mixing Length and Kinematic Eddy Viscosity in a Compressible Boundary Layer", AIAA Journal, Vol. 6, No. 1, pp 73-79, January 1968
18. Lee, R.E. and Smith, R.A., "Evaluation of the Turbulent Transport Terms for a Two-Dimensional Nozzle Wall Boundary Layer Flow at Mach 5 and with Pressure Gradient, Heat Transfer and Upstream Effects", Paper No. 74-96, AIAA 12th Aerospace Sciences Meeting, January 1974
19. Watson, R.D., "Wall Cooling Effects on Hypersonic Transitional/Turbulent Boundary Layers at High Reynolds Numbers", Paper No. 75-834, AIAA 8th Fluid and Plasma Dynamics Conference, June 1975
20. Bushnell, D.M., Cary, Jr., A.M., and Holley, B.B., "Mixing Length in Low Reynolds Number Compressible Turbulent Boundary Layers", AIAA Journal, Vol. 13, No. 8, pp 1119-1121, August 1975
21. Watson, R.D., "Prediction of Outer Layer Mixing Lengths in Turbulent Boundary Layers", AIAA Journal, Vol. 15, No. 4, pp 591-592, April 1977
22. Fletcher, R.H., "Prediction of Turbulent Boundary Layers at Low Reynolds Numbers," AIAA Journal, Vol. 14, No. 5, pp 696-698, May 1976

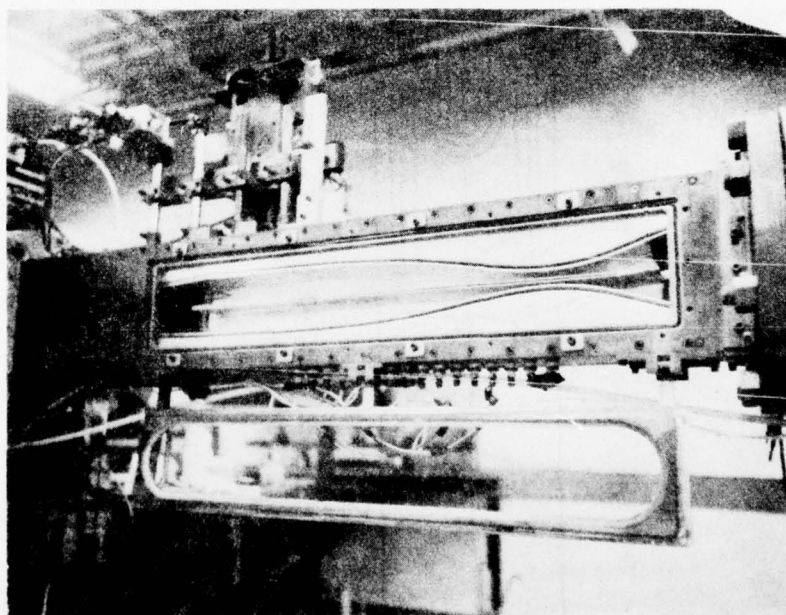
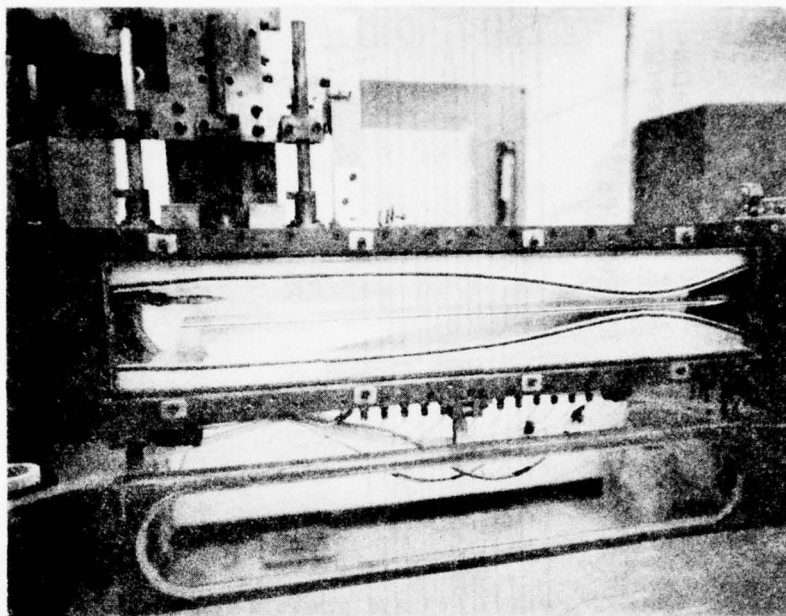


Figure 1. Photograph of flat plate installed in wind tunnel

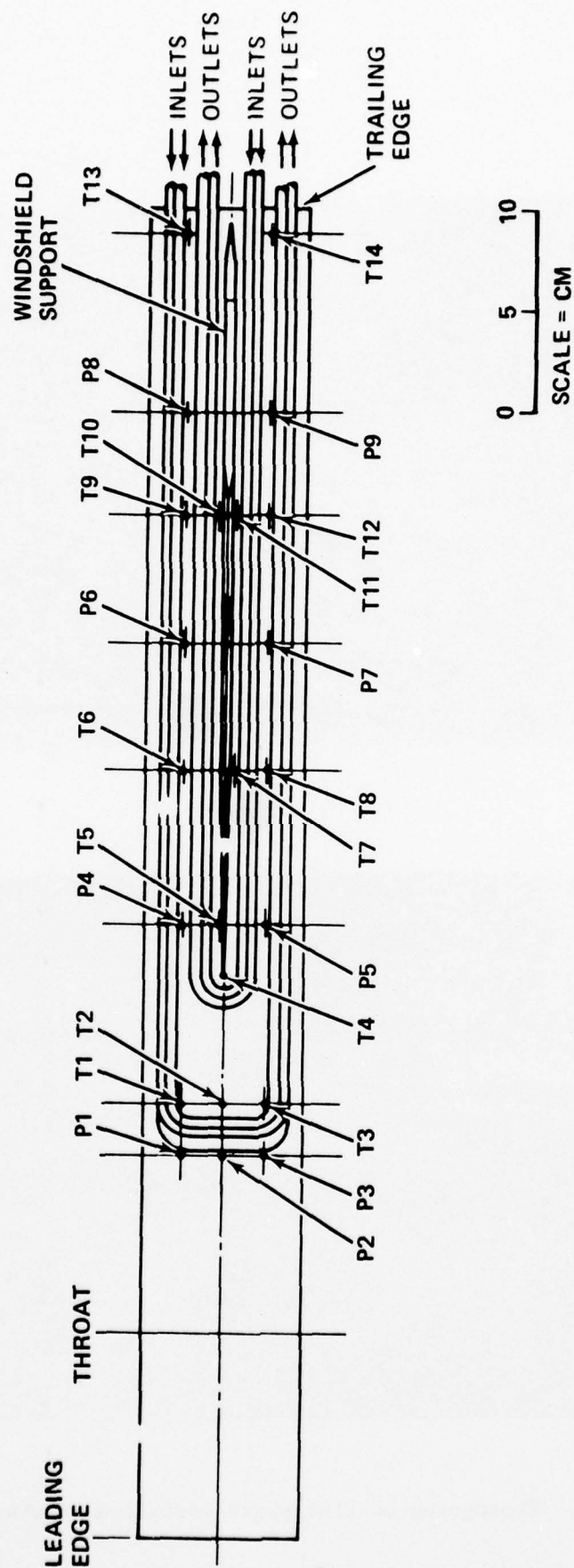


Figure 2. Schematic of flat plate underside showing coolings and location of thermocouples (T1, T2,...) and static pressure taps (p1, p2,...)

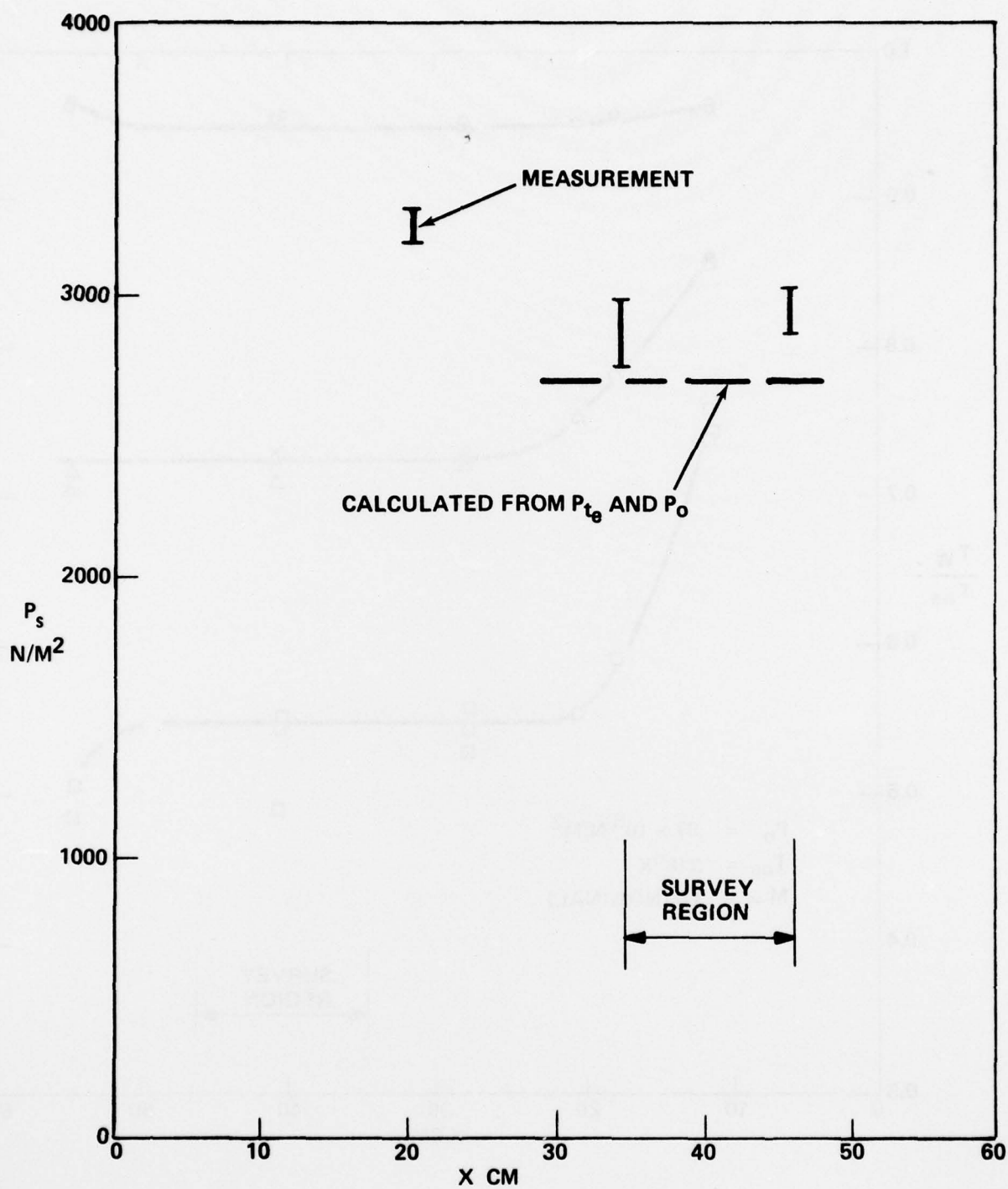


Figure 3. Typical surface pressure distribution

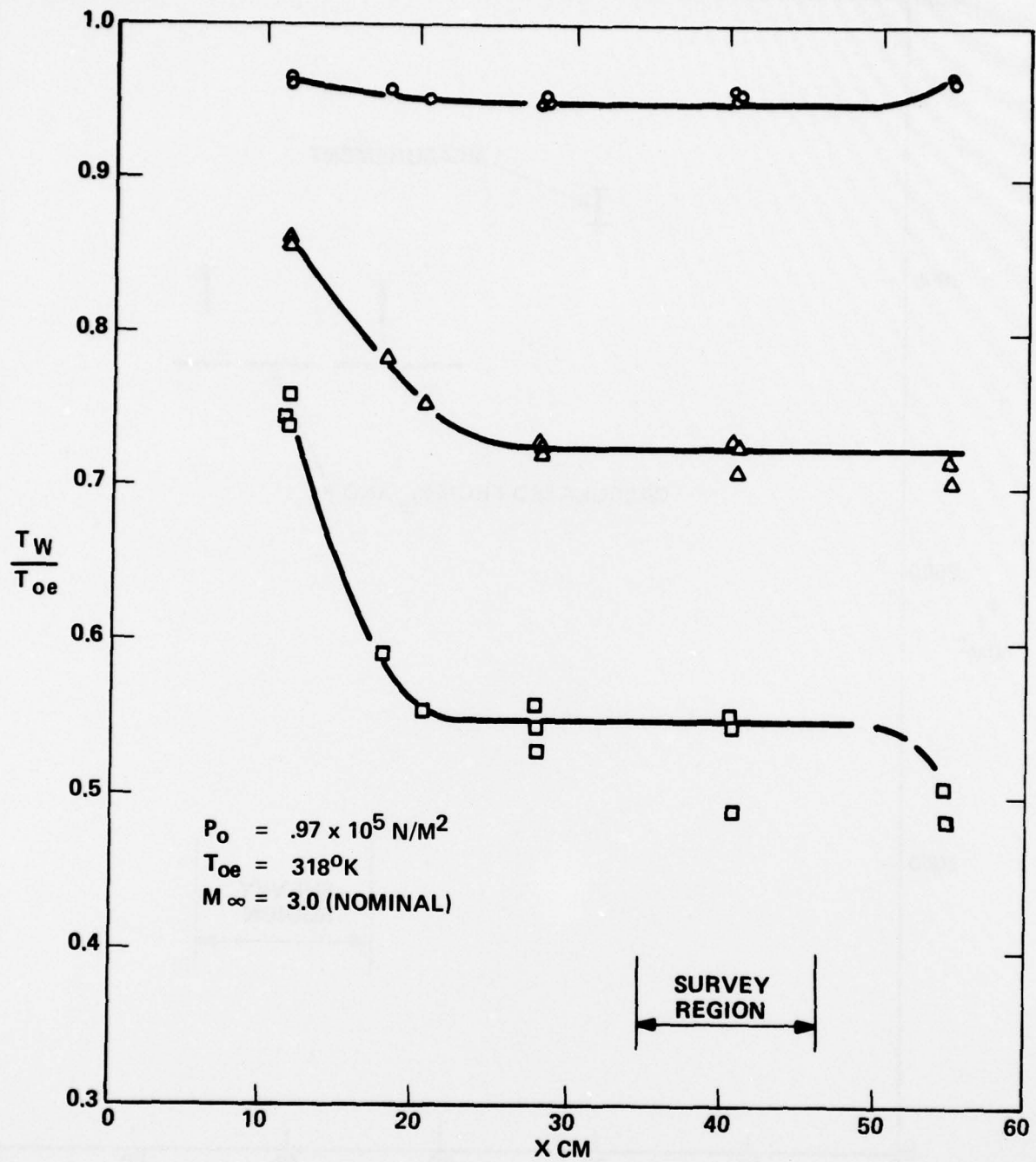


Figure 4. Typical surface temperature distributions

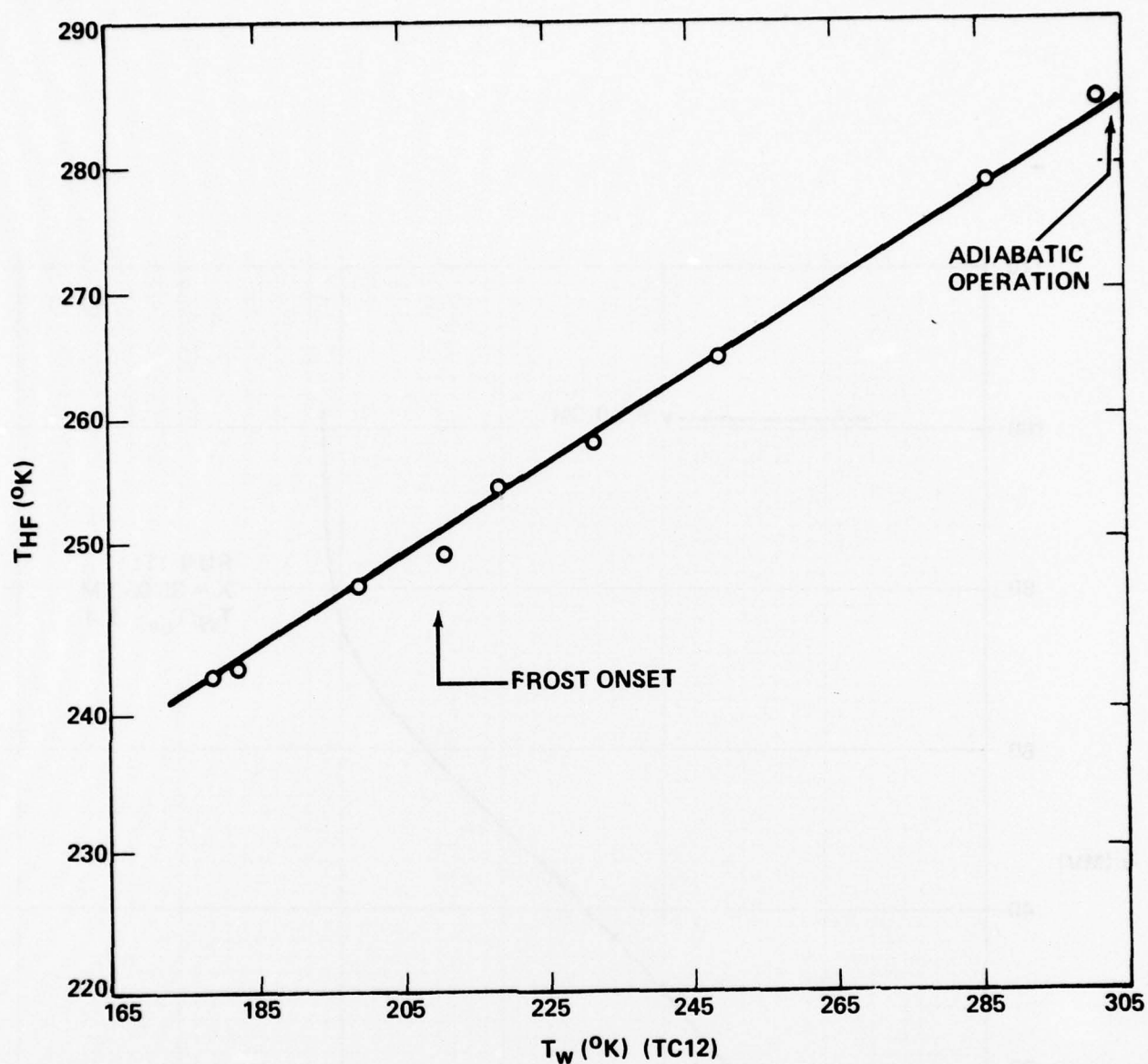


Figure 5. Variation of hot film temperature T_{HF} held just above plate surface, as a function of wall temperature. Calibration of T_{HF} is approximate and is only meant to indicate smoothness of response through the frost formation stage.

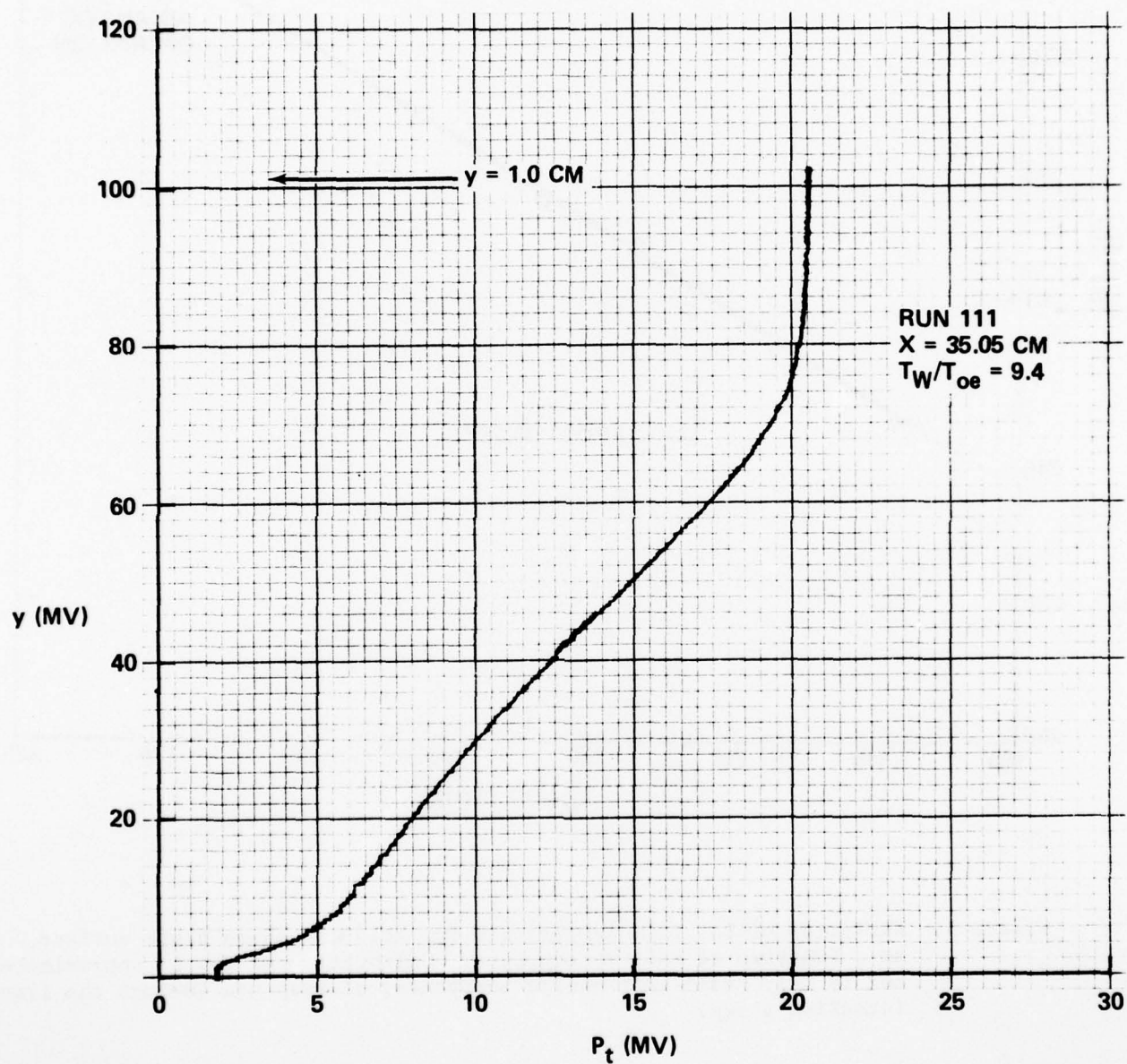


Figure 6. Typical X-Y plotter record of pitot pressure profile

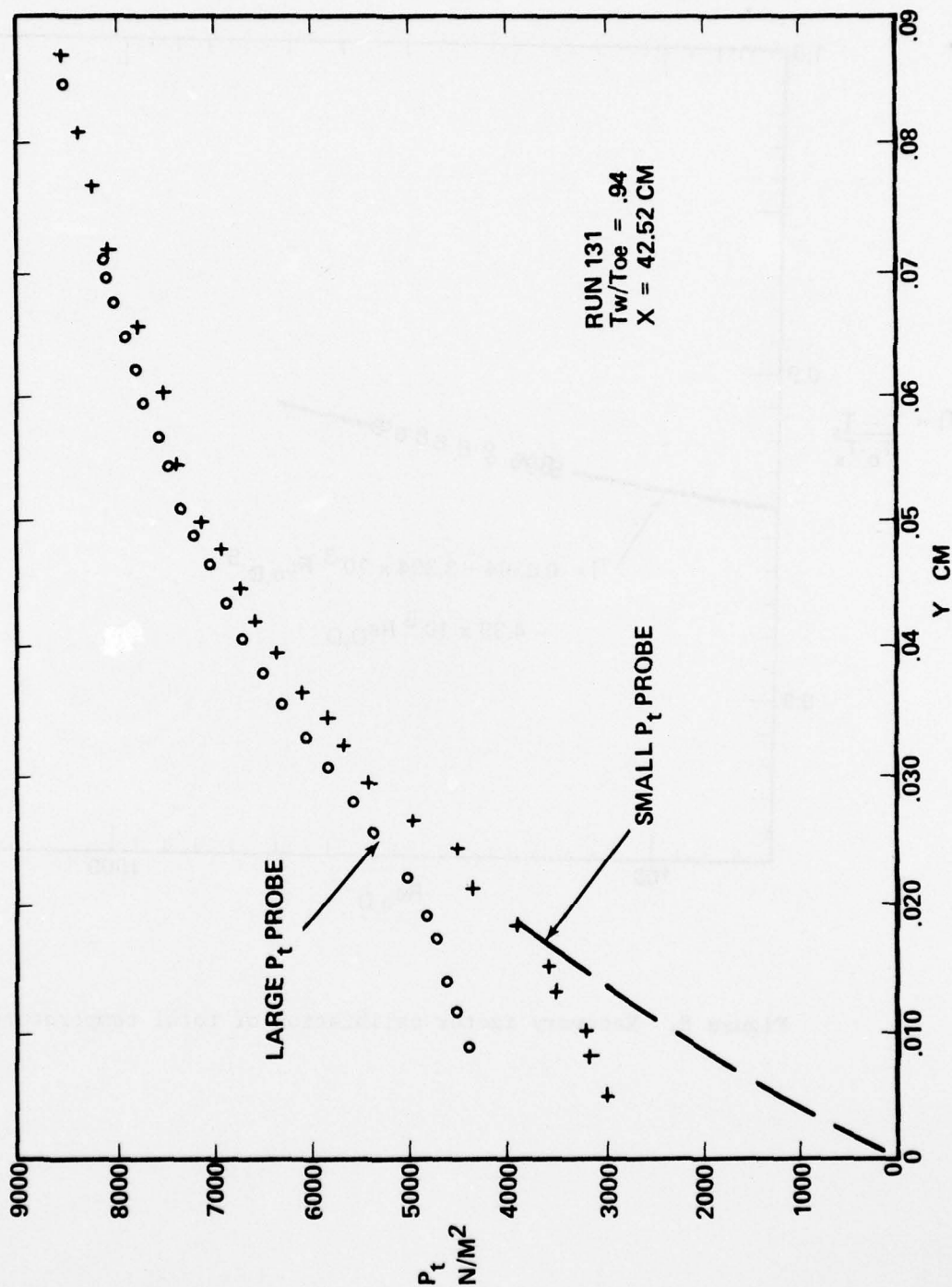


Figure 7. Typical pitot pressure measurements showing effect of probe size

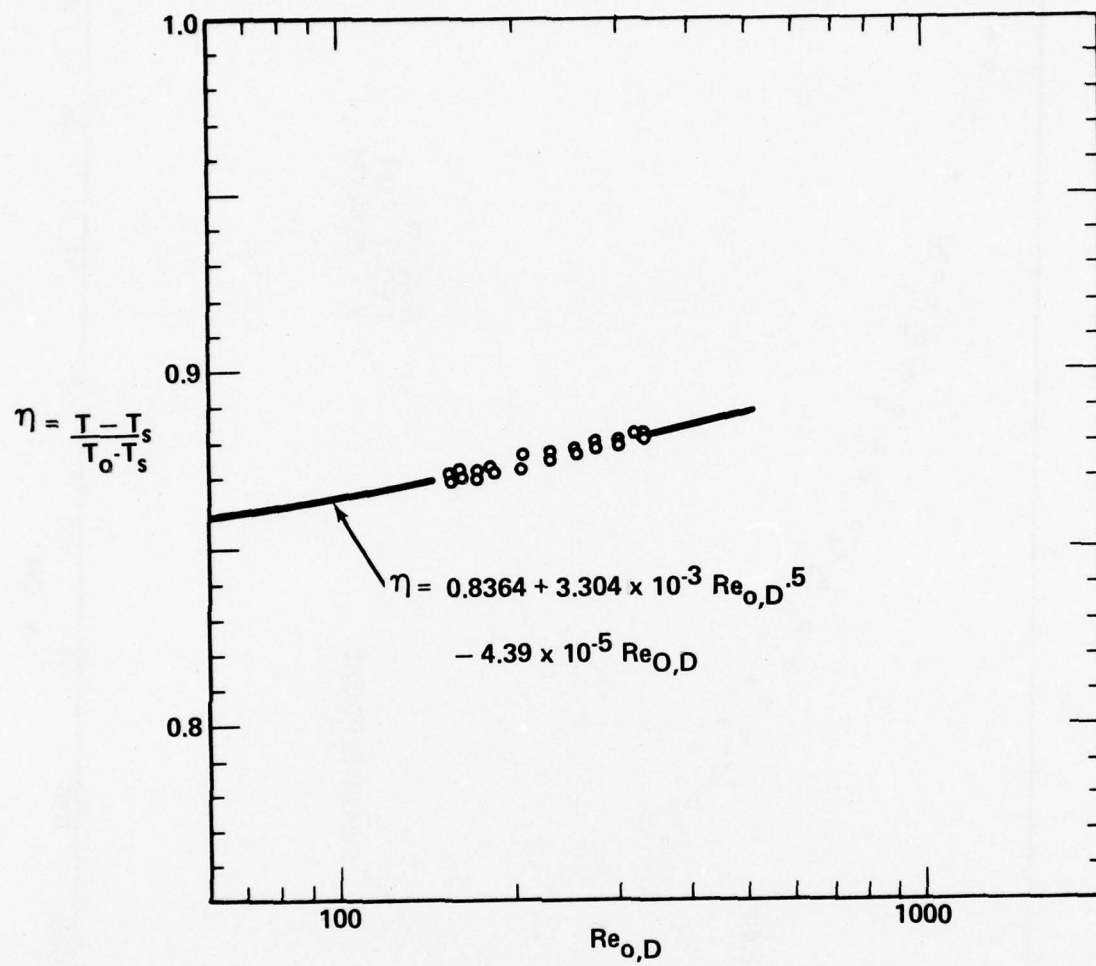


Figure 8. Recovery factor calibration of total temperature probe

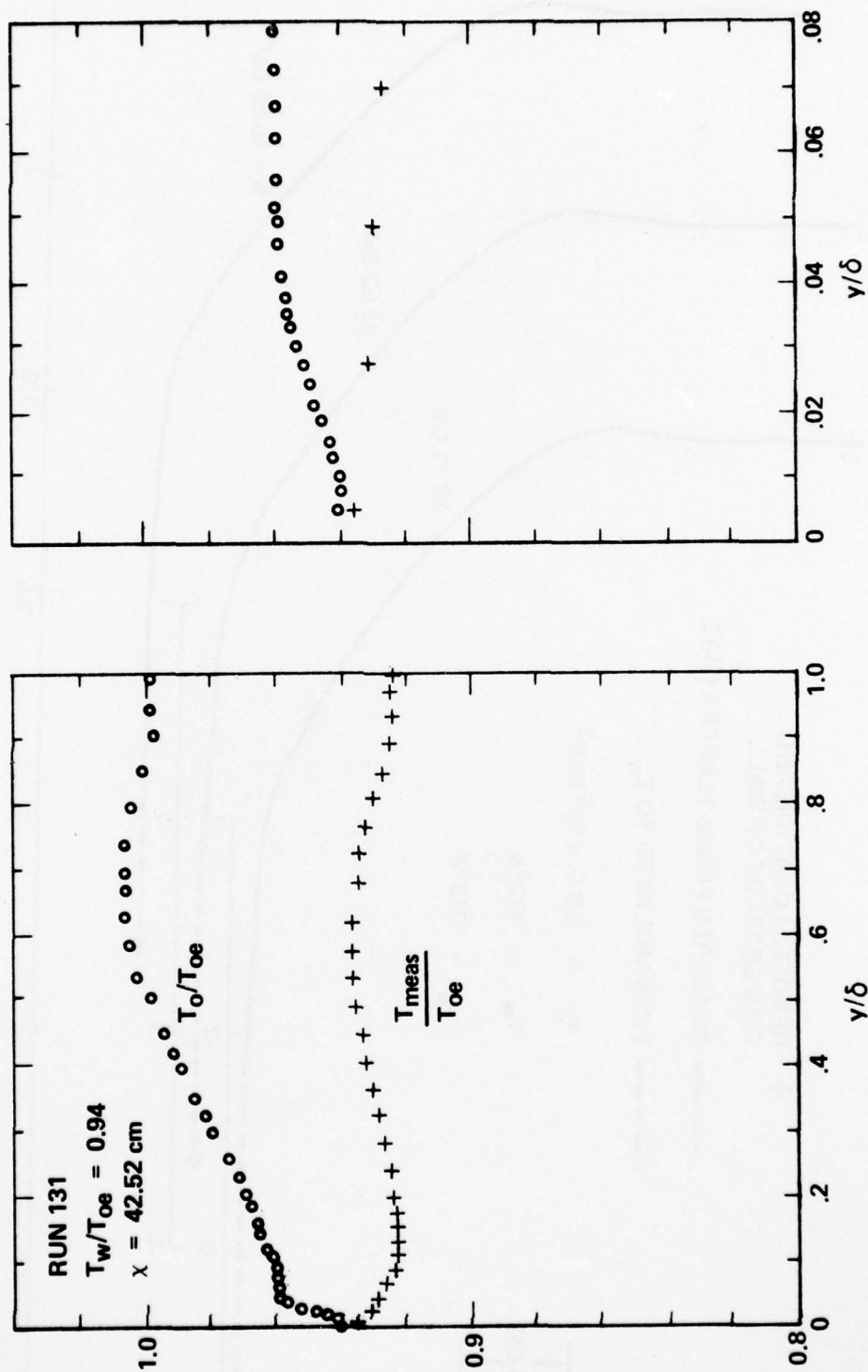


Figure 9. Recovery temperature and computed total temperature profiles for adiabatic wall condition

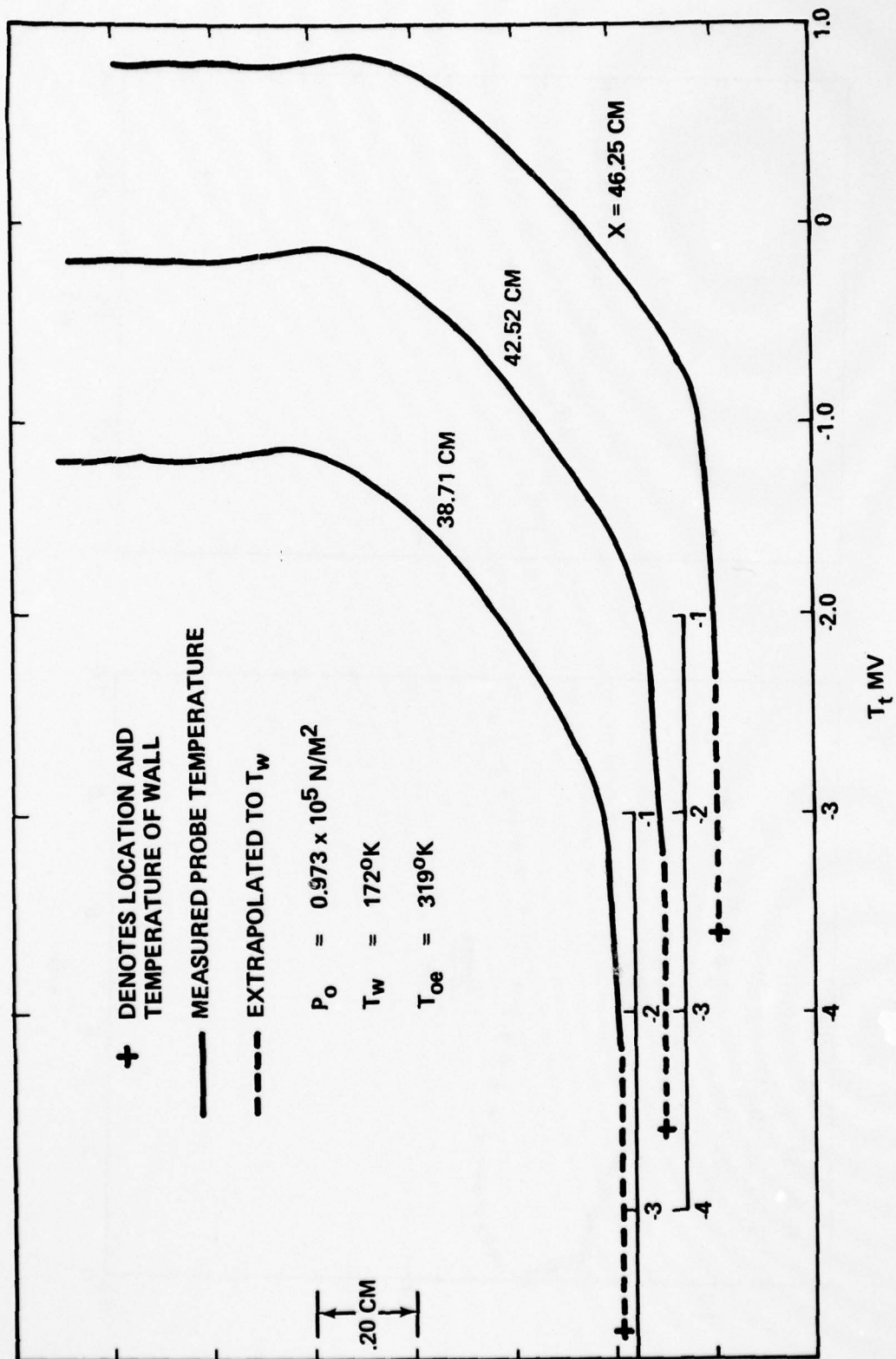


Figure 10. Typical recovery temperature profiles for $T_W = 172^\circ\text{K}$

AD-A046 365

FORD AEROSPACE AND COMMUNICATIONS CORP NEWPORT BEACH --ETC F/G 20/4
INVESTIGATION OF THE STRUCTURE OF A COOLED WALL TURBULENT SUPER--ETC(U)
OCT 77 A J LADERMAN, A DEMETRIADES DAA629-75-C-0014

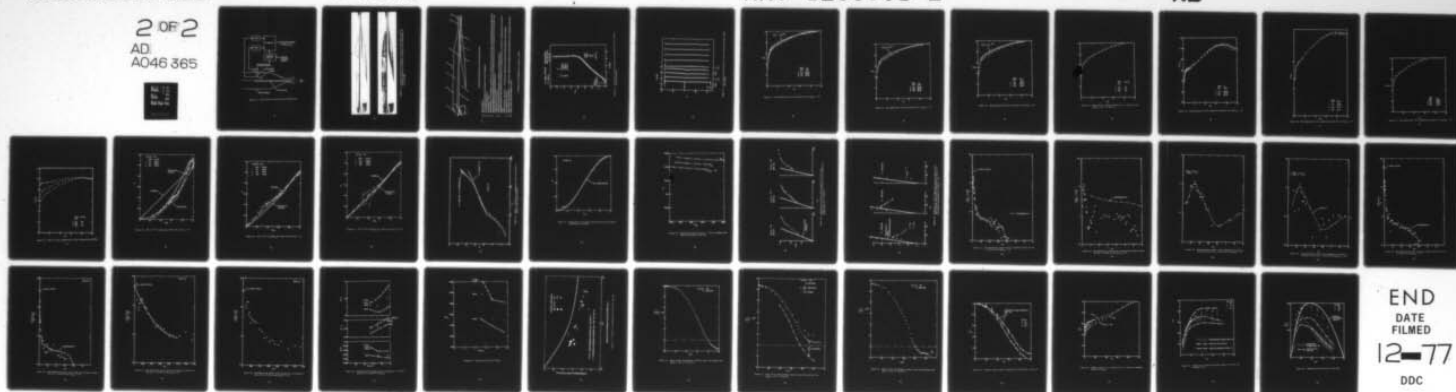
UNCLASSIFIED

U-6370

ARO-12505.1-E

NL

2 OF 2
AD
A046 365



END
DATE
FILMED
12-77
DDC

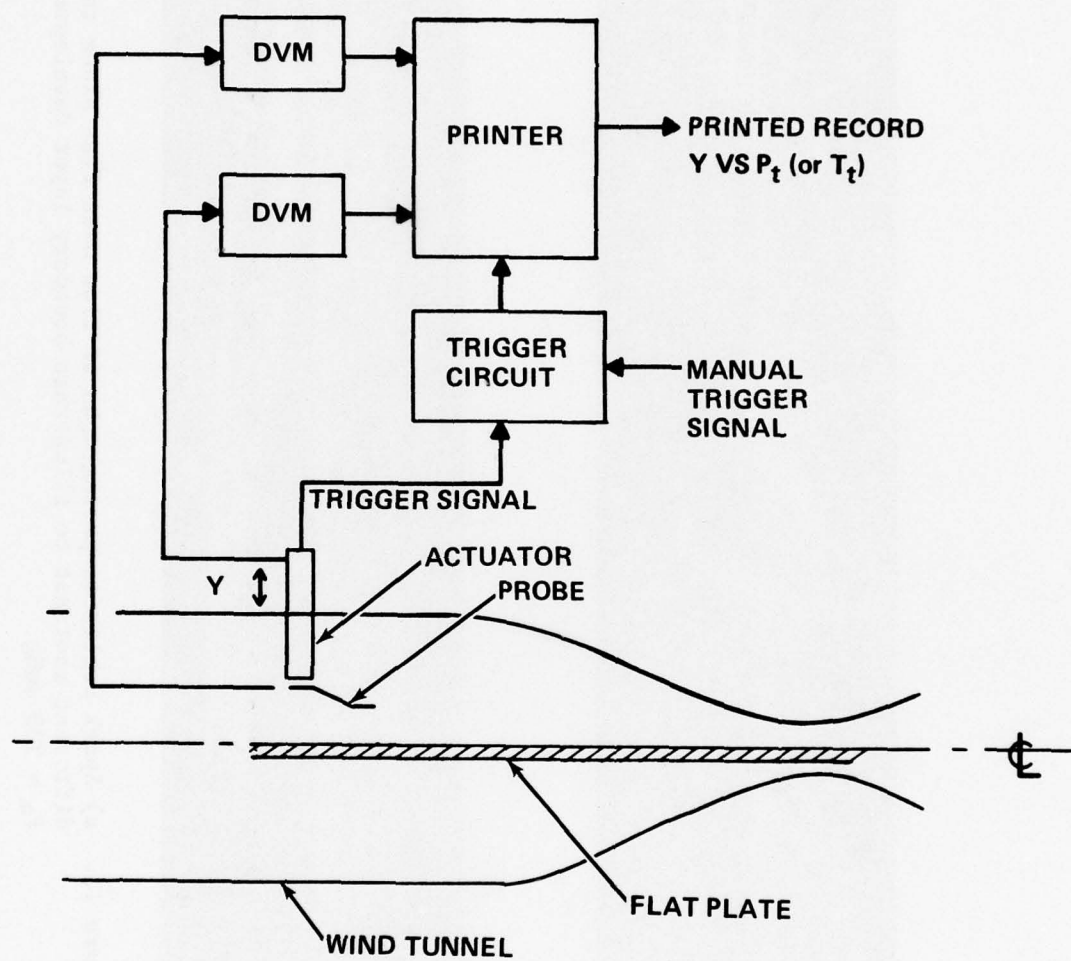


Figure 11. Block diagram of mean flow instrumentation

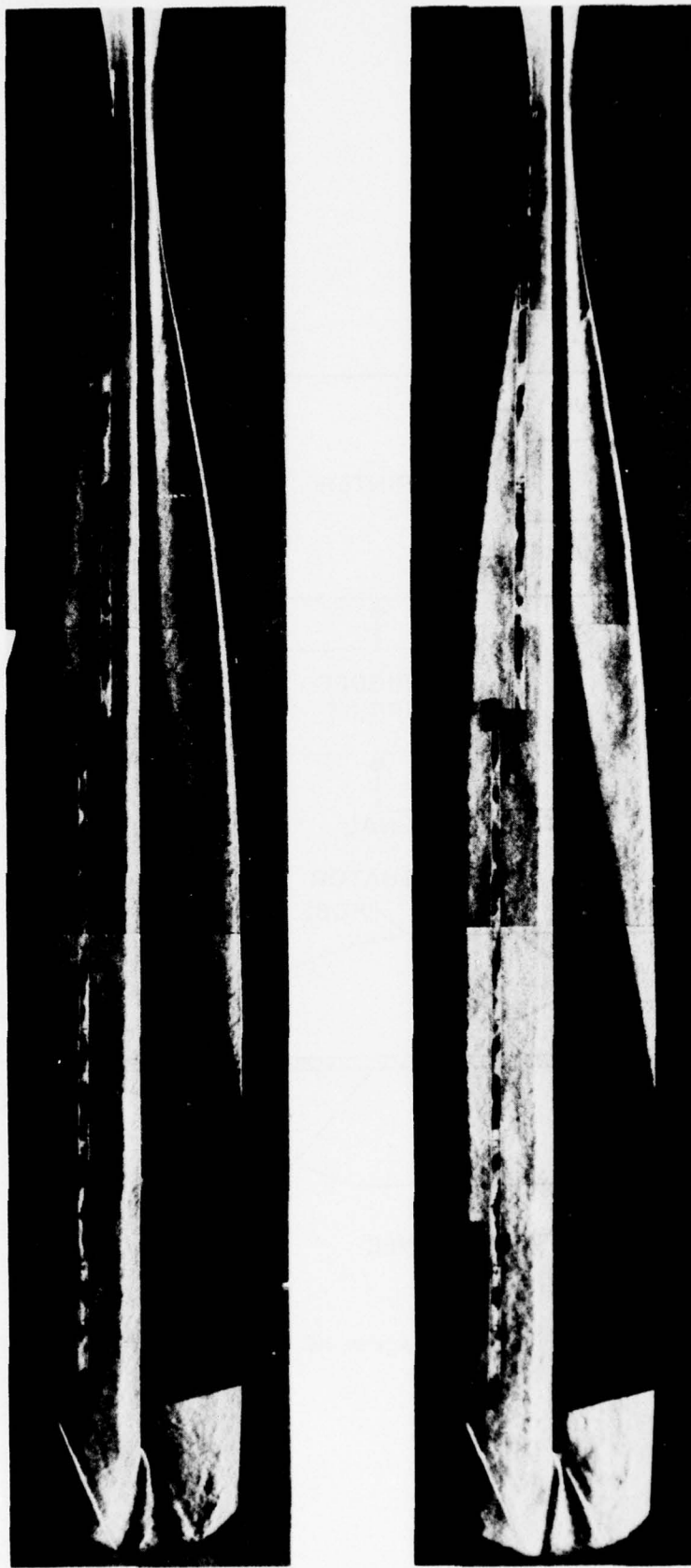
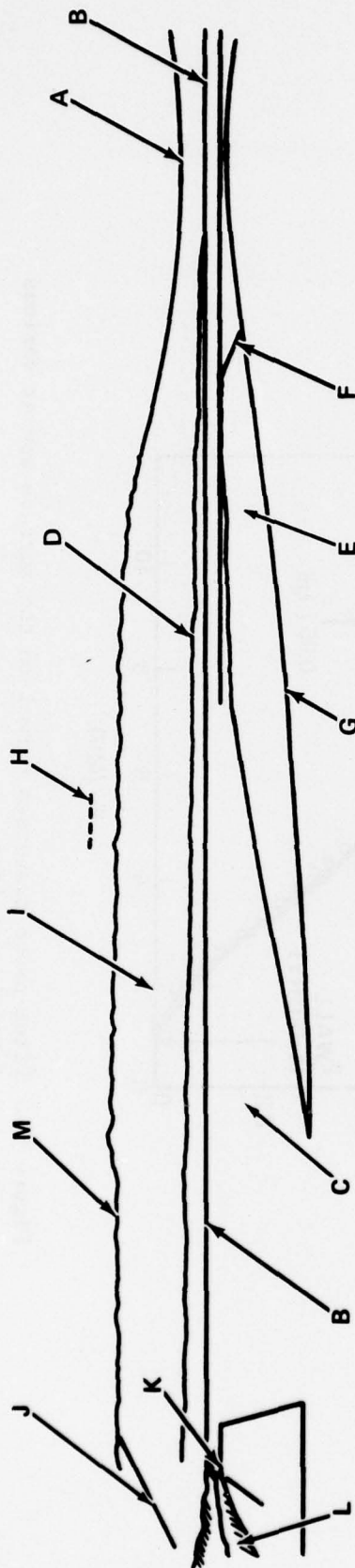


Figure 12. a) Spark Schlieren photographs of flow over flat plate taken at different contrast to illustrate boundary layer development at $P_0 = 730 \text{ mmHg}$



FEATURES DISTINGUISHED IN THE TBL-H SCHLIEREN TESTS

- A. NOZZLE THROAT
- B. PLATE (WORKING) SURFACE (LIES ON NOZZLE PLANE OF SYMMETRY)
- C. PLATE SUPPORT WINDSHIELD
- D. TEST BOUNDARY LAYER
- E. NON-UNIFORM ($M_{\infty} \approx 4$) SUPERSONIC FLOW UNDER PLATE, GENERATED BY AREA RATIO HIGHER THAN CORRESPONDING RATIO ABOVE PLATE
- F. SHOCKLET EMANATING FROM OPEN .08 CM DIA. STATIC TAP ON LOWER NOZZLE BLOCK SURFACE, DEMONSTRATING THE SUPERSONIC FLOW IN REGION E AND THE SCHLIEREN SYSTEM SENSITIVITY.
- G. LOWER NOZZLE BLOCK SURFACE
- H. UPPER NOZZLE BLOCK SURFACE, OBSCURED BY BOUNDARY-LAYER GROWTH OVER IT
- I. UNIFORM SUPERSONIC FLOW IN WORKING VOLUME ABOVE PLATE (LONG OBJECT SEEN IN THIS REGION IS TRANSPARENT SCALE TAPED ON GLASS.)
- J. SHOCK FROM PARTLY PROTRUDING TUATOR STRUT, GENERATED ON PURPOSE TO SHOW SUPERSONIC FLOW IN REGION I
- K. PLATE SQUARE TRAILING EDGE
- L. WAKE OF PLATE, DEFLECTED DOWNWARD BECAUSE OF HIGHER MACH NUMBER AND LOWER PRESSURE IN PLATE UNDERSIDE (SEE ITEM E).
- M. EDGE OF NOZZLE CEILING BOUNDARY LAYER

b) Features distinguished in Schlieren records

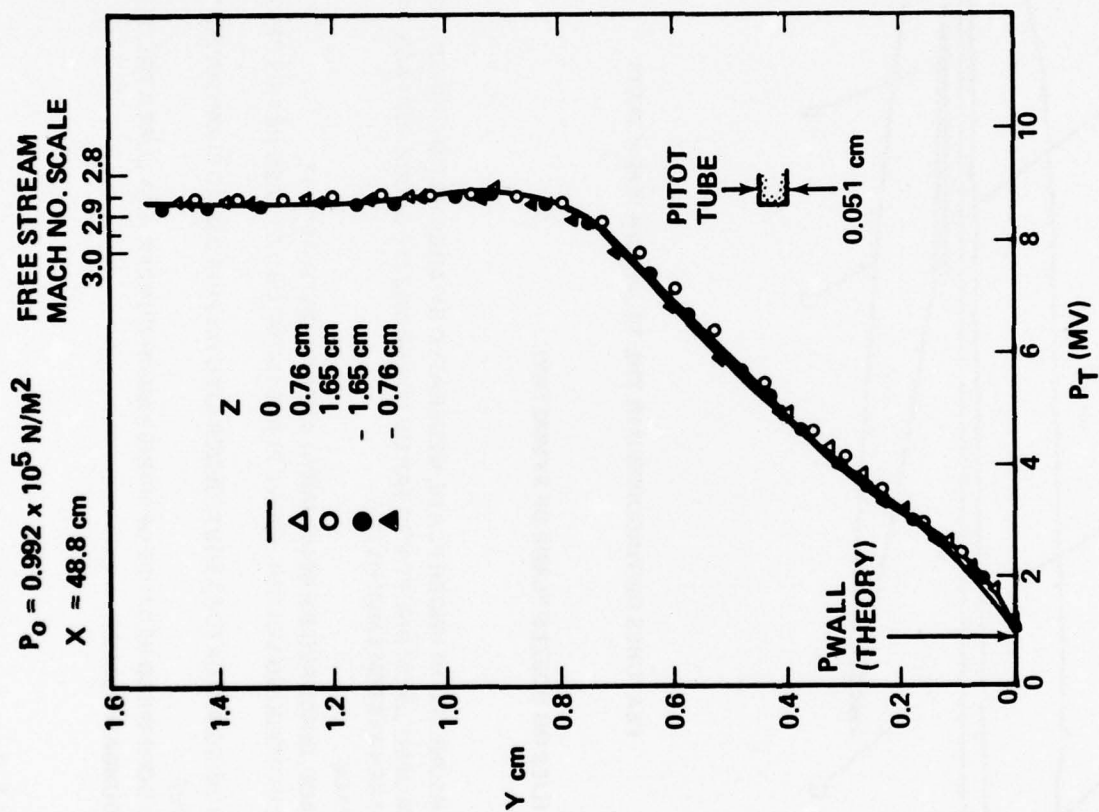


Figure 13. Pitot probe traverses normal to the surface and at various lateral positions

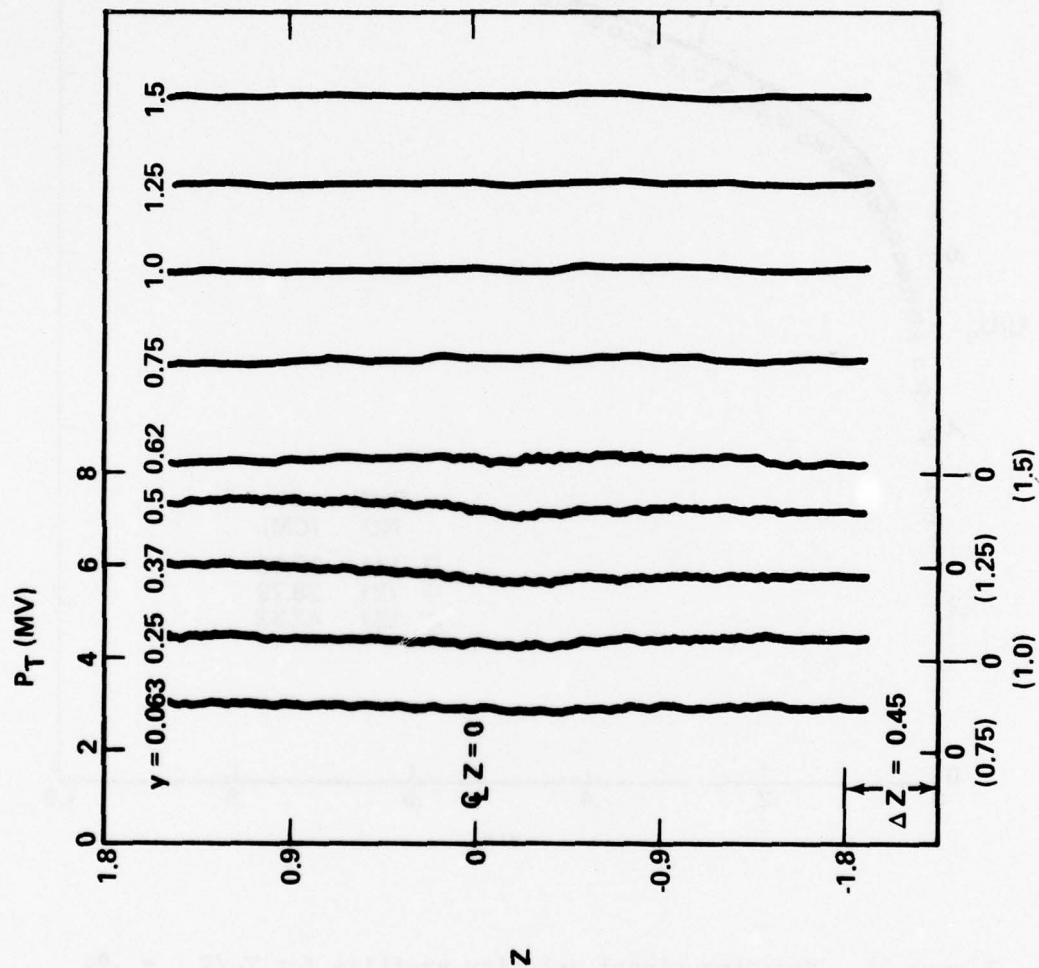


Figure 14. Pitot probe traces parallel to and at various distances from the surface

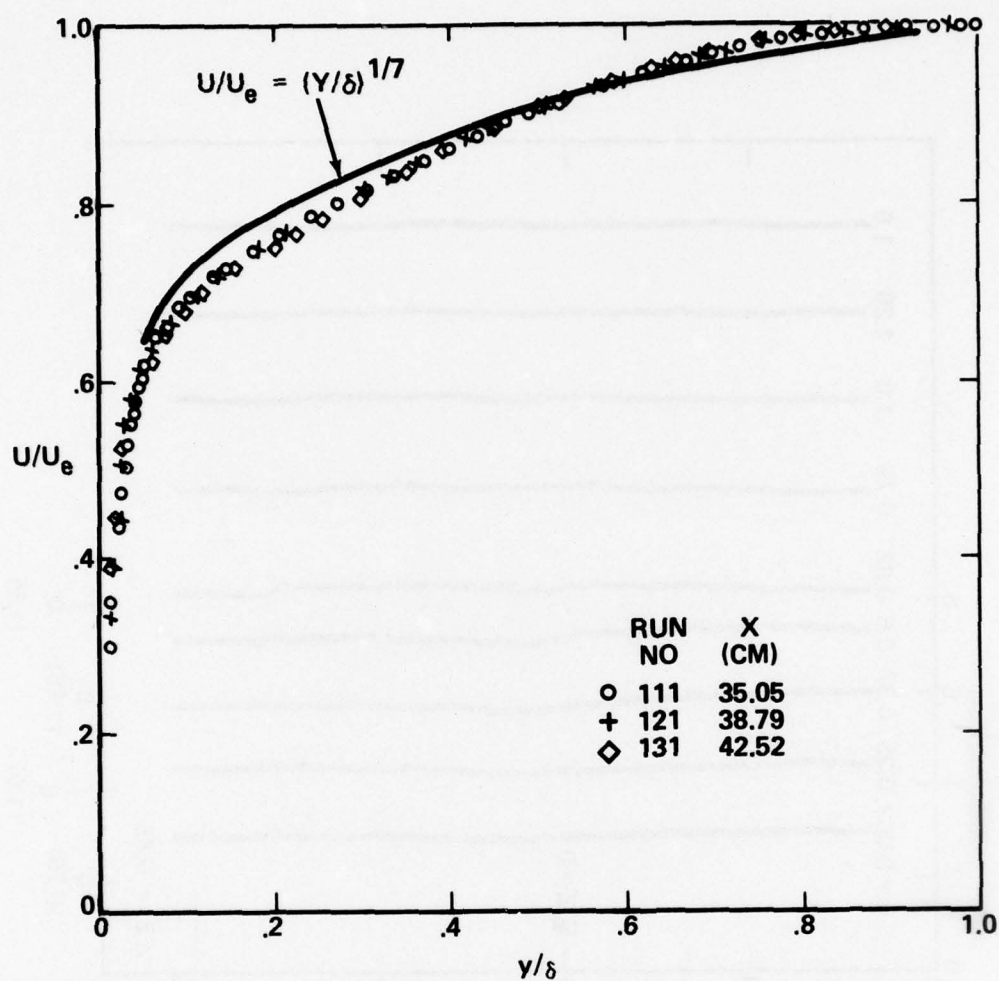


Figure 15. Non-dimensional velocity profiles for $T_w/T_{oe} = .94$

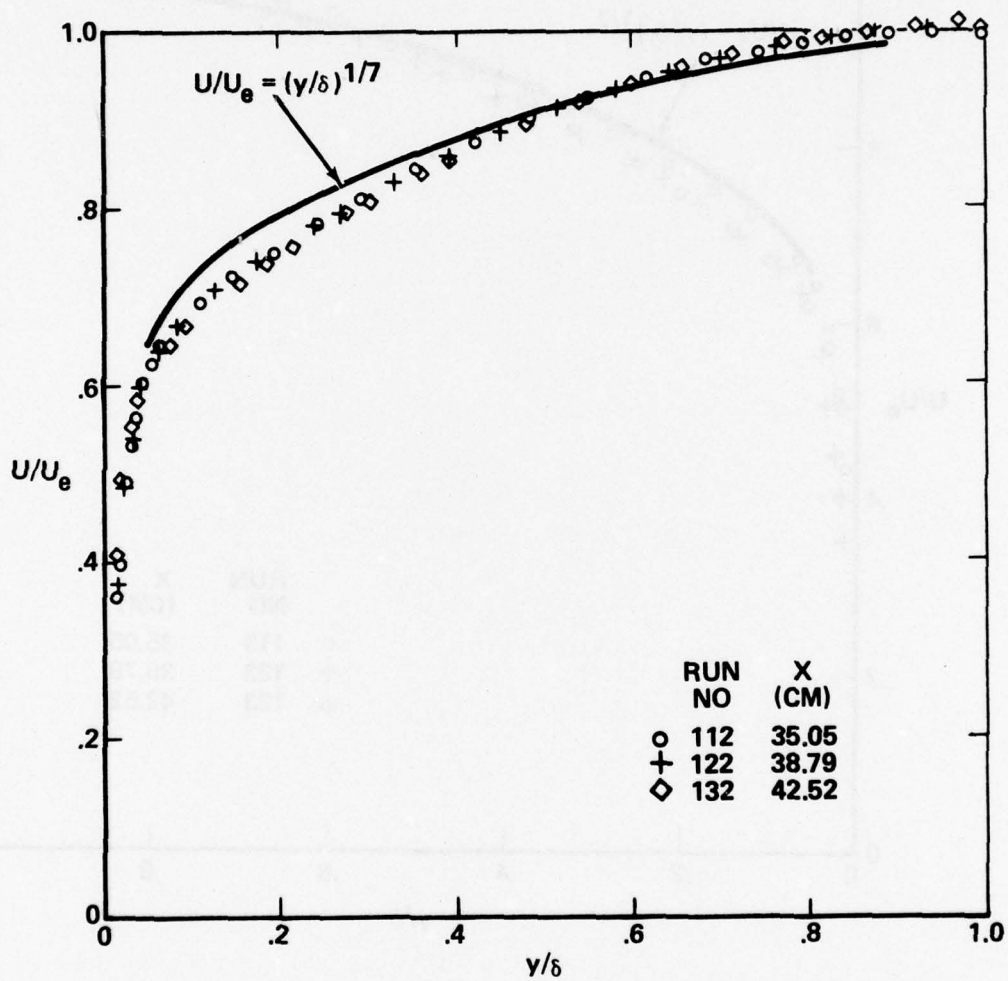


Figure 16. Non-dimensional velocity profiles for $T_w/T_{oe} = .71$

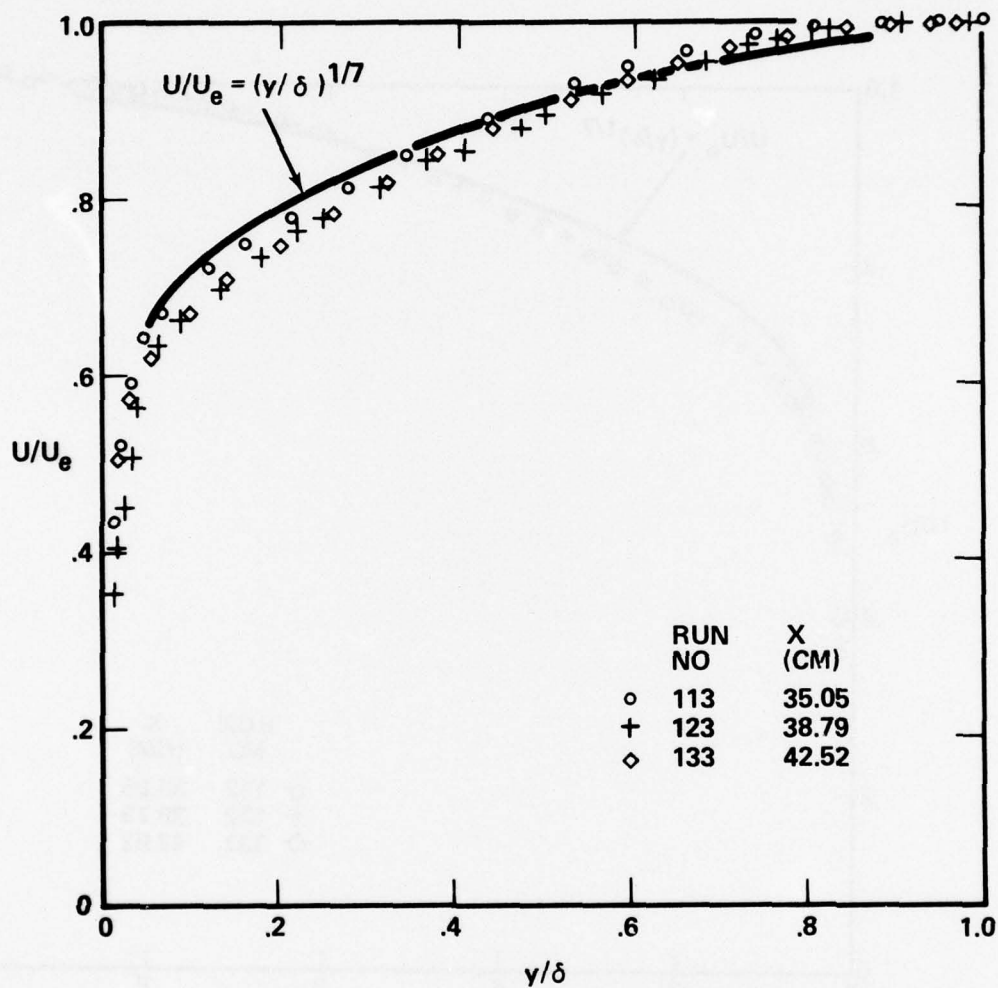


Figure 17. Non-dimensional velocity profiles for $T_w/T_{oe} = .54$

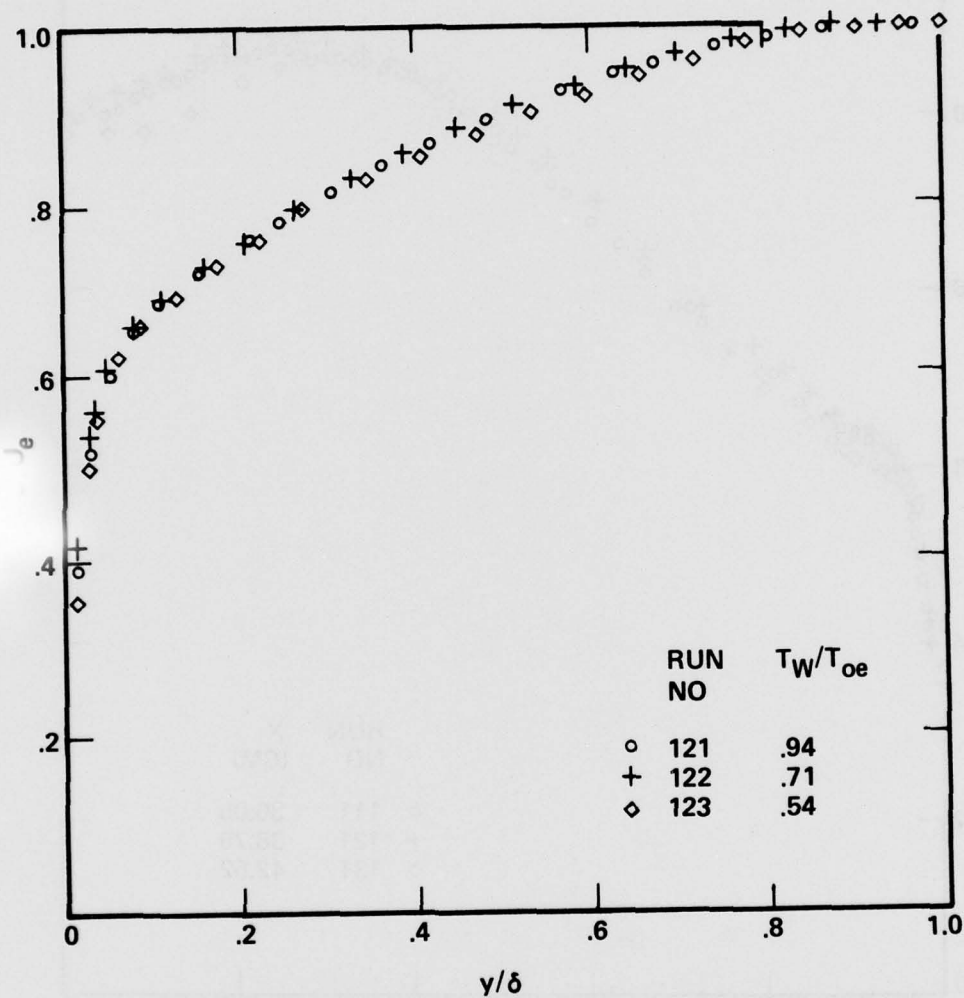


Figure 18. Comparison of velocity profiles at $x = 38.79$ cm for $T_w/T_{oe} = .94, .71$ and $.54$

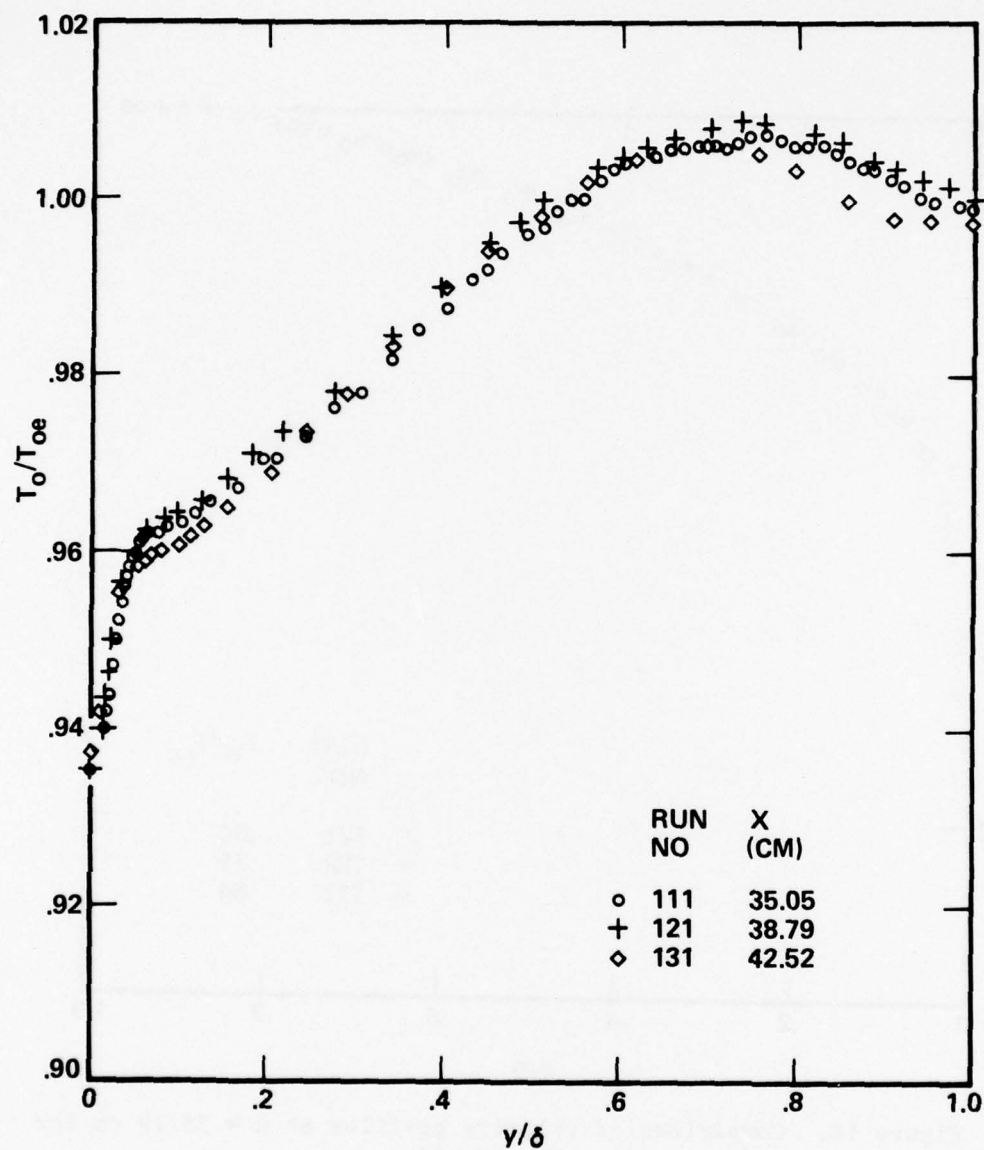


Figure 19. Non-dimensional total temperature profiles for $T_w/T_{oe} = .94$

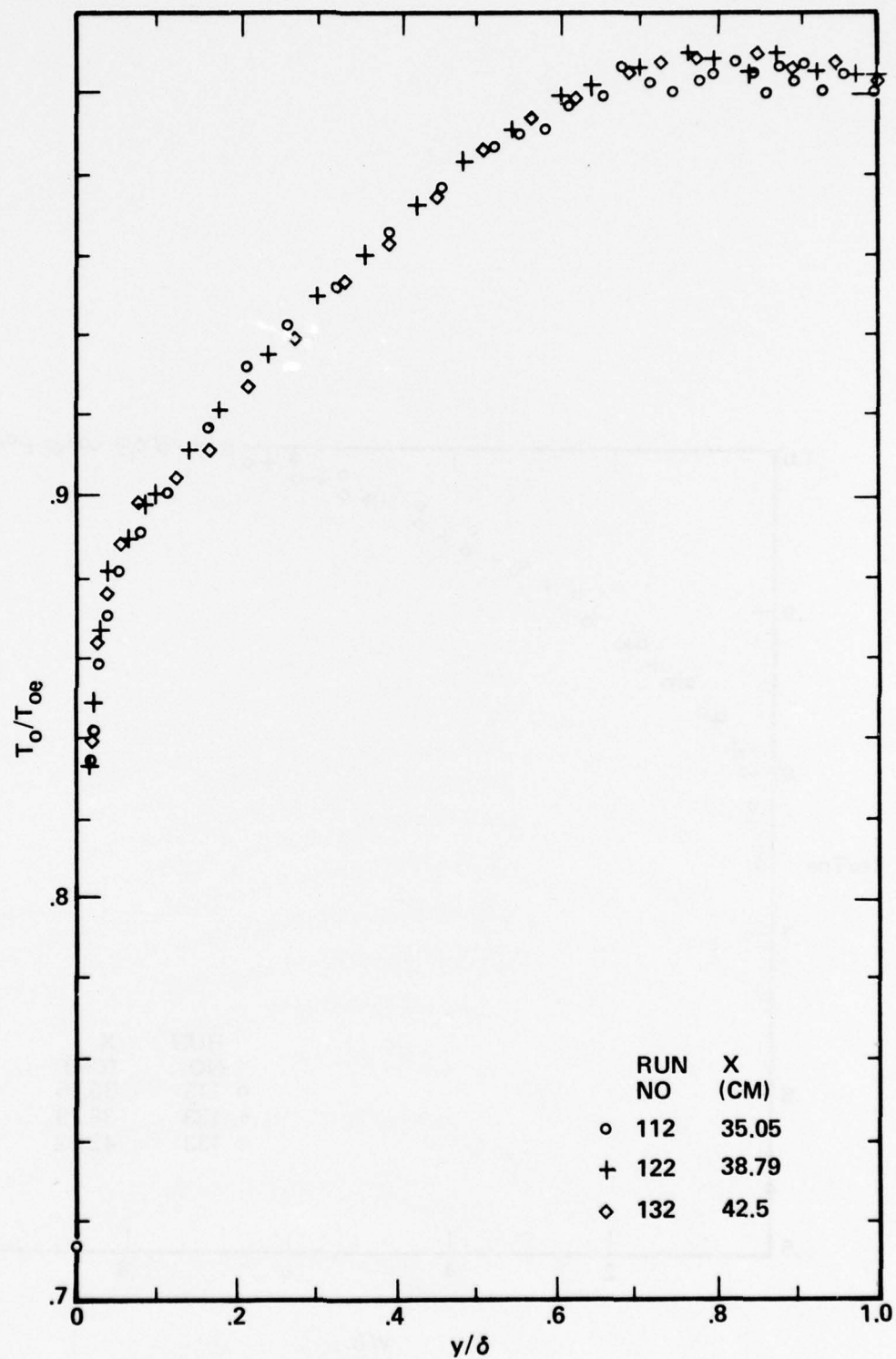


Figure 20. Non-dimensional total temperature profiles for $T_w/T_{oe} = .71$

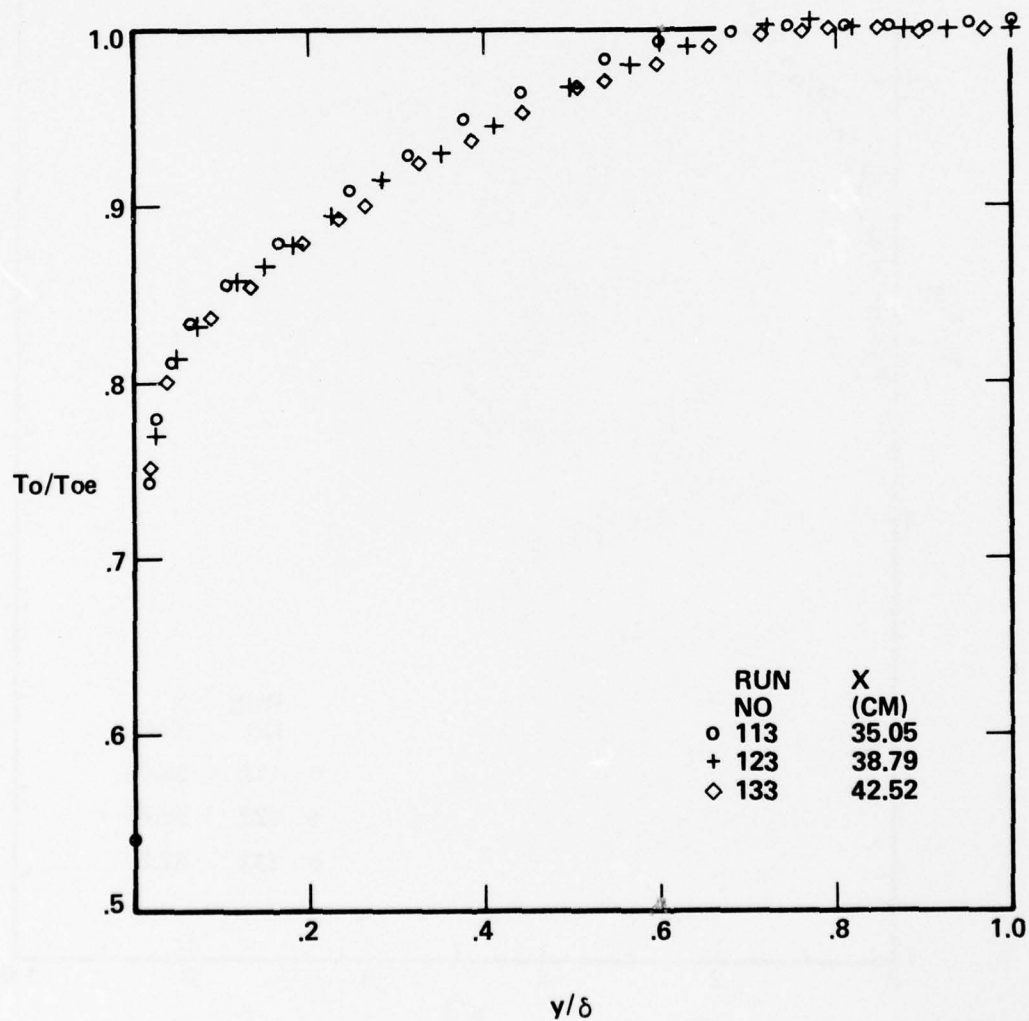


Figure 21. Non-dimensional total temperature profiles for $T_w/T_{oe} = .54$

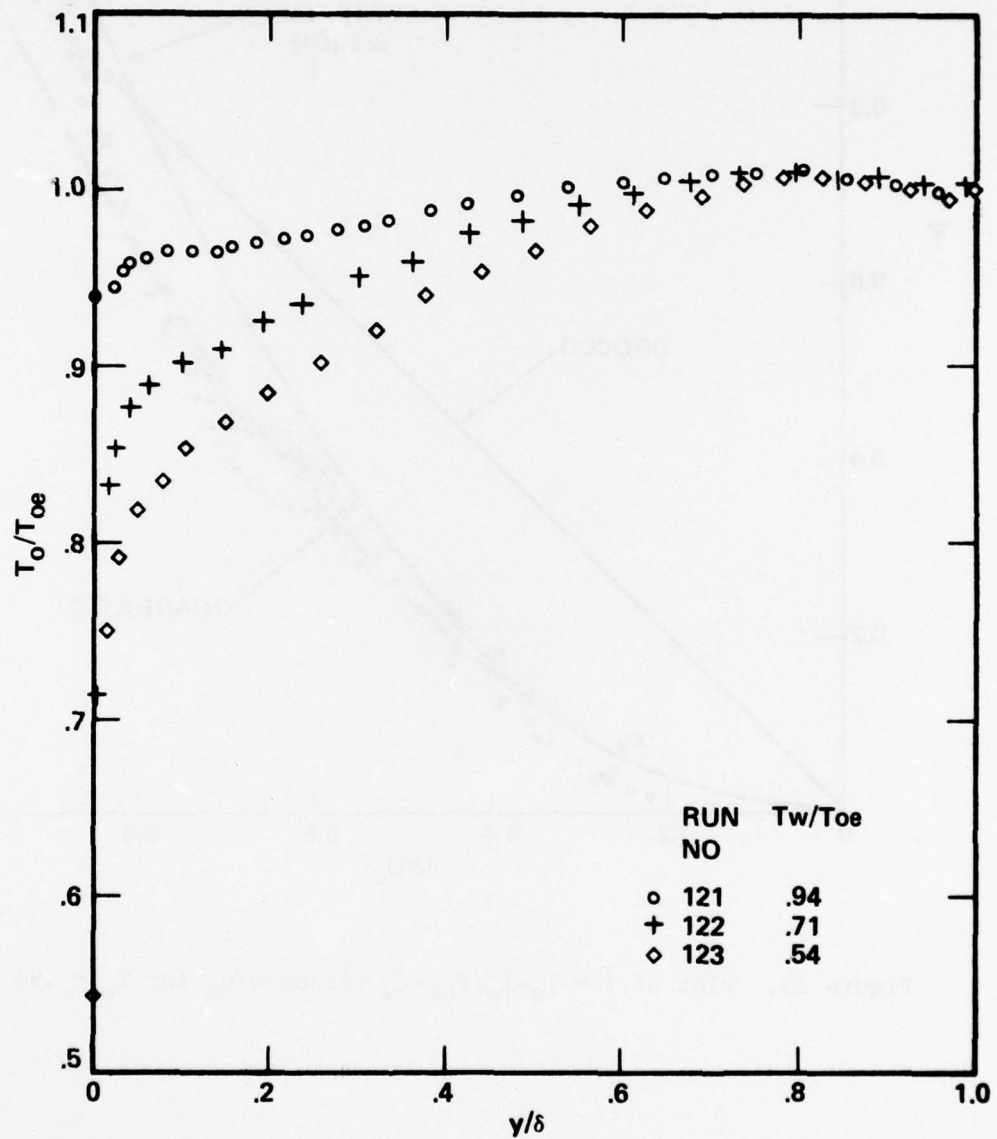


Figure 22. Effect of wall temperature on total temperature profiles

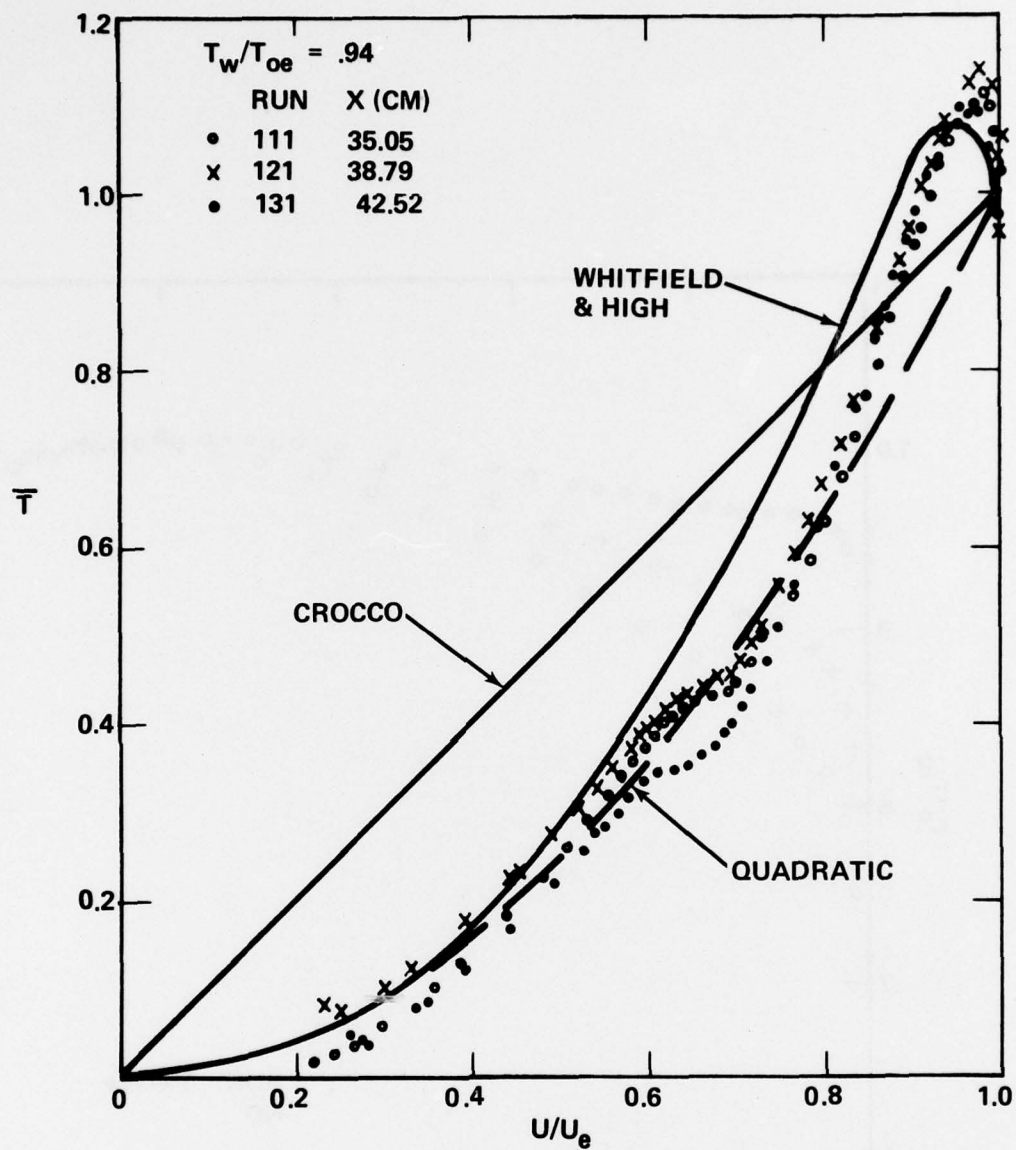


Figure 23. Plot of $\tilde{T} = T_o - T_w / T_{oe} - T_w$ versus u/u_e for $T_w = .94$

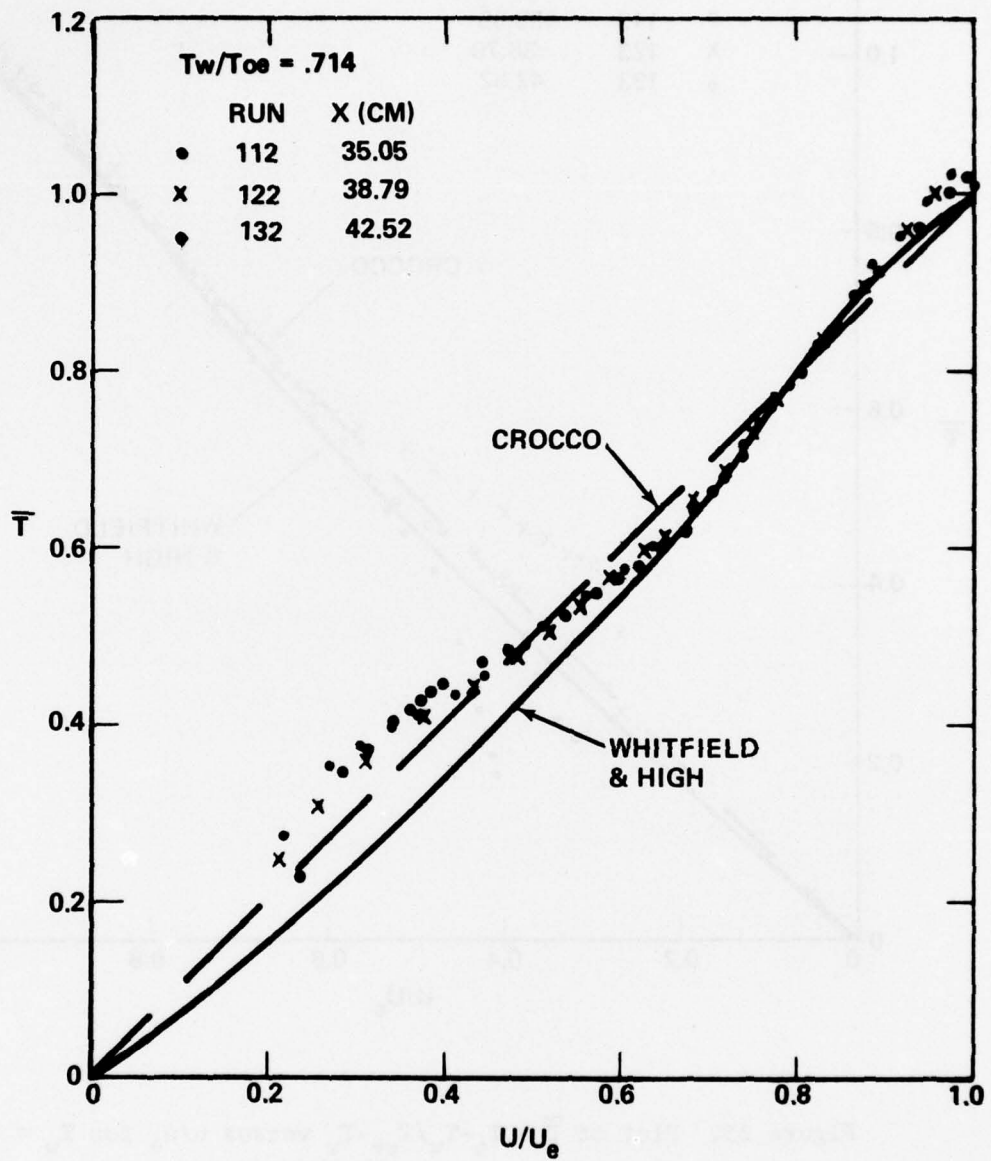


Figure 24. Plot of $\tilde{T} = T_o - T_w / T_{oe} - T_w$ versus u/u_e for $T_w = .71$

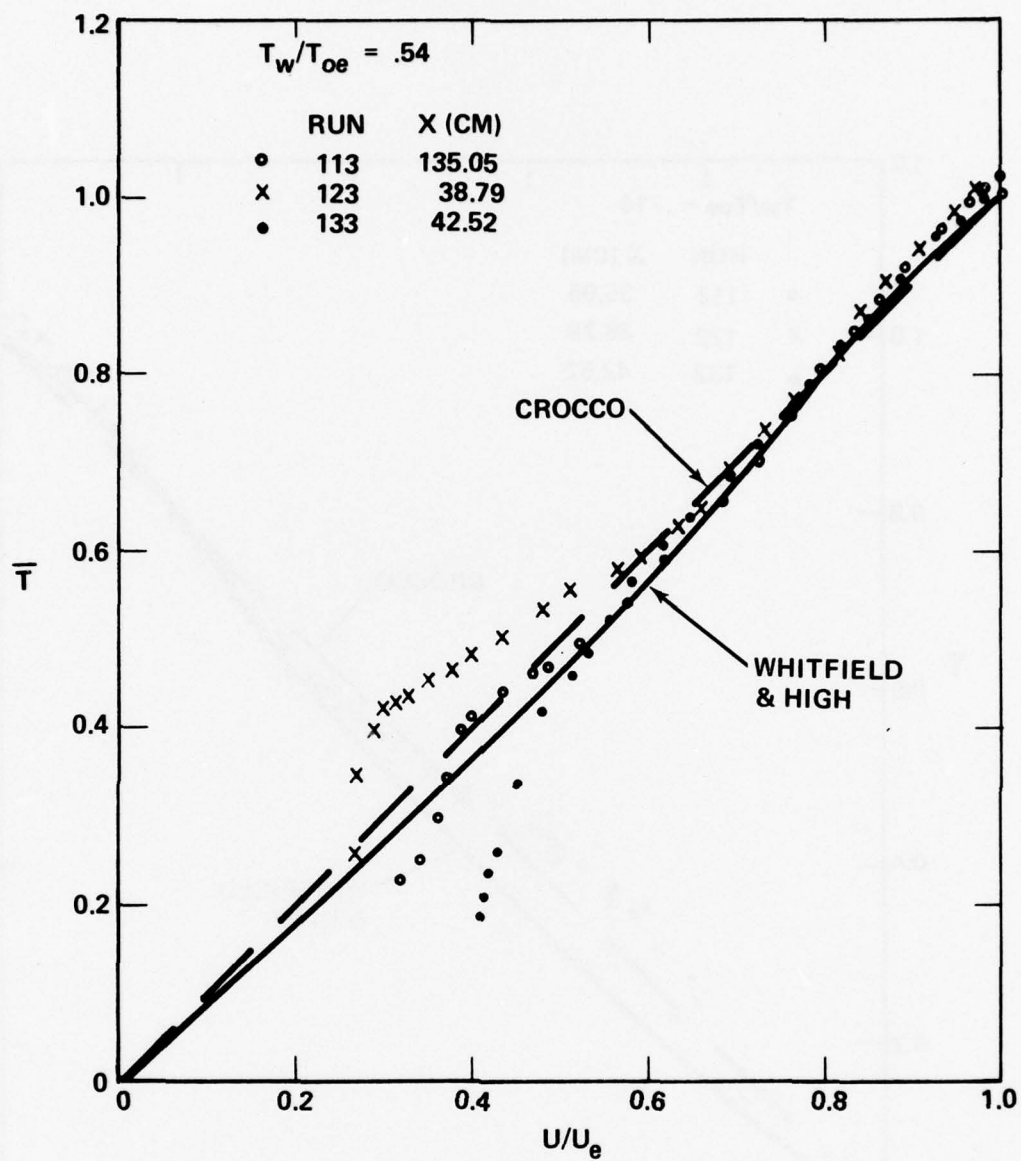


Figure 25. Plot of $\tilde{T} = T_o - T_w / T_{oe} - T_w$ versus u/u_e for $T_w = .54$

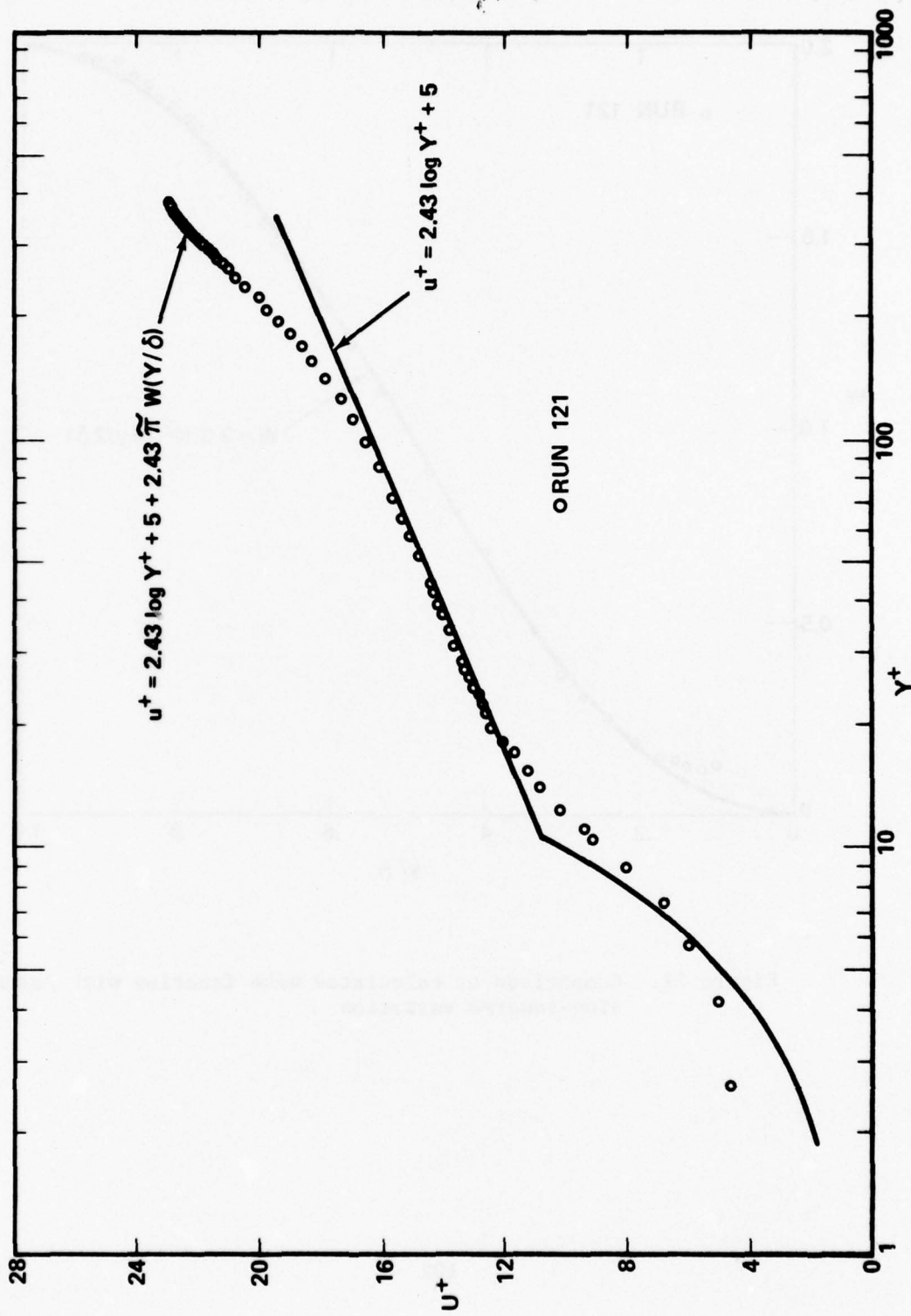


Figure 26. Typical correlation of experimental velocity profile in terms of the Law-of-the-Wake

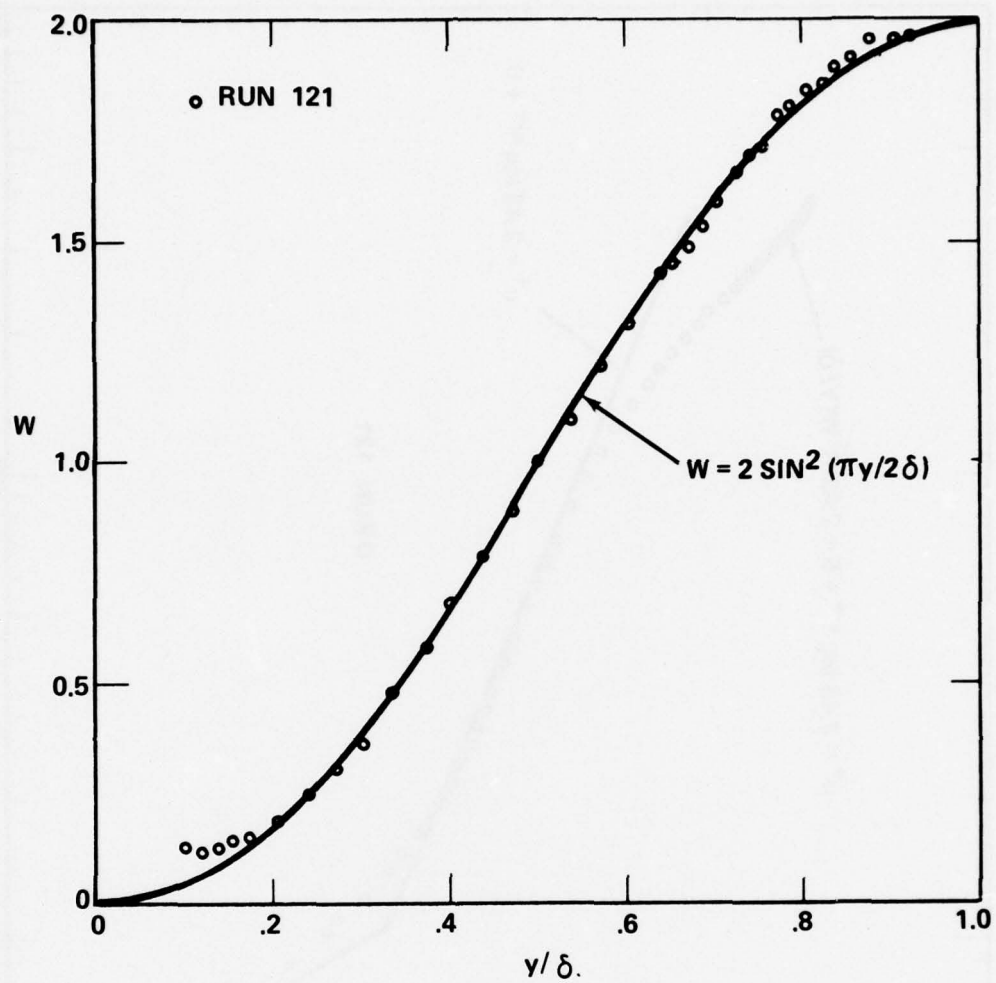


Figure 27. Comparison of calculated wake function with assumed sine-squared variation

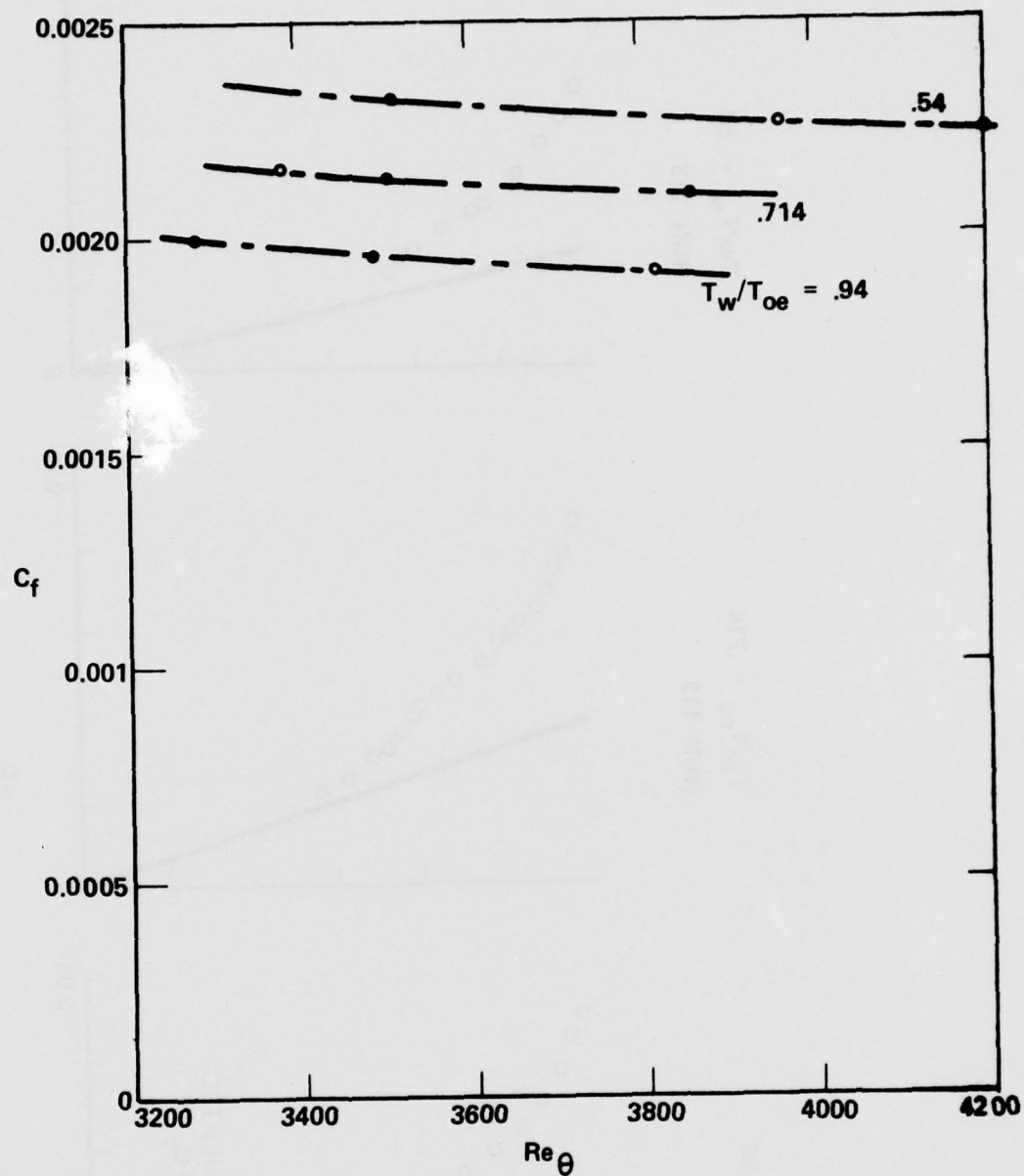


Figure 28. Variation of skin friction c_f , based on Hopkins and Inouye correlation, with Re_θ

$T_w/T_{oe} = .94$
RUN 111

$T_w/T_{oe} = .714$
RUN 112

$T_w/T_{oe} = .54$
RUN 113

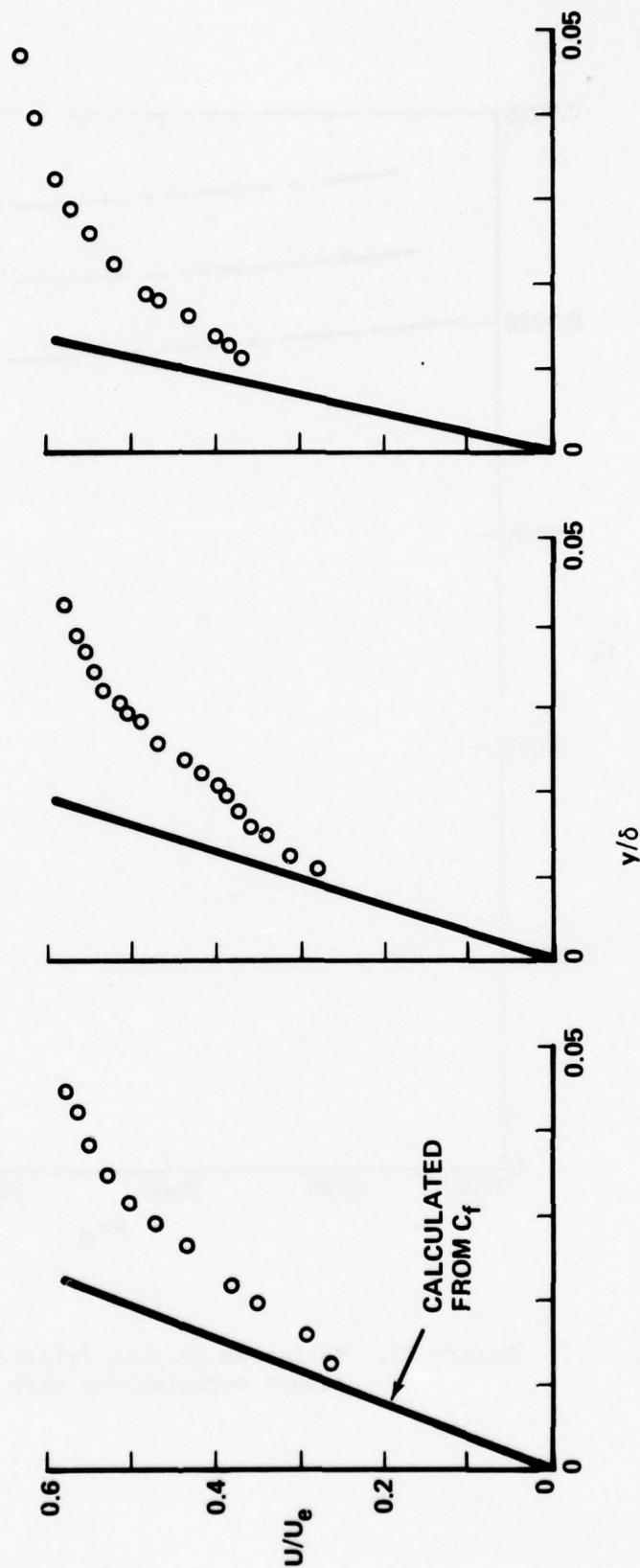


Figure 29. Comparison of linear velocity profile near the wall, deduced from skin friction coefficient, with experimental measurements at $x = 38.79$ cm

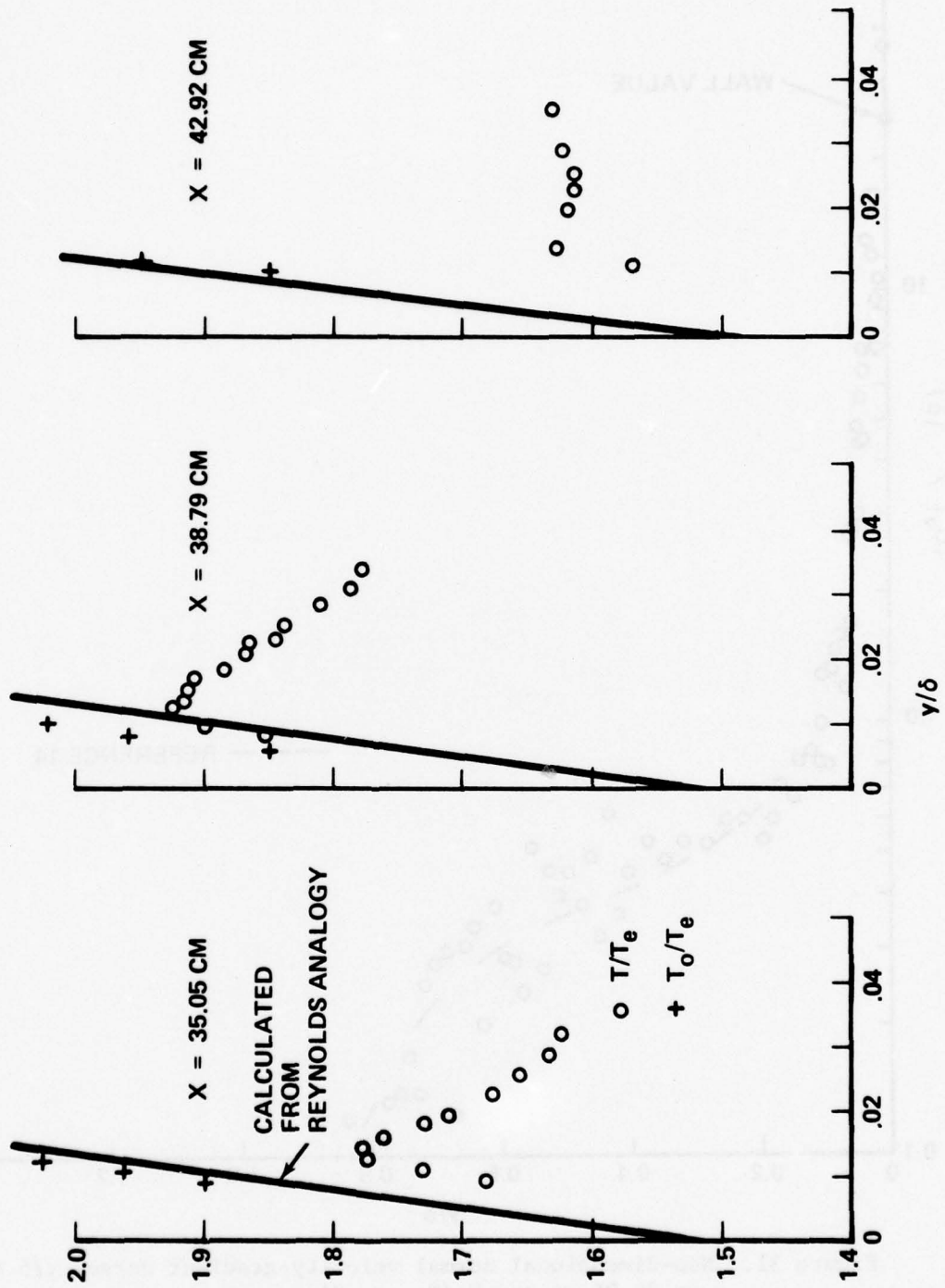


Figure 30. Comparison of linear temperature profile, deduced from skin friction coefficient and Reynolds analogy, with experimental measurements at $T_w/T_{oe} = .54$

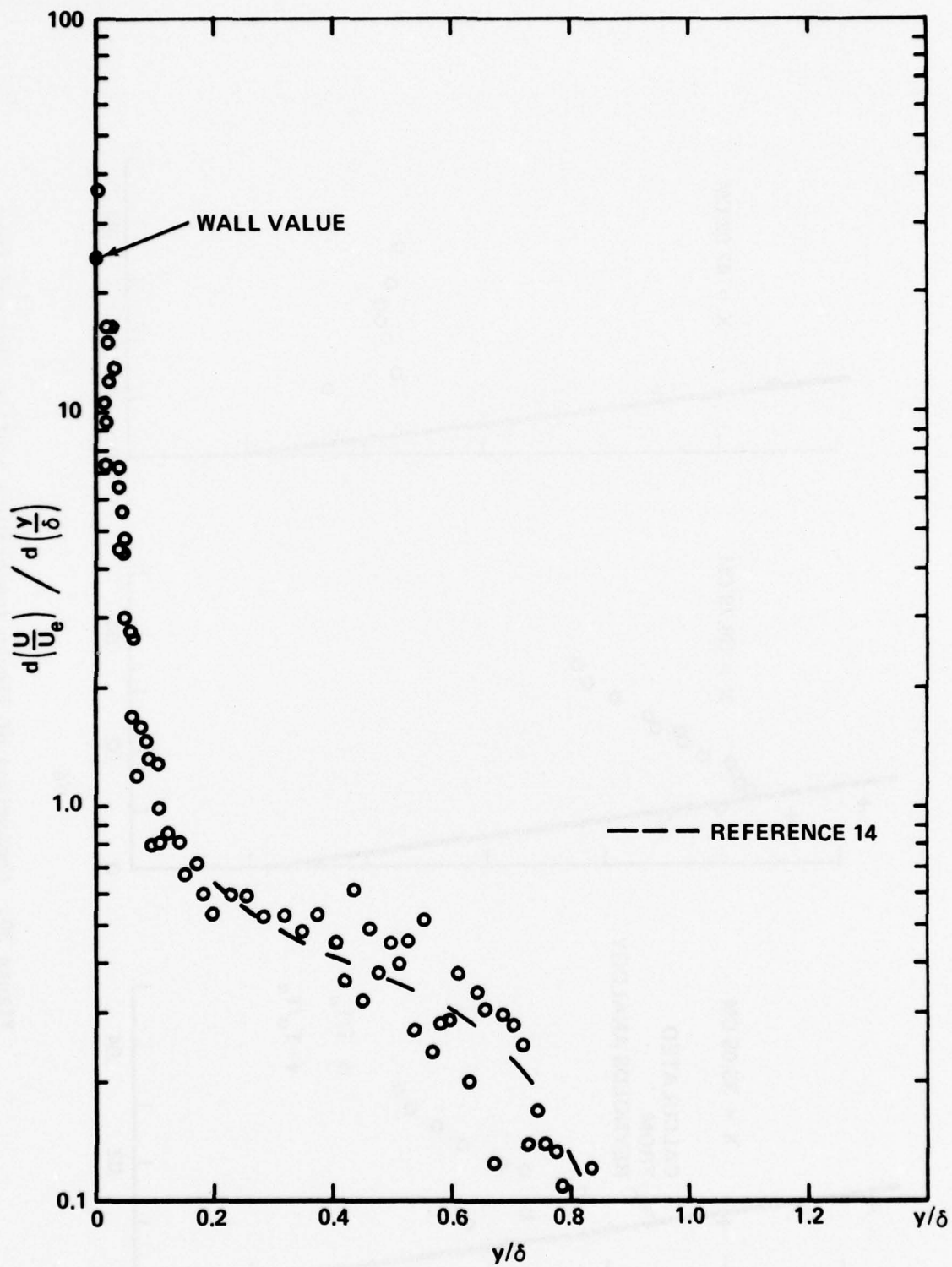


Figure 31. Non-dimensional normal velocity gradient versus y/δ for $x = 35.05$ cm and $T_w/T_{oe} = .94$

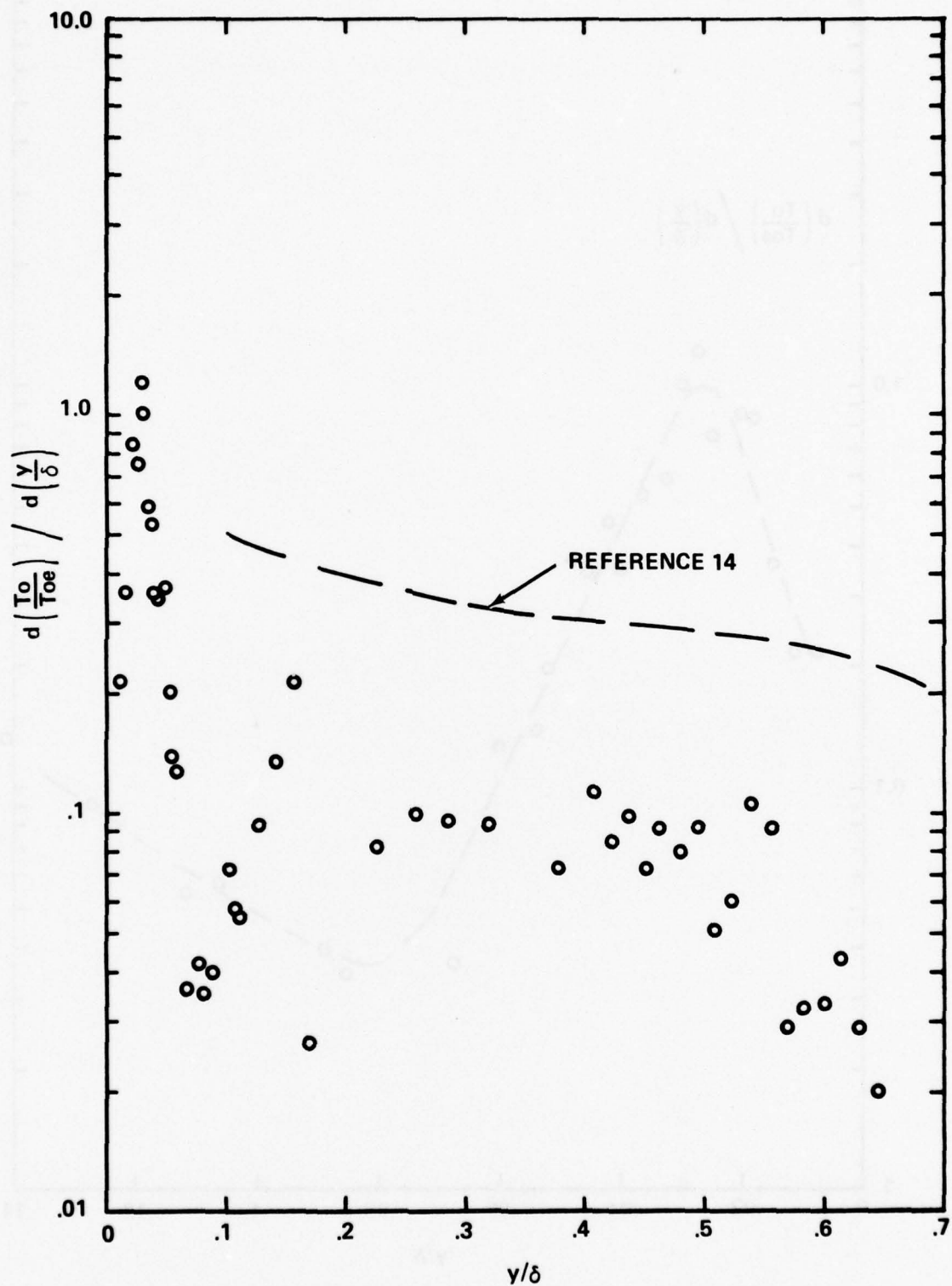


Figure 32. Non-dimensional normal total temperature gradient versus y/δ for $x = 35.05$ cm and $T_w/T_{oe} = .94$

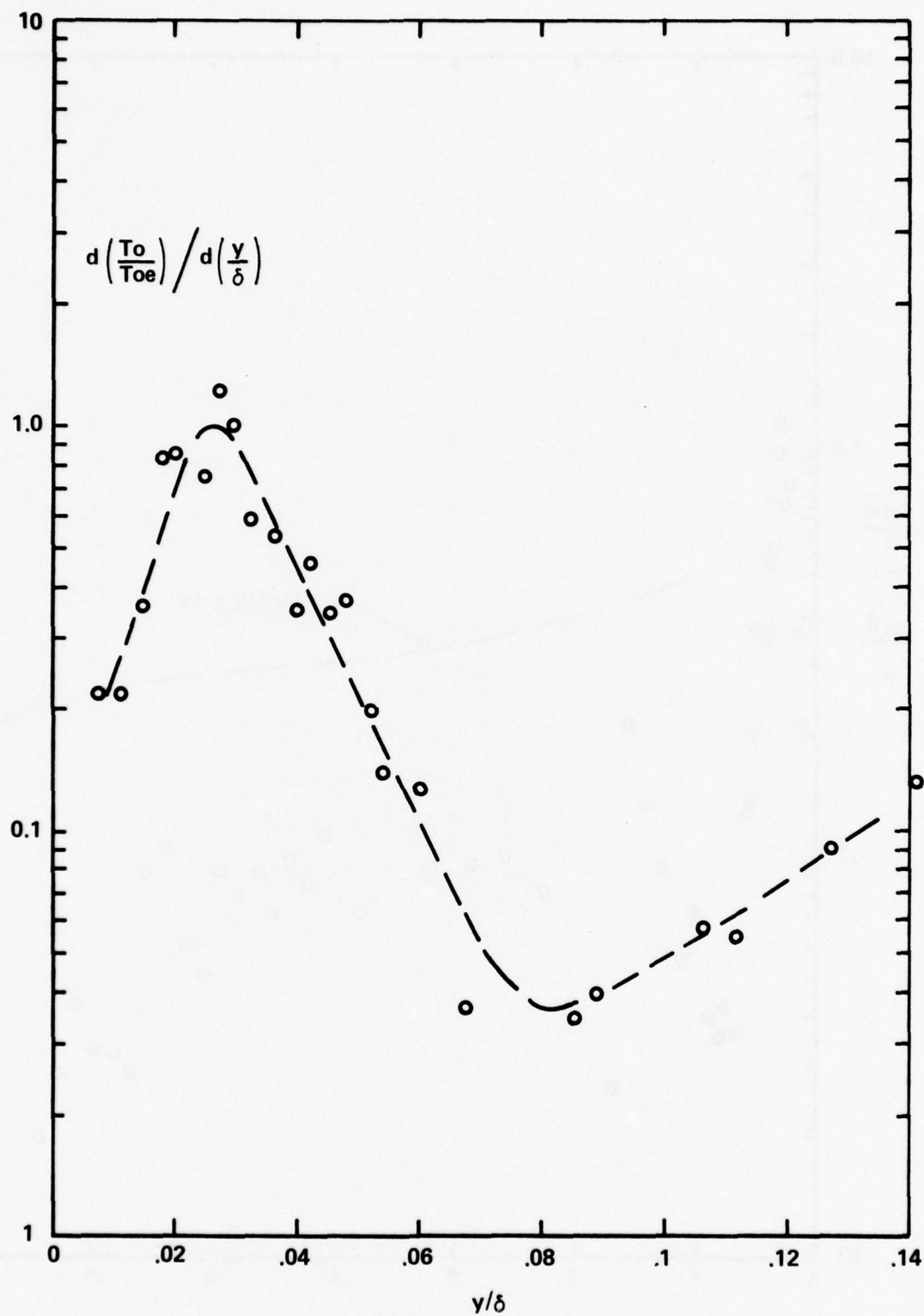


Figure 33. Non-dimensional normal total temperature gradient in vicinity of wall for $x = 35.05$ cm and $T_w/T_{oe} = .94$

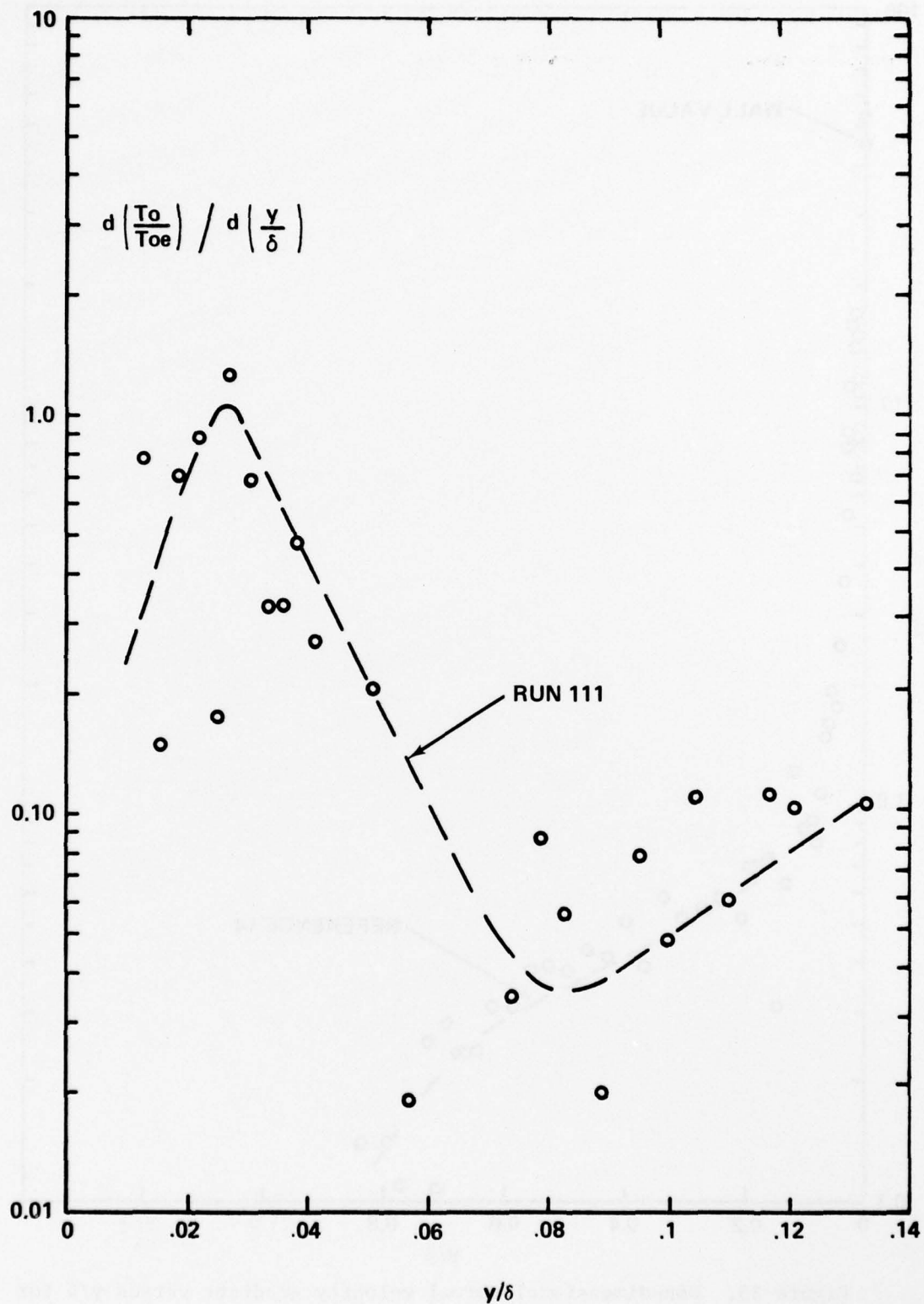


Figure 34. Non-dimensional normal total temperature gradient in vicinity of wall for $x = 42.52$ cm and $T_w/T_{oe} = .94$

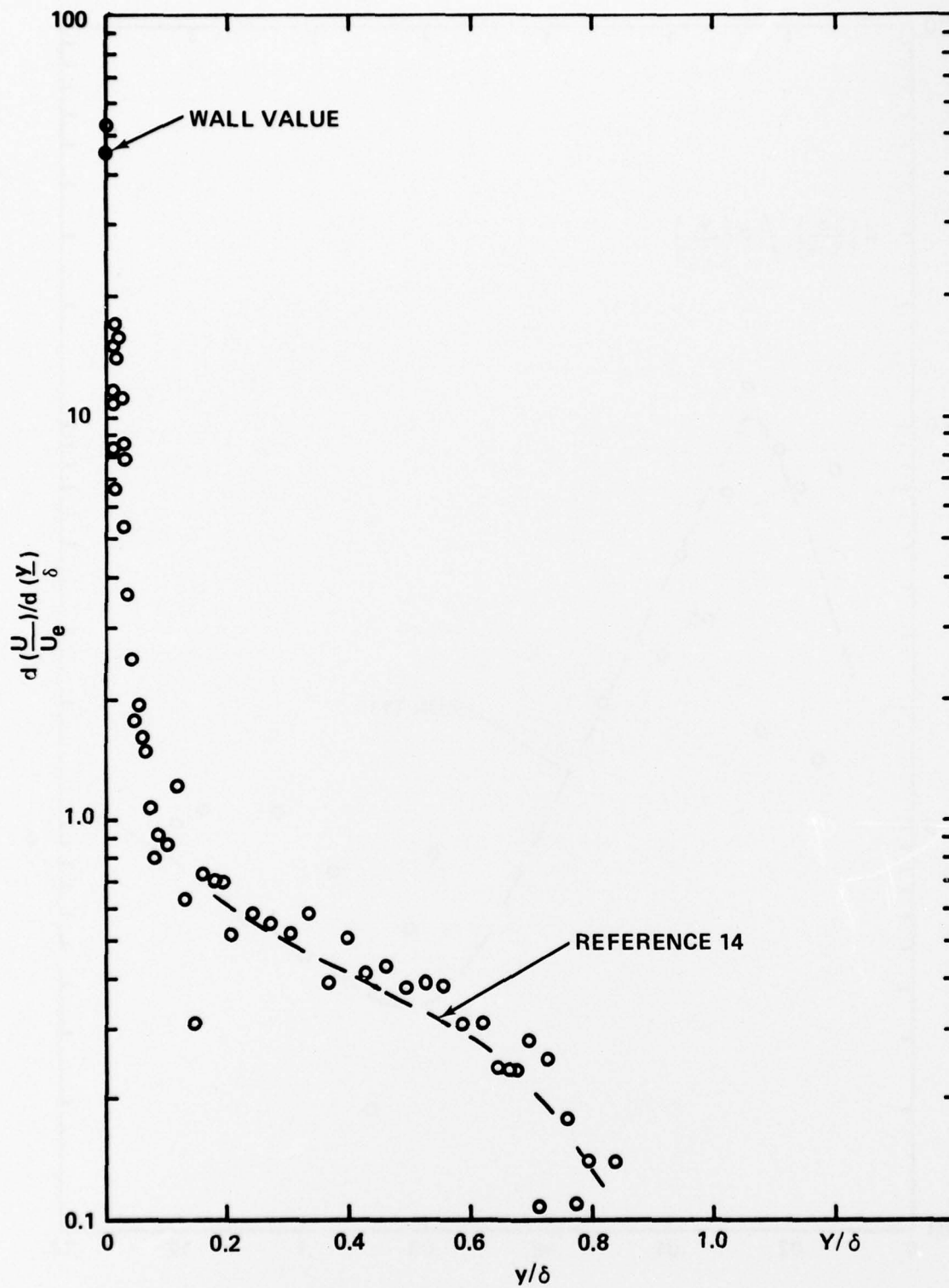


Figure 35. Non-dimensional normal velocity gradient versus y/δ for $x = 35.05$ cm and $T_w/T_{oe} = .54$

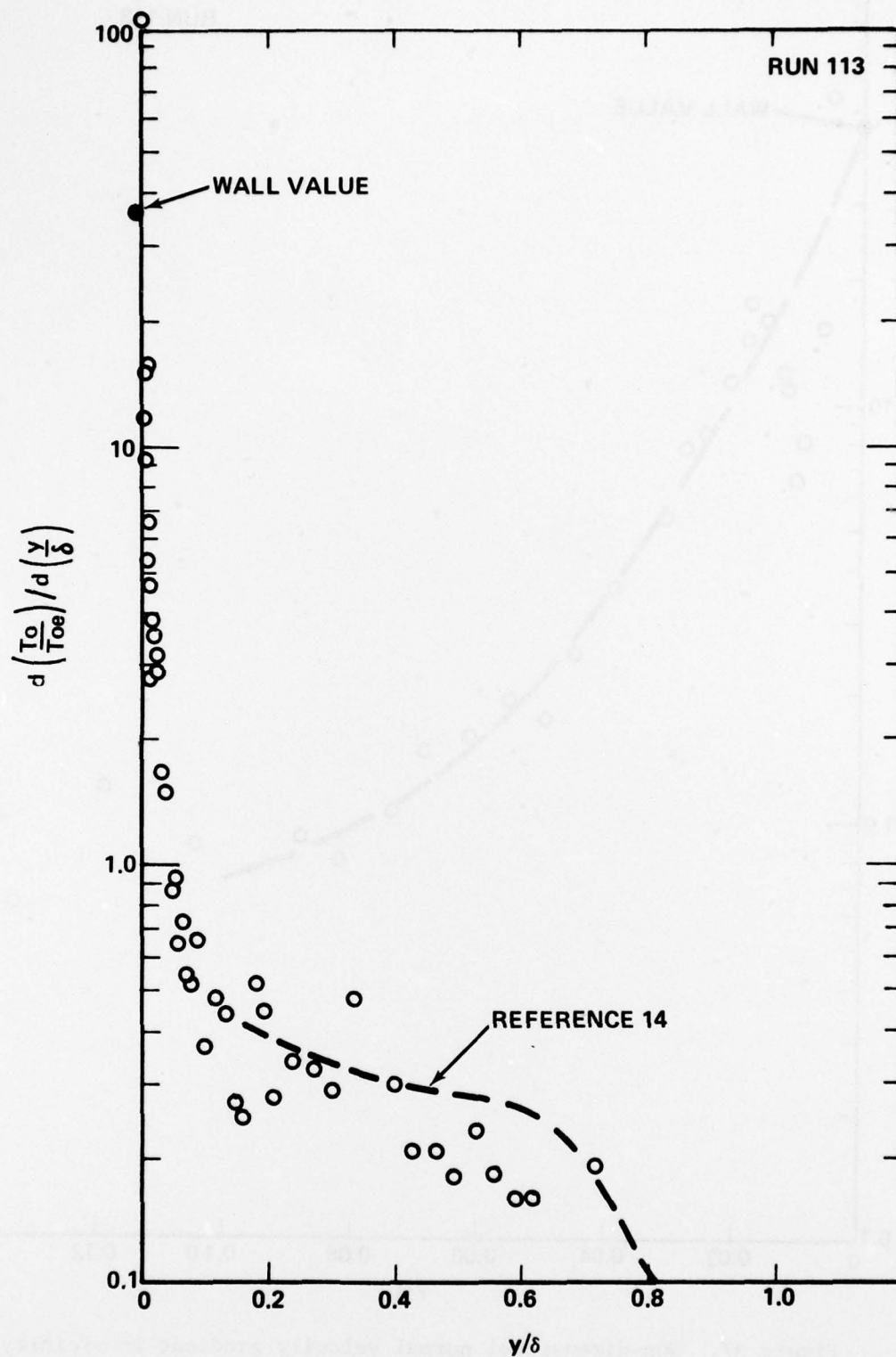


Figure 36. Non-dimensional normal total temperature gradient versus y/δ for $x = 35.05$ cm and $T_w/T_{oe} = .54$

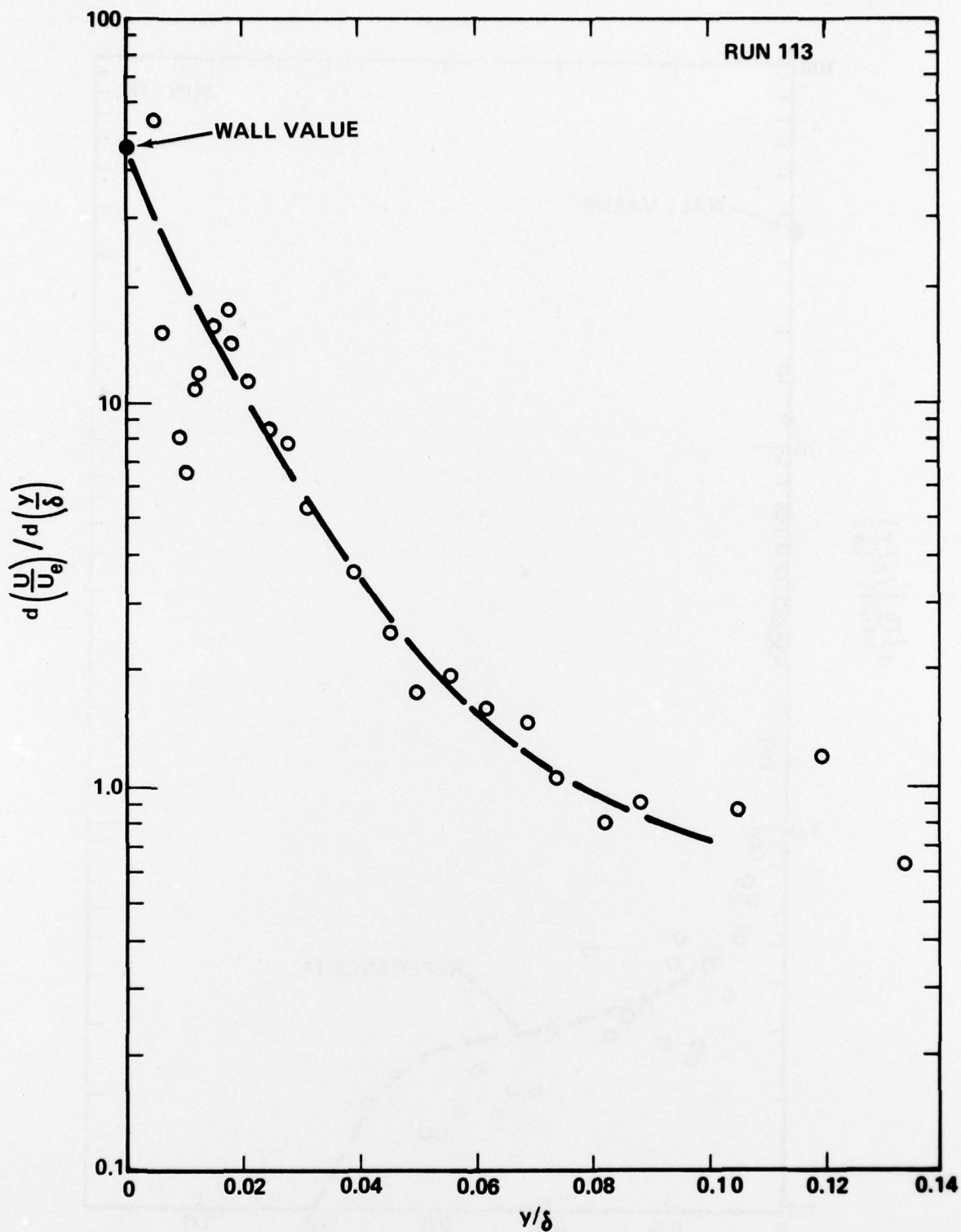


Figure 37. Non-dimensional normal velocity gradient in vicinity of wall for $x = 35.05$ cm and $T_e/T_{oe} = .54$

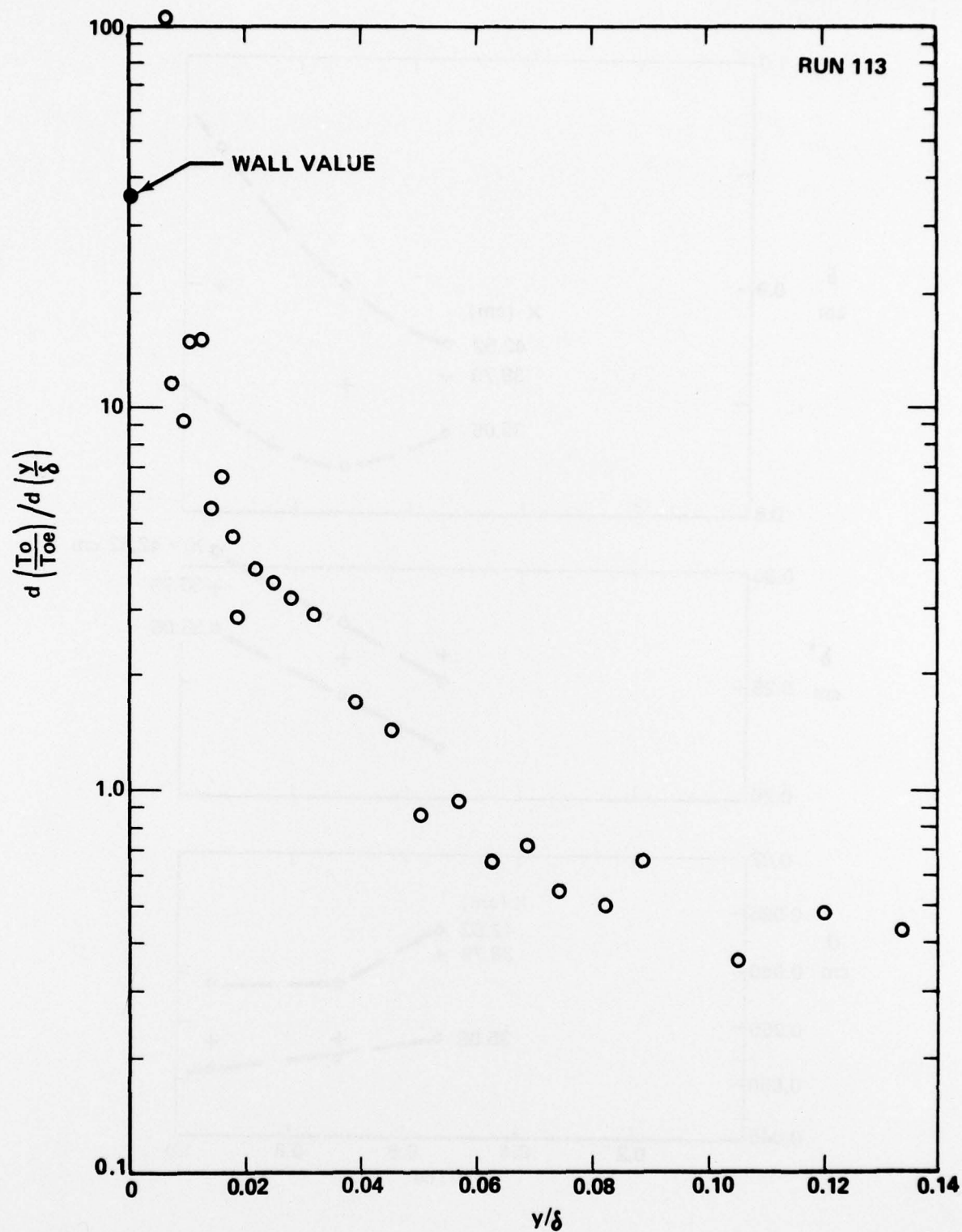


Figure 38. Non-dimensional normal total temperature in vicinity of wall for $x = 35.05$ cm and $T_w/T_{oe} = .54$

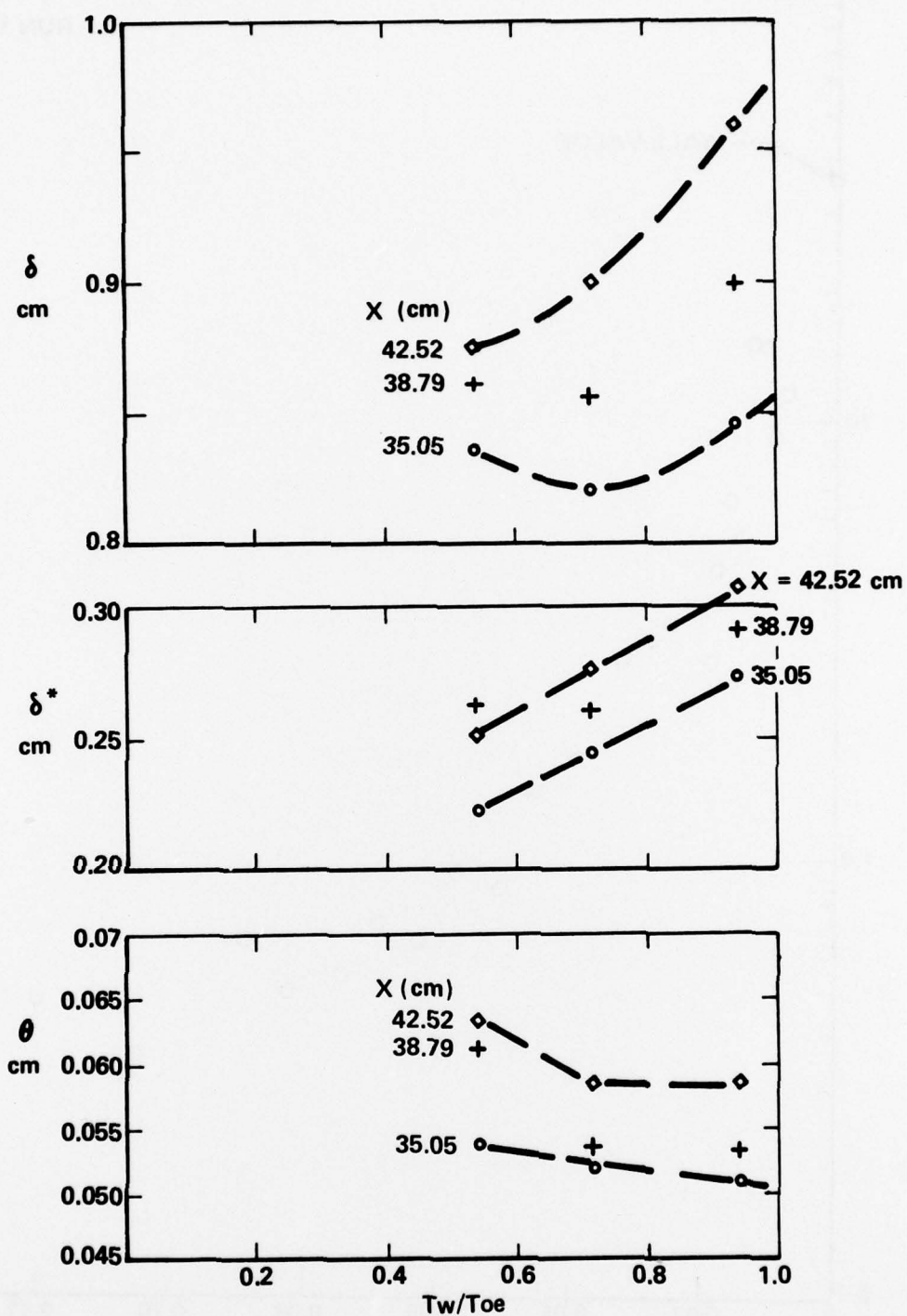


Figure 39. Characteristic boundary layer thicknesses δ , δ^* and θ plotted as a function of T_w/T_{oe}

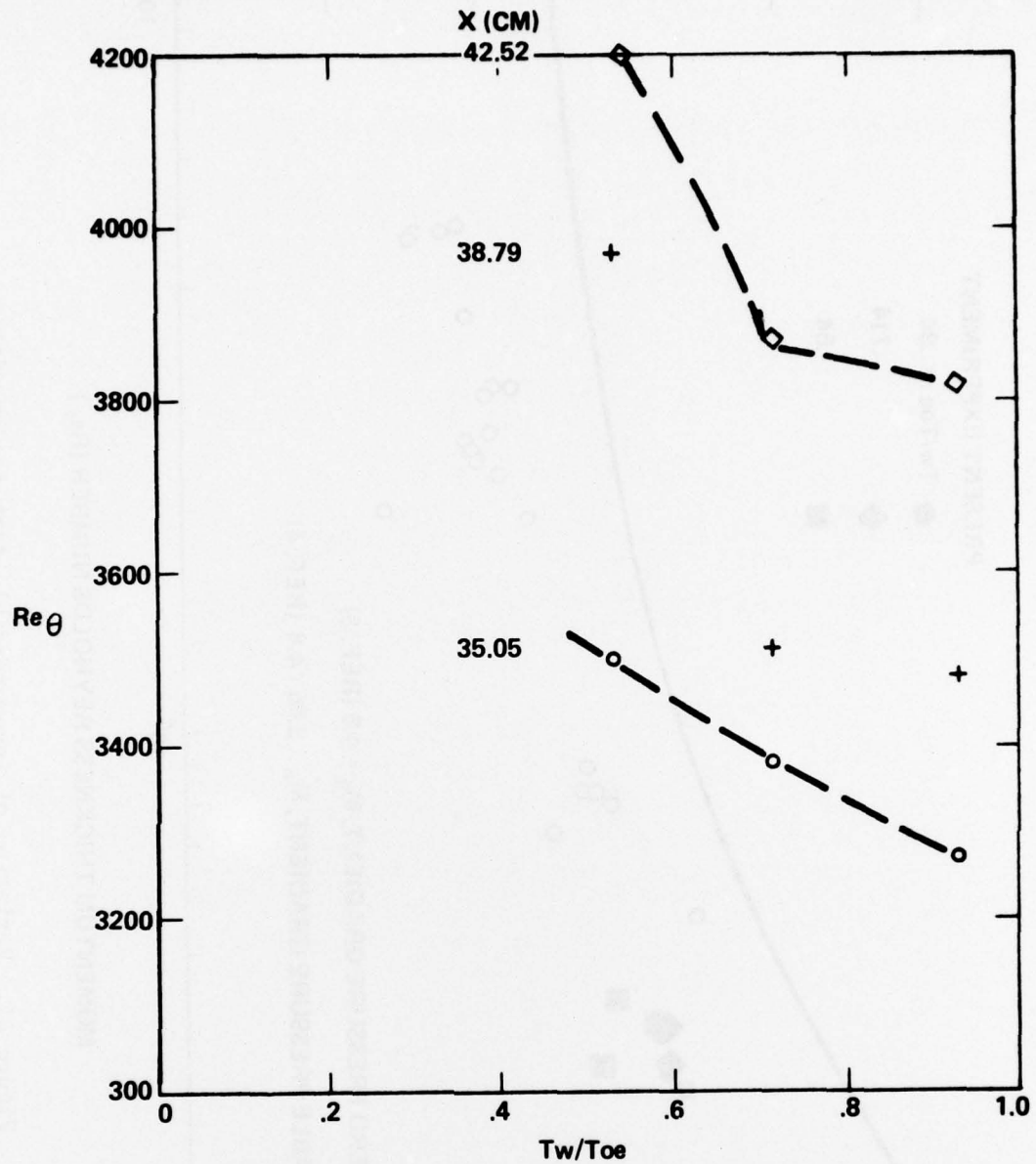


Figure 40. Variation of Re_θ with T_w/T_{oe}

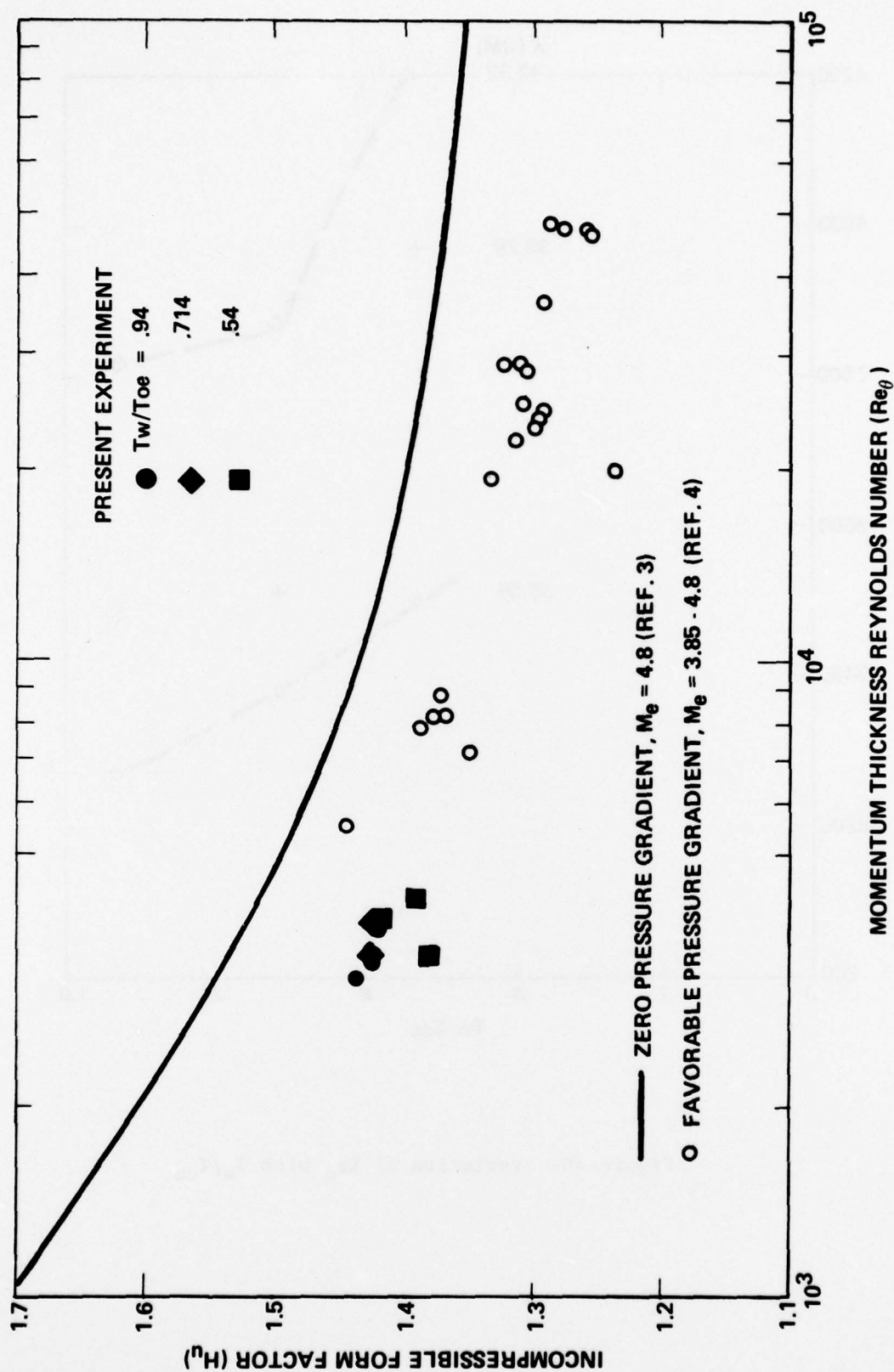


Figure 41. Variation of incompressible form factor with Re_θ

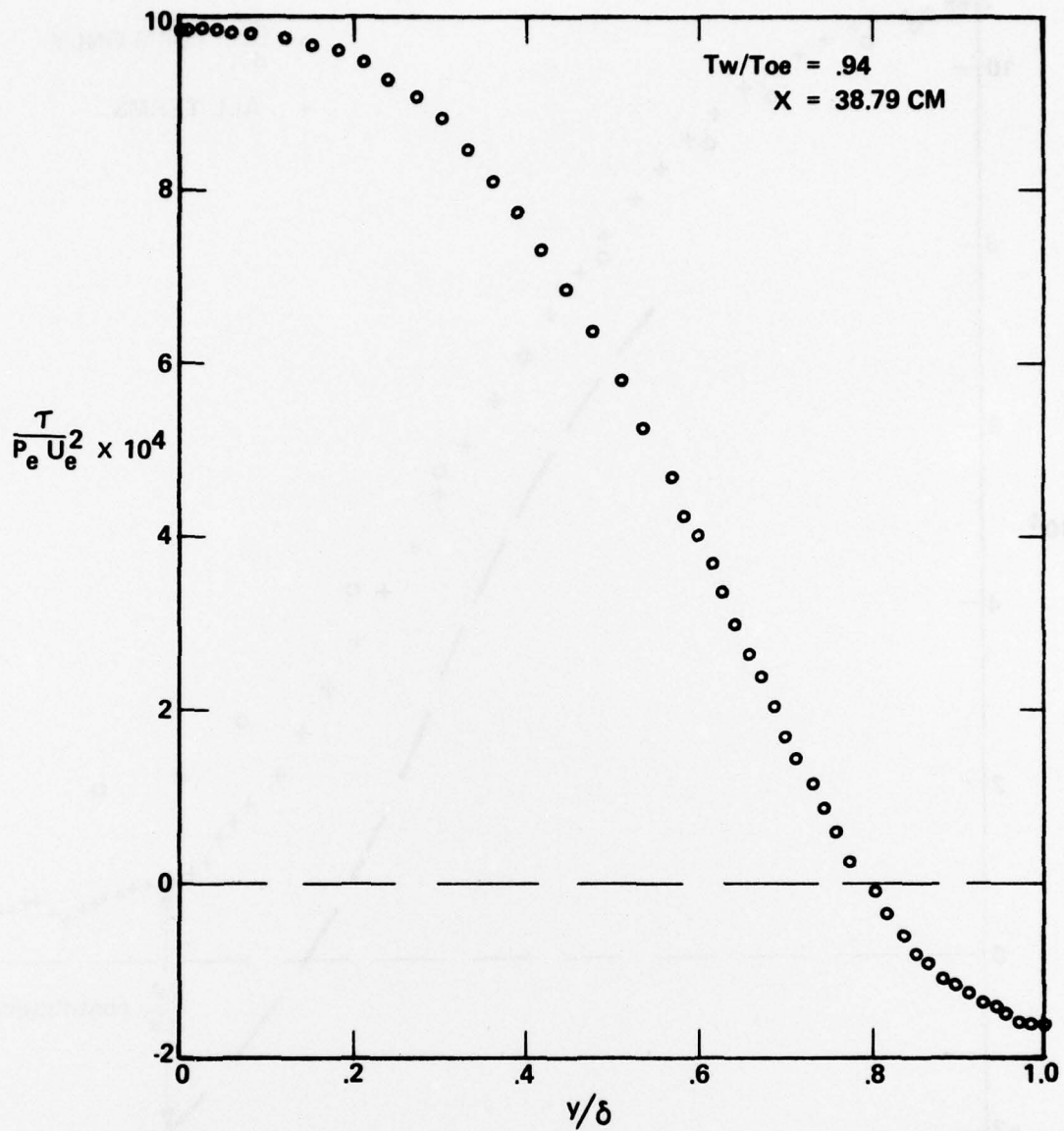


Figure 42. Shear stress distribution, based on mean flow profiles for $T_w/T_{oe} = .94$, $x = 38.79 \text{ cm}$

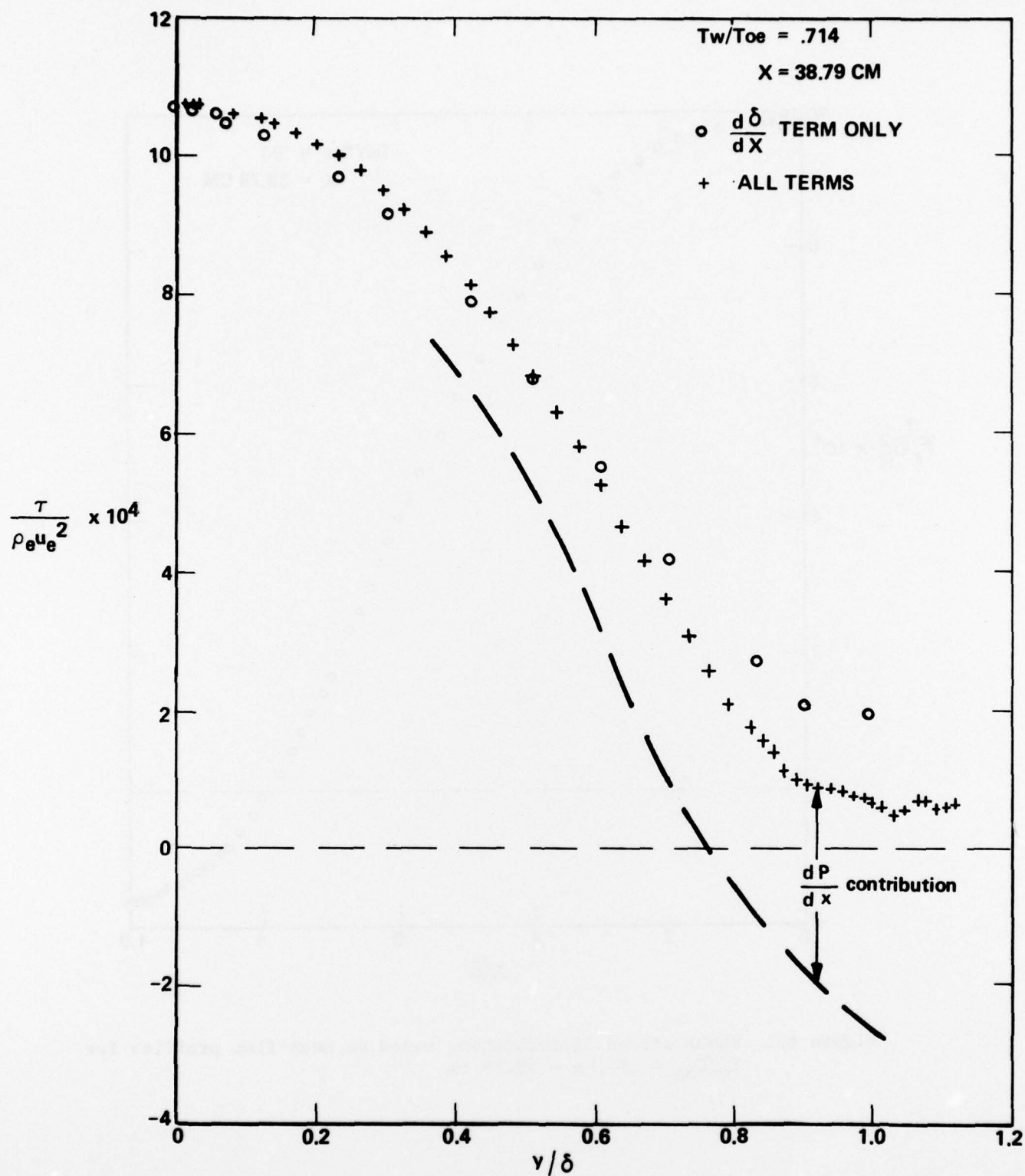


Figure 43. Shear stress distribution, based on mean flow profiles for $T_w/T_{oe} = .71$, $x = 38.79 \text{ cm}$

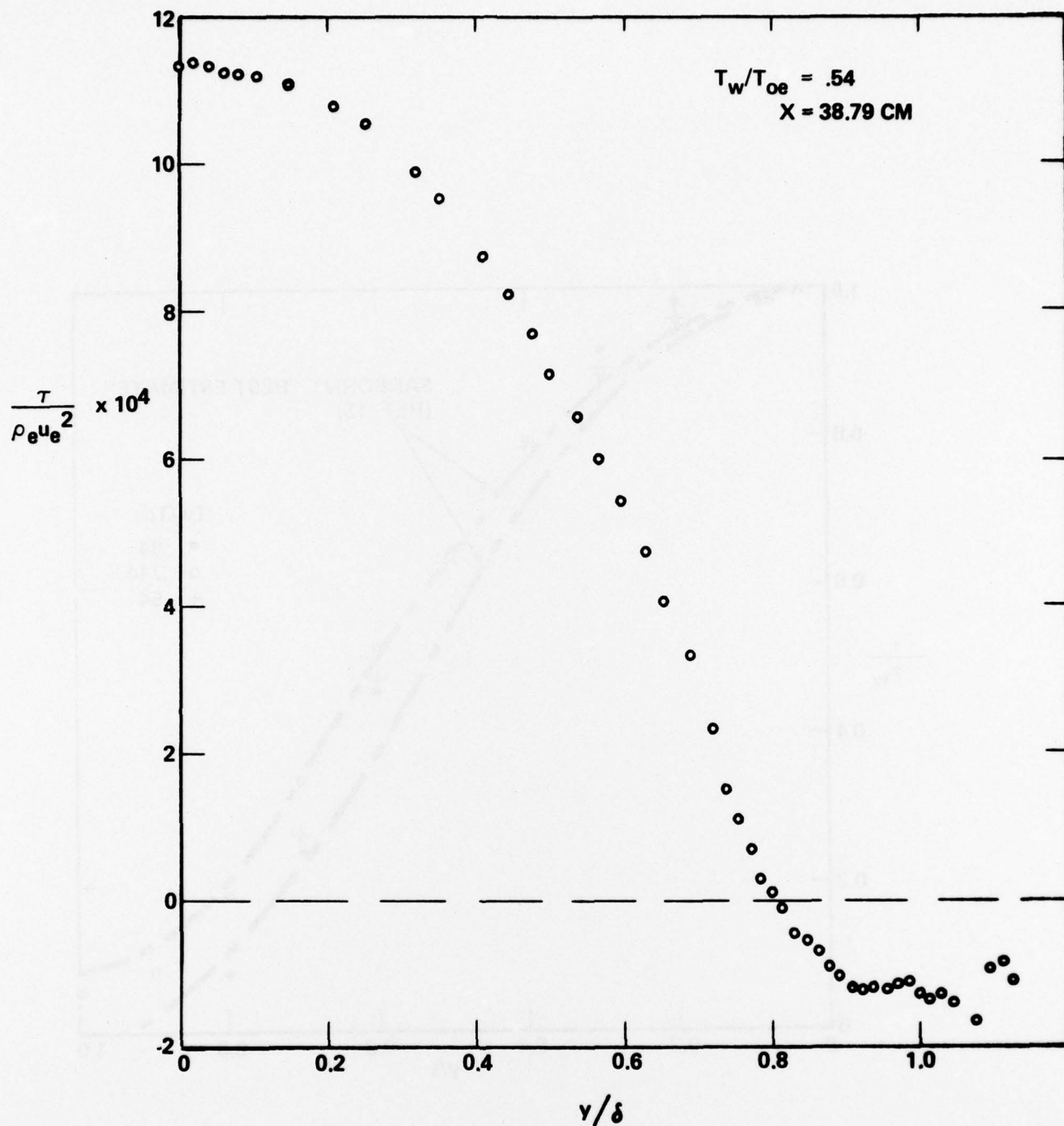


Figure 44. Shear stress distribution, based on mean flow profiles for $T_w/T_{oe} = .54$, $x = 38.79 \text{ cm}$

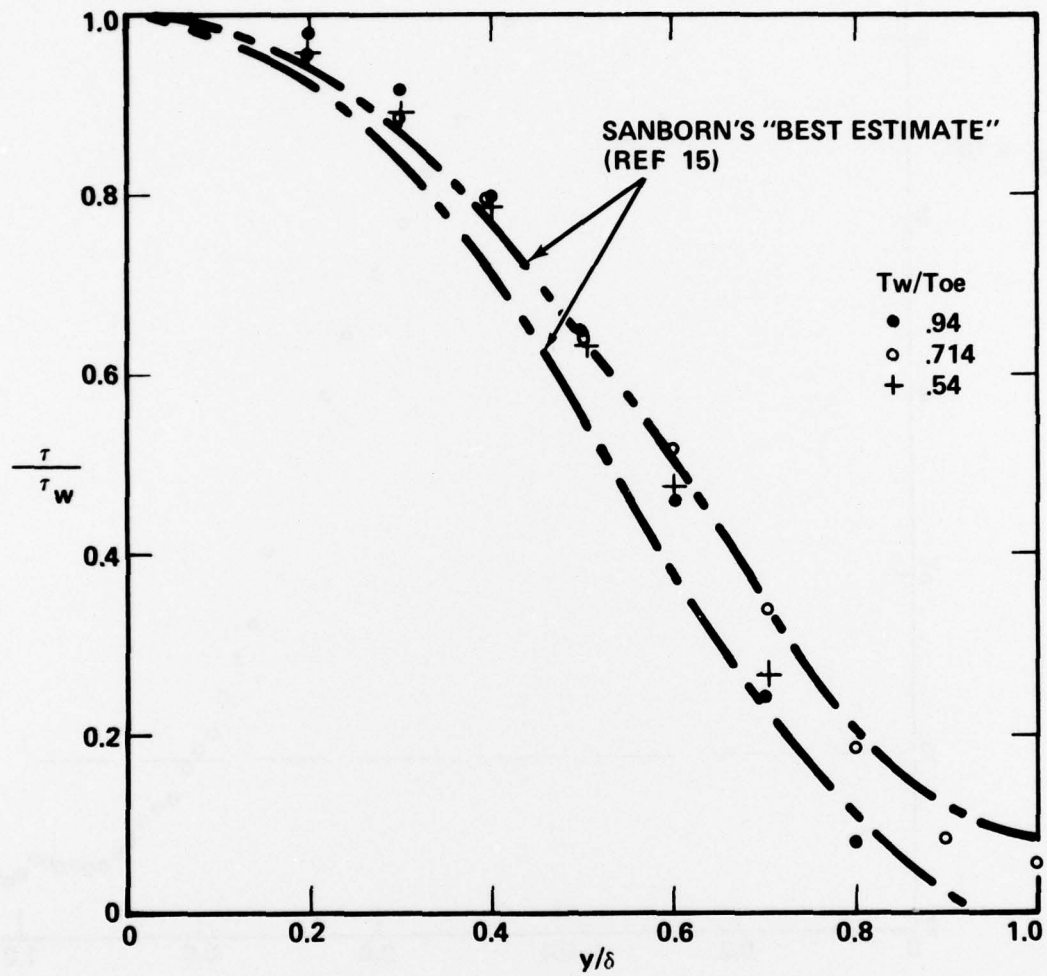


Figure 45. Turbulent shear stress, normalized by wall shear, versus y/δ

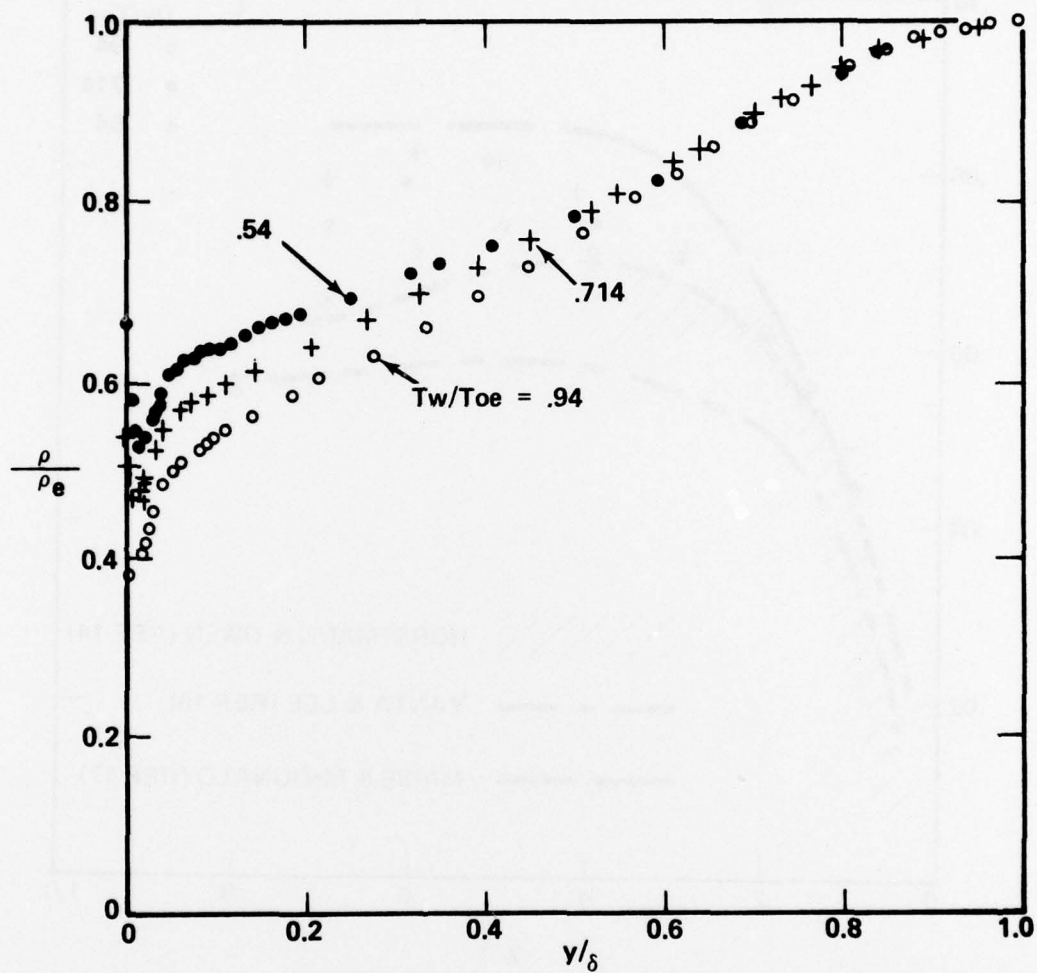


Figure 46. Density ratio, ρ/ρ_e , versus y/δ for $x = 38.79$ cm showing effect of T_w/T_{oe}

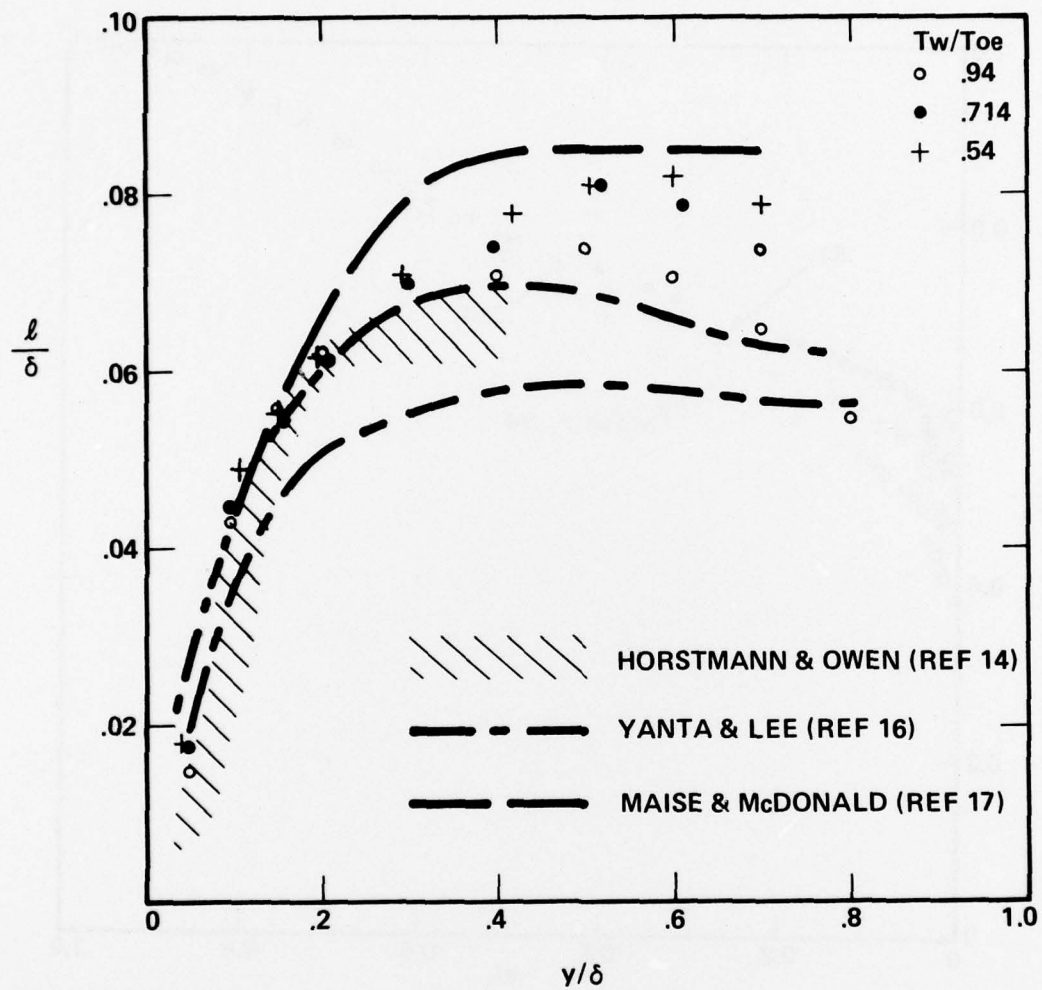


Figure 47. Variation of normalized mixing length l/δ across the boundary layer

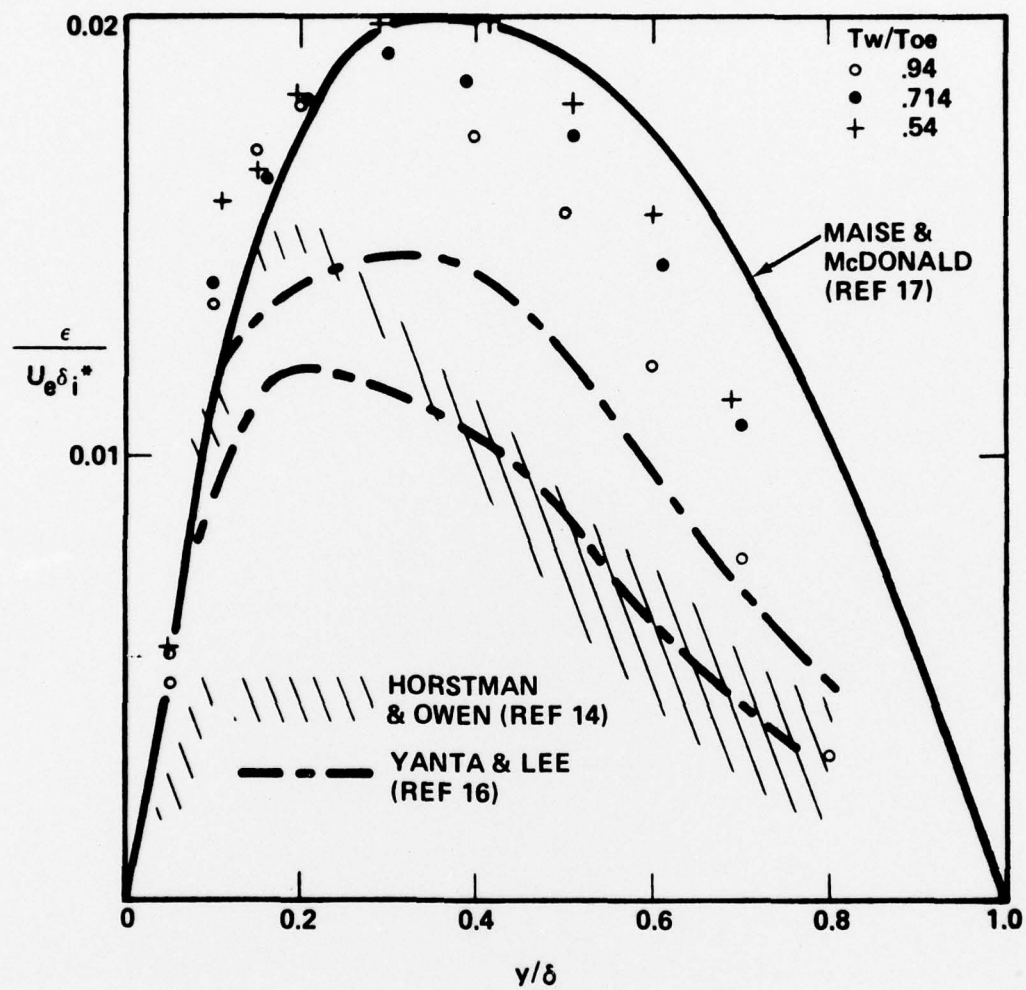


Figure 48. Normalized eddy viscosity versus y/δ